Ziegler–Natta Polymerization: HDPE, PP, LLDPE and EPDM

Chapter · August 2023

DOI: 10.1002/9783527843831.ch5

2 authors, including:

Niket Sharma
Aspen Technology, Inc.
20 PUBLICATIONS **278** CITATIONS

SEE PROFILE

Ziegler-Natta Polymerization: HDPE, PP, LLDPE and EPDM

Y.A. Liu and Niket Sharma

Department of Chemical Engineering, Virginia Polytechnic Institute and State University, Blacksburg, Virginia 24061, U.S.A

Abstract

This chapter presents a novel approach to modeling the manufacturing processes of high-density polyethylene (HDPE), polypropylene (PP), linear low-density polyethylene (LLDPE), and ethylene-propylene-diene monomer (EPDM) using Ziegler-Natta (ZN) catalysts. By leveraging Aspen Polymers simulation software, the chapter introduces an innovative methodology for estimating kinetic parameters directly from plant data, enabling more accurate and optimized simulation models for commercial polyolefin processes.

The chapter covers key aspects of ZN polymerization kinetics, such as catalyst site activation, chain propagation, transfer, inhibition, and deactivation, while offering a unique framework to model complex processes through reactor-specific considerations, molecular weight distributions, and thermodynamic modeling. A significant contribution is the integration of validated plant data with advanced simulation tools, offering new possibilities for process improvement and optimization.

Through a series of hands-on workshops, the chapter showcases groundbreaking applications for simulating and optimizing HDPE, PP, LLDPE, and EPDM production, utilizing novel approaches such as slurry and gas-phase operations. This methodology introduces a transformative toolset for kinetic parameter estimation and process enhancement, positioning it as a pioneering resource for the next generation of polyolefin manufacturing advancements.

This chapter deals with modeling of HDPE, PP, LLDPE and EPDM manufacturing processes using Ziegler-Natta (ZN) catalyst. We use simulation software Aspen Polymers for this study. We deal with the methodology and procedure to model the ZN polymerization kinetics.

We present an effective methodology for estimating the kinetic parameters based on plant data in the development of simulation and optimization models for commercial polyolefin processes using efficient software tools. We cover conceptual development, modeling methodology, illustrative examples and hands-on workshops.

This is a preprint version of a chapter from our book - Integrated Process Modeling, Advanced Control and Data Analytics for Optimizing Polyolefin Manufacturing [78,83] and also an extended version of our paper [3]. Please cite the original work if referenced

5.1 Ziegler-Natta (ZN) Polymerization

Section 5.1 introduces Ziegler-Natta polymerization. Section 5.2 discusses ZN polymerization kinetics. We cover catalyst site activation, chain initiation, chain propagation, chain transfer, catalyst inhibition and deactivation, and copolymerization kinetics. Section 5.3 presents modeling considerations, including reactor types, polymer types, process flowsheets, molecular weight distributions (MWD) and multi-modal distributions, thermodynamics, and global kinetics versus local kinetics. Section 5.4 describes commercial polyolefin production targets, including general and polymer-specific production targets. Section 5.5 presents an effective methodology for kinetic parameter estimation for modeling commercial polyolefin processes from plant data using efficient software tools, including data fit, sensitivity analysis, and design specification. This section also illustrates the applications of simulation models validated by plant data to process improvement. Section 5.6 presents a detailed hands-on workshop to develop the simulation model for the slurry HDPE process. Section 5.7 is a hands-on workshop to illustrates how to simulate and optimize a gas-phase PP process using stirred-bed reactors. Section 5.8 gives a hands-on workshop of producing LLDPE using a condensed mode cooling operation of a fluidized-bed process. Section 5.9 present a hands-on workshop to simulate an ethylene-propylene rubber copolymerization (EPM) or an ethylene-propylene-diene rubber terpolymerization (EPDM) by a metallocene catalyst system. Section 5.10 presents the biography.

5.1.1 Introduction

Ziegler-Natta (ZN) catalyst is one of the most widely used catalysts for manufacturing commercial HDPE, PP, LLDPE and EPDM. Polyethylene and polypropylene are two commodity polymers of the highest demands. Polyolefins have a wide application requiring different properties with different molecular weight distribution and branching distribution. The polymerization follows the coordination mechanism which is different from the free radical polymerization mechanism used for producing high-pressure LDPE. The microstructure of polyolefins made with coordination catalysts is different from that made with free radical kinetics. The LDPE made using the free radical mechanism consists of both short chain branching (SCB) and long chain branching (LCB), while that made by coordination mechanism consists of only SCB. Thus, catalyst design plays an important role in polyolefin processes. Different process types with different reactors and phases are other variable able to modify polyolefin properties. The process for producing polyolefins can be in three phases, including solution, slurry and gas phase. Autoclaves/CSTR, loop reactors, fixed bed reactors (FBR) are some of the main reactors used for polyolefin processes for different phases. For example, the loop reactors are used for slurry-phase process and FBR are used for gas-phase process. The book by Soares and McKenna [1] covers different polyolefin processes in detail.

The modeling of the ZN kinetics is complex because of the multiple active catalyst sites in the ZN catalyst. The most common type of ZN catalyst is titanium tetrachloride $TiCl_4$ supported on $MgCl_2$ or SiO_2 which is heterogeneous in nature. ZN catalysts give high activity and productivity. Multiple active sites of the ZN catalyst enable the production of polymers with broad molecular weight distributions and allow good polymer microstructural control.

This chapter focuses mostly on ZN catalysts, not other catalyst types, such as Phillips, metallocene and late transition metal catalysts discussed in Chapters 3 and 5 of Soares and McKenna [1]. Phillips catalyst is similar to the ZN catalyst with multiple active sites and is used for producing HDPE consisting of chromium compounds like CrO_3 supported on SiO_2. Metallocene catalyst and late transition metal catalysts are used to produce HDPE/LLDPE with uniform properties and narrow MWD. The metallocene

catalysts are considered to be single site and homogeneous, i.e., soluble in the reaction medium. In Section 5.9, we present a hands-on workshop to simulate an ethylene-propylene rubber copolymerization (EPM) by a metallocene catalyst system. This chapter also does not deal with any processes that may use more than one catalyst type. Our limitation results from the lack of sufficient published plant data that would enable us to develop an effective methodology for kinetic parameter estimation for other catalyst types.

5.1.2 Ziegler-Natta Catalysts

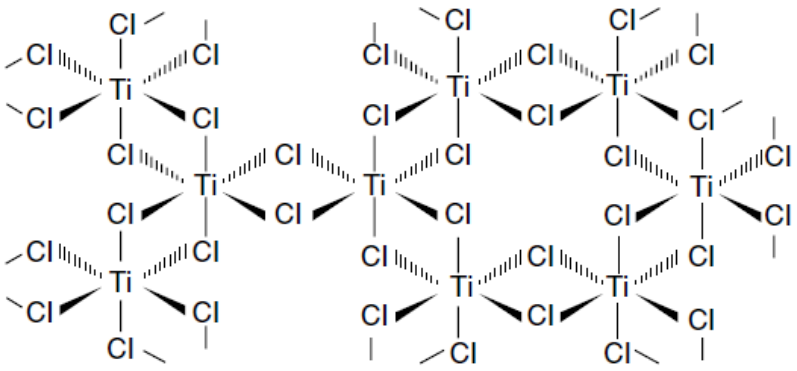

Figure 5.1 The structure of ZN catalyst (Soares and McKenna [1])

The ZN catalyst (Figure 5.1) requires a co-catalyst AlR_3 such as triethyl aluminum (TEAL), $Al(C_2H_5)_3$, for activation. A shown in Figure 5.2, the co-catalyst is used to alkylate the Ti salt to yield an active site. The catalyst and co-catalyst react in a series of reactions to form a complex. The co-catalyst extracts the chlorine atoms and transfer the alkyl group to the catalyst. Thus, the co- catalyst acts as a reducing agent and the electron-deficient site acts as the active site initiating the polymerization.

Figure 5.2 ZN catalyst mechanism

5.2 Ziegler-Natta Polymerization Kinetics

The most important reactions in the ZN kinetics are the same as in any polymerization kinetics, namely, the chain initiation, propagation and chain transfer reactions which can be with a monomer, hydrogen, or solvent. The ZN catalyst consists of different catalyst site types with each having its own relative reactivity, because of variations in the local chemical composition of each site type. The catalyst activation, deactivation and inhibition reactions are also specific to ZN catalyst. Site activation reactions convert potential sites to active sites, while site deactivation reactions convert active sites to dead sites. As discussed previously, Aspen Polymers builds the kinetic model in terms of repeating units or segments. All the main reactions in ZN kinetics are as follows.

5.2.1 Catalyst Activation (ACT)

The catalyst site activation step involves the generation of reactive vacant active sites from potential sites. There are several different site activation reactions included in the built-in kinetic scheme. They include site activation by co-catalyst, electron donors, hydrogen, monomer, and spontaneous site

activation. Different catalyst systems tend to be activated by a different subset of the reactions. The $TiCl_4$ catalyst is usually activated using TEAL co-catalyst or by spontaneous activation.

(1a) ACT-SPON: Spontaneous catalyst activation ($P_{0,i}$ is vacant site of type *i)*:

$$CAT_i \xrightarrow{k_{as,i}} P_{0,i}$$

(1b) ACT-COCAT: Catalyst site activation by cocatalyst:

$$CAT_i + COCAT \xrightarrow{k_{act,i}} P_{0,i}$$

(1c) ACT-H2: Catalyst site activation by hydrogen:

$$CAT_i + H_2 \xrightarrow{k_{acth,i}} P_{0,i}$$

5.2.2 Chain Initiation (CHAIN-INI)

Chain initiation involves the reaction of a monomer molecule at a vacant active site to form a live polymer molecule of one unit length at that site. This reaction converts a vacant active site to a propagation site.

(2) CHAIN-INI: Chain initiation by monomer (M) ($P_{1,i}$ is a propagation site of type *i* with an attached polymer chain containing one segment):

$$P_{0,i} + M \xrightarrow{k_{ini,i}} P_{1,i}$$

(2') CHAIN-INI: Chain initiation by monomer j (M_j) for copolymerization:

$$P_{0,i} + M_j \xrightarrow{k^j_{ini,i}} P^j_{1,i}$$

5.2.3 Chain Propagation (PROP)

The live polymer at each active site type grows or propagates through the addition of monomer molecules to form long polymer chains

(3a) PROP: Chain propagation by monomer (M):

$$P_{n,i} + M \xrightarrow{k_{p,i}} P_{n+1,i}$$

$P_{n,i}$ and $P_{n+1,i}$ are polymer chains of length *n* and *n* + 1 segments.

(3b) ATACT-PROP: Atactic propagation is a reaction considered in Aspen Polymers accounting for the formation of atactic polymer (see section 2.10.1 about tacticity and Figure 2.63), while the main propagation reaction represents the formation of all polymers including isotactic or atactic

$$P_{n,i} + M \xrightarrow{k_{pa,i}} P_{n+1,i}$$

$k_{pa,i}$ is the rate constant for atactic chain propagation at site type *i.* We define *the atactic fraction* by dividing the amount of polymer produced by atactic propagation by that produced by total propagation*:*

Atactic fraction = (rate of atactic propagation)/ (rate of total propagation)

It is not possible to determine the rate constants for chain initiation and propagation separately, because of the limited types of data measurements available from experiments. Therefore, we set the rate constant for ethylene or propylene monomer chain initiation equal to the rate constant for propagation of ethylene or propylene monomer on ethylene or propylene active segments. Likewise, we set rate constants for comonomer chain initiation equal to the rate constants for homopropagation of these monomers.

5.2.4 Chain Transfer Reaction (CHAT)

Chain transfer to monomer, solvent or chain transfer agent usually involves the extraction of hydrogen from the small molecule by the active site and leads to the termination of the live chain. At the same time, a new vacant site is formed which can undergo chain initiation to start polymerization.

(4a) CHAT-MON: Chain transfer to monomer ($k_{tm,i}^{jk}$ is the rate constant for chain transfer to a monomer of type *k* reacting with a growing chain transfer ending with a monomer unit of type *j* at site type *i*):

$$P_{n,i}^{j} + M_k \xrightarrow{k_{tm,i}^{jk}} D_n + P_{1,i}^{k}$$

(4b) CHAT-H2: Chain transfer to hydrogen (chain transfer to hydrogen generates a vacant site of type *i,* $P_{0,i}$. D_n is a dead polymer chain of length *n).*

$$P_{n,i} + H_2 \xrightarrow{k_{th,i}} D_n + P_{0,i}$$

(4b') CHAT-H2: Chain transfer to hydrogen for copolymerization (chain transfer to hydrogen and other transfer reactions generates a vacant site of type *i,* $P_{0,i}$. D_n is a dead polymer chain of length *n).*

$$P_{n,i}^{j} + H_2 \xrightarrow{k_{th,i}^{j}} D_n + P_{0,i}^{j}$$

5.2.5 Catalyst Deactivation (DEACT)

The catalyst site deactivation involves the deactivation of active sites, vacant and propagation, to form dead sites. The catalyst site deactivation can occur spontaneously or by agents like cocatalyst, electron donors, hydrogen, monomers, or poisons. Different catalyst systems tend to be deactivated by a different subsets of these reactions, but spontaneous catalyst deactivation is most common.

(5) DEACT-SPON: Spontaneous catalyst deactivation ($DCAT_i$ is deactivated catalyst site of type *i*. D_n is a dead polymer chain of n segments):

$$P_{0,i} \xrightarrow{k_{ds,i}} DCAT_i$$

$$P_{n,i} \xrightarrow{k_{ds,i}} D_n + DCAT_i$$

5.2.6 Catalyst Inhibition (INH)

Inhibited sites have small molecules such as hydrogen or poisons attached. As a result, inhibited sites are temporarily blocked from becoming propagation sites. The site inhibition reaction is reversible.

Therefore, the small molecule may dissociate from an inhibited site which then becomes a vacant site once again.

(6) FSINH-H2 and RFINH-H2: Forward and reverse catalyst Inhibitions by hydrogen ($ICAT_i$ is the inhibited catalyst of site type *i*):

$$CAT_i + xH_2 \xrightarrow{k_{finh,i}} ICAT_i$$

$$ICAT_i \xrightarrow{k_{rinh,i}} CAT_i + xH_2$$

5.2.7 Copolymerization Kinetics

Comonomers are used to produce polyolefins of varying densities. We assume that the rate of propagation of a monomer (or comonomer) depends only on the active segment (last monomer added to the chain) and the propagating monomer. This is commonly referred to as the terminal model for copolymerization kinetics.

(7) COMONOMER-PROP: For a system with two monomers, we write the propagation reactions as follows ($k_{p,i}^{jk}$ is the rate constant for propagation, associated with site type *i*, for a monomer of type *k* adding to a chain with an active segment of type *j*):

$$P_{n,i}^1 + M_1 \xrightarrow{k_{p,i}^{11}} P_{n+1,i}^1$$

$$P_{n,i}^1 + M_2 \xrightarrow{k_{p,i}^{12}} P_{n+1,i}^2$$

$$P_{n,i}^2 + M_1 \xrightarrow{k_{p,i}^{21}} P_{n+1,i}^1$$

$$P_{n,i}^2 + M_2 \xrightarrow{k_{p,i}^{22}} P_{n+1,i}^2$$

We note that the reaction rate constants listed in the chemical reactions above have the following standard Arrhenius form:

$$k = k_0 * e^{-\frac{E}{R}(\frac{1}{T} - \frac{1}{T_r})} \quad (5.1)$$

where k_o is the pre-exponential factor, E is the activation energy, R is the ideal gas constant, and T is the temperature of the reaction system and T_r is the reference temperature.

We discuss below our reasoning for including certain model reactions, and our simplification in ignoring other model reactions [1].

(1) Touloupidis [6] and Zacca and Ray [7] include the catalyst site activation by monomer (ACT-MON) and by electron donor (ACT-EDONOR) in their modeling studies. These reactions are available within the ZN kinetic model in Aspen Polymers when needed.

(2) Chain transfer to transfer agent (CHAT-AGENT), to solvent (CHAT-SOL), to co-catalyst (CHAT-COCAT), to electron donor (CHAT-EDONOR) follows a similar reaction to 4b, chain transfer to hydrogen (CHAT-H2). These reactions are available within the ZN kinetic model in Aspen Polymers. We ignore them as in references [4,5].

(3) Zhang et al. [9] include the beta-hydride elimination in their slurry HDPE modeling study. Soares and McKenna [1, p.162] state that this reaction produces metal hydride sites that are indistinguishable from those made by chain transfer to hydrogen. Therefore, it would be appropriate to consider only the reaction of chain transfer to hydrogen, without the reaction of beta-hydride elimination, as in references [4,5]

(4) After considering chain-transfer reactions, Touloupidis [6] includes site-transformation reactions that convert one vacant catalyst site type to another by means of specific reactions, such as transformation to hydrogen, to cocatalyst, to solvent and to poison, as well as spontaneous site transformation. Touloupidis further states that "site transformation reactions do not seem to play an important role, as they are rarely employed. Moreover, they pose difficulties on the way site transformation can be experimentally measured and validated" [6, p. 518]. Therefore, we ignore site-transformation reactions.

(5) As explained in reference [2], by adding hydrogen to polyolefin processes with ethylene as a monomer, the rate of polymerization decreases. We can model this effect by including the forward and backward catalyst site inhibition reactions because of hydrogen (FSINH-H2 and RFINH-H2). The rate constants of these inhibition reactions affect the polymer production rate. The Aspen Polymers model also calculates the equilibrium mole of inhibited catalyst sites (CISFRAC).

(6) In certain polyolefin systems such as HDPE [4], we may get a bimodal homopolymer from a single reactor. This is different from the bimodal copolymer produced in a reactor series for HDPE [9,10,11], PP [12,13] or LLDPE [14] because of the difference in the hydrogen concentrations of the two reactors in series. We can model this bimodal copolymer by the forward and reverse catalyst-hydrogen inhibition reactions (FSINH-H2 and RFINH-H2) [4]. The Aspen Polymers model also calculates the equilibrium mole fraction of inhibited catalyst sites (CISFRAC).

(7) Many HDPE [4,8, 9, 10, 11], PP [5, 12,13] and LLDPE [14] models include the reaction of spontaneous catalyst deactivation (DEACT-SPON). For PP, the tacticity control agent deactivates a portion of the catalyst sites that produces atactic polymer. We account for this by the reaction of catalyst deactivation by tacticity control agent (DEACT-TCA) [5]. The Aspen Polymers model also includes catalyst deactivation reactions by hydrogen (DEACT-H2), by cocatalyst (DEACT-COCAT), by

monomer (DEACT-MON), by poison (DEACT-POISON), and by electron donor (DEACT-EDONOR), as listed in [6]. In our workshops, we include DEACT-POISON and DEACT-H2 reactions.

5.3 Modeling Considerations

5.3.1 Reactor Types Chapter 4 of Soares and McKenna [1] describes the various types of reactors used for polyolefin processes, depending on the type of polyolefin, process technology and reactant phase. The most common reactors used in polyolefin processes are *stirred autoclave or continuous stirred tank reactor (CSTR), loop reactor, fluidized-bed reactor (FBR), and horizontal stirred-bed reactor (HSBR).* The modeling of the reactors requires certain assumptions.

Table 5.1 gives examples of common reactor types in commercial polyolefin processes. We can model the stirred autoclave reactors in the Mitsui slurry HDPE process [4,9,10] and in the DOWLEX solution LLDPE process [25] as continuous stirred tank reactors (CSTRs). Loop reactors are used in the Borstar slurry HDPE process [1, p. 120; 8, 11] as well as the Basell Spheripol [12,13; 1, p. 106] and Mitsui HYPOL [18,19] PP processes. In the modeling of a loop reactor when the recycle ratio is 30 or higher as calculated by Zacca and Ray [7], we can simulate the loop reactor as a CSTR. High recycle ratios give very low axial concentration gradient of the reactant and uniform temperature and residence time distribution (RTD) so that we can model a loop reactor as a CSTR. The loop reactors have a higher space-time yield and a high ratio of heat transfer per unit volume. Luo et. al. [18], Zheng [26], among others, have modeled the loop reactor series as CSTRs for PP production.

Table 5.1 Examples of Common Reactors for Producing Polyolefins

Polymer	**Stirred autoclave, or continuous stirred tank reactor (CSTR)**	**Slurry Loop Reactors (SLRs)**	**Fluidized-Bed Reactors (FBRs)**	**SLRs + FBRs**	**Stirred-Bed Reactors (SBRs)**
HDPE	Mitsui slurry process [4, 9, 10]			Borstar bimodal process [8, 11]	

PP		Loop reactor series [18,26]	Univation UNIPOL [27]	Basell Spheripol process [5, 12, 13], HYPOL process [19,20]	Innovene [5]
LLDPE	DOWLEX solution process [1, 25]	Loop reactor series [14]	Basell Spherilene [25], Univation UNIPOL [23]		

Fluidized-bed reactors (FBRs) are mainly used for gas-phase and mixed-phase processes, such as the Borstar bimodal HDPE [10,11], Basell Spheripol PP [12,13], Mitsui HYPOL PP [19,20], Basell Spherilene [25] and Univation UNIPOL [23] LLDPE processes. FBRs have a high overall conversion as well as high heat removal capacity. FBRs are mostly used as a finishing reactor for making copolymers in a series polyolefin process, as varying levels of comonomers can be added without any solubility issues. The high recycle ratios of the recycle gas lead to uniform temperatures and low concentration gradients in the FBRs, making it reasonable to model the FBR as a CSTR. Chen et al. [8] and Zhao et al. [11] have modeled the FBR as a CSTR in the finishing reactor for making bimodal HDPE.

The HSBR (horizontal stirred-bed reactor) has been used for gas-phase polymerization processes, such as the Innovene (formerly BP Amoco) PP process [5]. It has a plug-flow characteristic and can be used for fast grade change and making wide variety of products. We can simulate the HSBR as a series of CSTRs to approximate the RTD of the plug flow [5].

5.3.2 Process Flowsheets

Figures 5.3 to 5.8 illustrate the simplified flowsheets of several commercial polyolefin production processes that we use below to demonstrate our methodology for kinetic parameter estimation from plant data using simulation software tools.

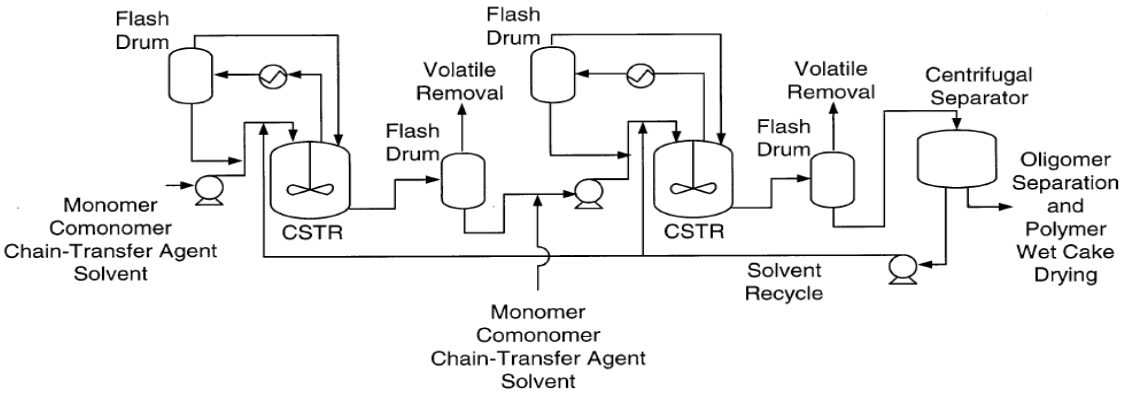

Figure 5.3 Mitsui slurry HDPE process: serial reactor configuration [4]

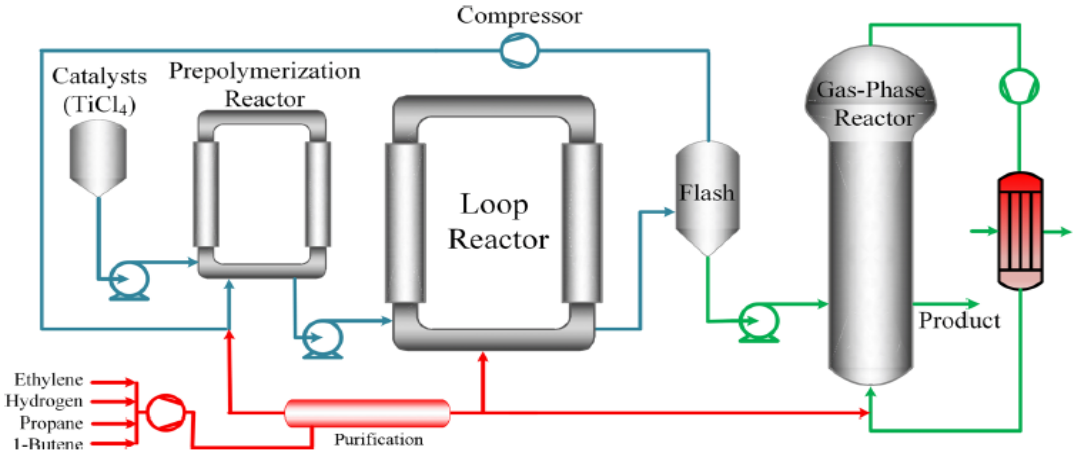

Figure 5.4 Borstar bimodal HDPE process with a prepolymerization reactor, a slurry loop reactor (SLR), a flash unit, and a finishing fluidized-bed reactor (FBR) [11].

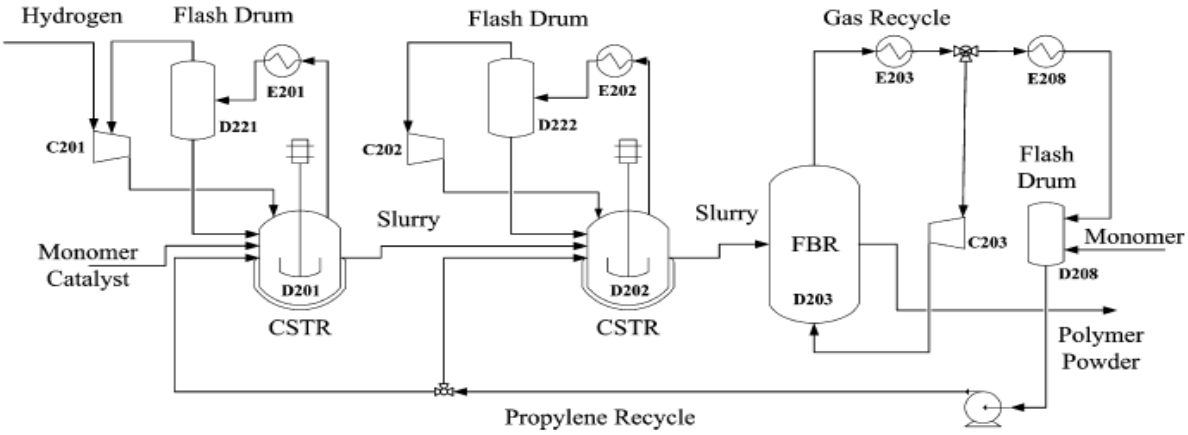

Figure 5.5 Polymerization section of the Mitsui HYPOL PP process: C201, C202 and C203- compressor; D201 and D202- slurry polymerization reactor (SLR); D203- fluidized-bed reactor (FBR); D221, D222, and D228- flash drum; E201, E202, E203 and E208- heat exchanger [20].

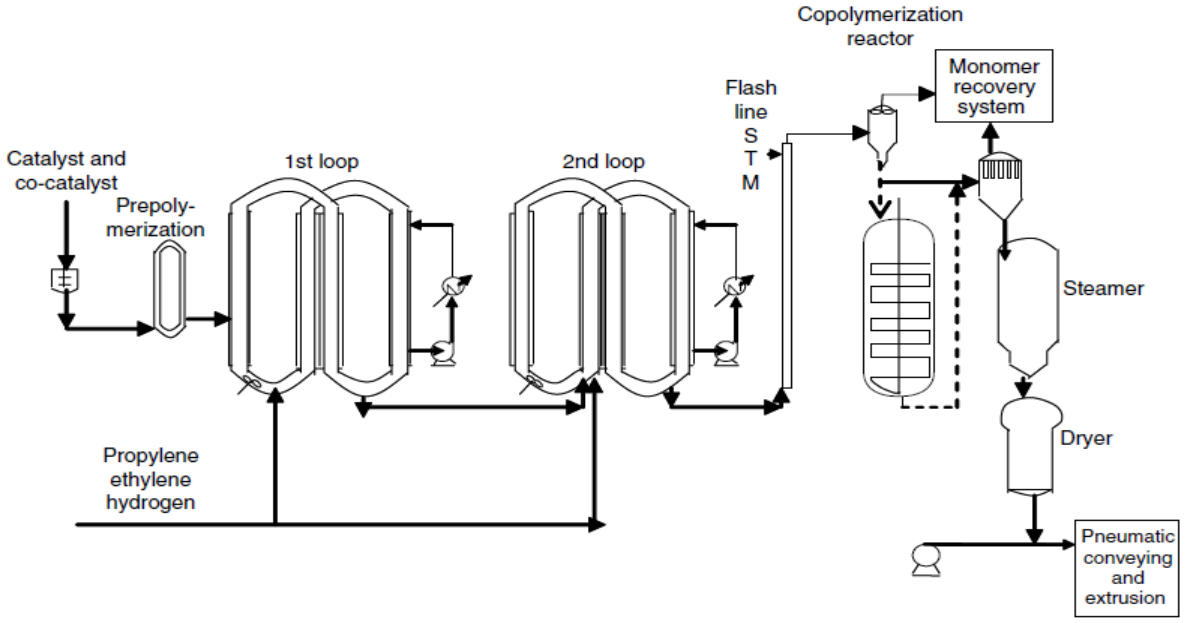

Figure 5.6 Basell Spheripol PP process using two slurry loop reactors (SLRs), followed by a flash unit and a fluidized-bed reactor (FBR) for copolymerization [1]

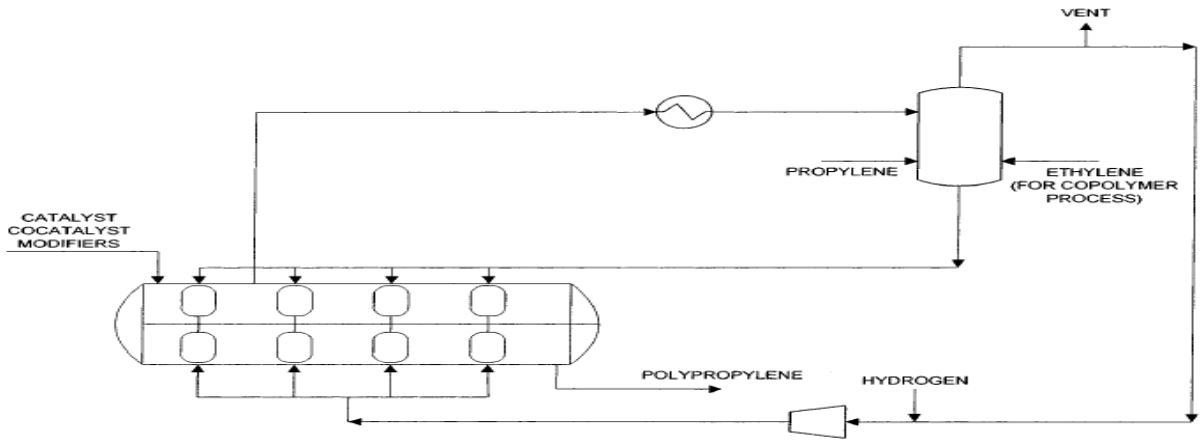

Figure 5.7. Innovene gas-phase PP process using a horizontal stirred-bed reactor [5].

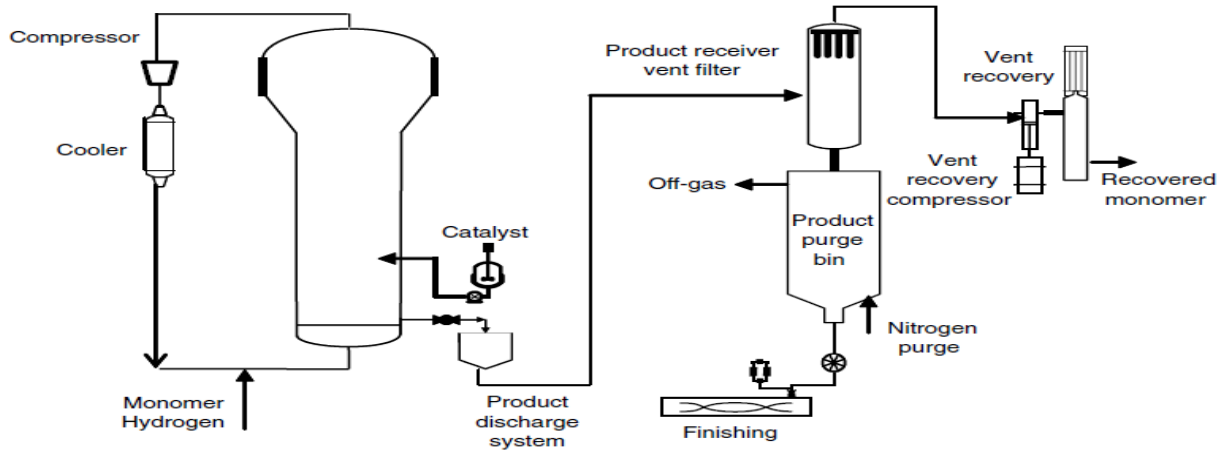

Figure 5.8 Univation UNIPOL LLDPE process using a fluidized-bed reactor [15]

5.3.3 Polymer Types

HDPE, PP and LLDPE are mostly made using ZN catalysts. The strategy for process modeling and kinetic parameter estimation does not change when considering different polymers. We only need to include certain reactions specific to the polymers. For HDPE processes, it is appropriate to consider the forward and reverse catalyst inhibition reactions by hydrogen (FSINH-H2 and RFINH-H2) since the rate of polymerization for ethylene polymer decreases with the addition of hydrogen. For PP processes, we may consider the atactic propagation reaction (ATACT-PROP), depending on the atactic content of the polymer. The atactic polymer is amorphous and has a low commercial value; it is desirable to have a high isotactic PP (see Figure 2.63).

5.3.4 Molecular Weight Distribution (MWD) and Multi-Modal Distributions

The MWD of the polymer can be unimodal or multi-modal, depending on the operating conditions. The kinetic estimation and modeling strategy remain the same whether the MWD distribution is unimodal or bimodal. The homopolymer MWD is usually unimodal.

For obtaining bimodal MWD in many polyolefin processes, the catalyst is exposed to two different operating conditions in a cascade of reactors. We can use two reactors in series to produce bimodal HDPE. The first reactor makes a low MWN HDPE with the help of a high hydrogen concentration, while the second reactor has a low hydrogen concentration producing a high-molecular-weight polymer. A comonomer alpha olefin is often added to make a copolymer. Chen et. al. [8] and Meng, et al. [10] have modeled the Borstar HDPE process to predict the bimodal MWD. In the Borstar process, the low-molecular-weight homopolymer is made in the slurry loop reactor (SLR) and the high-molecular-weight

copolymer is made in the FBR. There can be other reasons for obtaining a bimodal MWD apart from operating conditions if we obtain a bimodal MWD in a single reactor. The other reasons for bimodal MWD can be different types of reacting sites in the catalyst, inhibition of catalyst sites because of hydrogen or other poisoning and non-ideal mixing in the reactor [28].

5.3.5 Thermodynamics

Thermodynamics is an essential part of process modeling. The polymer perturbed-chain statistical fluid theory (POLYPCSF) is one of the most useful thermodynamic models for simulating polyolefin processes [5,28]. The POLYPCSF model is based on the perturbation theory. The underlying idea is to divide the total intermolecular forces into repulsive and attractive contributions. The model uses a hard-chain reference system to account for the repulsive interactions. The attractive forces are further divided into different contributions, including dispersion, polar, and association.

Another popular modeling of phase equilibrium in polyolefin processes is the Polymer Sanchez-Lacombe (POLYSL) equation of state [29, 30, 31]. It is based on the lattice theory, which states that fluids are mixtures of molecules and holes that are confined to sites in a lattice.

We refer our readers to Chapter 2 for the details of the POLYSL (Section 2.6) and POLYPCSF (Section 2.8) models, and the guidelines for the selection of thermodynamic models for polymer process simulation.

A correct thermodynamic model is very important in predicting certain commercial targets like the polymer solution density (not the polymer pellet density which depends on MWW and SCB content [10,17]). We use the polymer solution density to match the reactor residence time before estimating the kinetic parameters.

5.3.6 Global Kinetics versus Local Kinetics [32]

Reaction kinetics, like thermodynamics, are expected to be a global phenomenon. If the same catalyst is used in all the reactors, a good model should be capable of covering the full range.

Using different kinetics in different reactors significantly raises the degrees of freedom in the problem, which is already quite complex. We should instead treat the data from the different stages of the process as a sort of ‘natural experiment’ to further confirm a single set of rate parameters.

If we had samples after each stage, we could use the molecular weight distribution to further enrich our understanding of what is happening within the process.

We have seen projects where engineers have used different kinetics in different reactors, or different kinetics for different product grades. We have also seen in some cases of force-fitting the kinetics where the concentration of catalyst sites per unit mass of catalyst (*max sites*) is not realistic (outside of the range from 1E-5 to 1E-3 mole of sites per g of catalyst [4]), or the inhibition reaction and catalyst poisoning reaction rate constants may not be correct, resulting in the incorrect catalyst activity predicted by the model. We always consider these as symptoms of an imperfect model. Using local kinetic models may be 'over-fitting' the limited available data, which can lead to bad extrapolations away from the base-case conditions. Since the goal of modeling is usually to optimize the process to increase throughput, improve quality, or reduce energy consumption, it is important to be able to predict behavior outside the current operating envelope.

Additionally, when fitting a kinetic model, we should always use the reference temperature form of the kinetic expression, Eq. (5.1). This form makes the pre-exponential factor k_o and the activation energy E independent of each other at T_r. Otherwise, small changes to E overwhelm the data fitting of the k values and the fitting algorithm usually fails. We also find it easier to compare rate constants when they are on a consistent reference temperature basis.

5.4 Commercial Polyolefin Production Targets

The important commercial production targets for kinetic parameter estimation of polyolefin processes are as follows.

5.4.1 General Production Targets

5.4.1a. Production Rate: We use the mass flow rate of polymer within the outlet stream from each reactor for a process with reactors in series for kinetic parameter estimation. It is an essential production target for process modeling since the production rates are important when considering production rate expansion for a process. The propagation reaction determines the polymerization rate hence directly affects the production rate.

5.4.1b. MWN: The number-average molecular weight (MWN) of the polymer is an important target. MWN varies for different polymer grades. The reaction rate constants for chain transfer to H_2 (CHAT-H2) and to monomer (CHAT-MON) significantly affect the molecular weight of the polymer since the reactions lead to breaking growing polymer chains and forming the dead polymer chains.

5.4.1c. MI: In the literature, most empirical correlations for polyolefin MI with broad MWD or large PDI are based on the weight-average molecular weight (MWW). For example, a general MI correlation with MWW is in the form of [15,16]:

$$MI = a\ (MWW)^{-b} \qquad (5.2)$$

where a and b are correlating parameters. For PP, the MI may depend on the MWW as well as the atactic fraction (ATFRAC), calculated by the atactic chain propagation reaction (ATACT-PROP) [3].

5.4.1d. Conversion: The conversion percentages of the monomer and the comonomer are required to determine the yield of the process.

5.4.1e. PDI: The polydispersity index is the ratio of the weight-average molecular weight to the number-average molecular weight, MWW/MWN. It is an important polyolefin property. It is measured by performing gel permeation chromatography (GPC) of the polyolefin sample obtained at the product outlet or at each reactor outlet in a process with reactors in series.

5.4.1f. SMWN and SPFRAC: SMWN represents the number-average molecular weight produced at each active catalyst site. SPFRAC is the weight fraction of polymer produced at each active site. They are determined by deconvolution of the polymer GPC curve and are required for estimating individual site-specific kinetic parameters. See Section 5.5.2.3.

5.4.1g. SFRAC and SCB: SFRAC is the mole fraction of segments of the comonomer and is usually determined by the short chain branching distribution (SCBD). The use of online Fourier transform infrared spectroscopy (FTIR) with gel permeation chromatography (GPC) permits the detection of the SCB as a function of the MWW [17]. We use this simulation target to predict the comonomer content in the copolymer. SFRAC depends on the comonomer kinetics.

5.4.1h. Rho: The polymer density is usually measured for the pellets and correlated as a function of the MWW. For copolymerization, we often correlate the polymer density as a function of mole fraction of the comonomer and the MWW [10, 17]. In reference [10], the HDPE density obtained from ethylene copolymerization with comonomer 1-butene follows the following correlation:

$$\rho = (\ 1 - 0.009165\ \mathrm{xB}^{0.148895}) \times [1.137247 - 0.014314 \ln (MWW)] \qquad (5.3)$$

where xB is the mole fraction of 1-butene. In reference [16], we see an example of correlating the polymer density to MWW and SCB content for a bimodal HDPE copolymer process:

$$\rho = 1.0748 - 0.0241 logMWW - 0.01145\left(\frac{\sum_{j=1}^{N} m(j)SCB(j)w_{logMWW}(j)}{\sum_{j=1}^{N} m(j)w_{logMWW}(j)}\right)^{0.47332} \quad (5.4)$$

where m(j) is mass fraction of polymer formed at active site j, SCB(j) is the average short chain branching in copolymer formed at active site j, and $w_{logMWW}(j)$ is the weight chain length distribution of the polymer formed at active site j.

5.4.1 Residence Time: This refers to the reactor residence time. It can be the residence time of each reactor in a process with a series of reactors. It is an important target affecting the polymer properties. The residence time is dependent on the polymer solution density, which depends on the thermodynamic property parameters.

5.4.2 Polymer-Specific Targets:

5.4.2a. CISFRAC: It is the ratio of the moles of the inhibited catalyst sites to the total number of moles of the catalyst sites. It may be considered as a target for HDPE process when catalyst inhibition reactions are considered.

5.4.2b. ATFRAC: It is the ratio of the atactic propagation to the total propagation. It is a commercial target for atactic PP production.

Table 5.2 gives examples of production targets for kinetic parameter estimation for modeling commercial polyolefin processes from plant data.

Table 5.2 Examples of production targets for kinetic parameter estimation for modeling commercial polyolefin processes from plant data

Polymer [reference]	**Prod. rate**	**MWN and MI**	**Conv**	**SFRAC**	**PDI**	**Rho**	**SMWN and SPFRAC**	**Res. time**	**Polymer specific**
HDPE, Khare et a. [2]	✓	✓	✓	✓	✓	✓	✓	✓	✓
HDPE, Chen et al. [8]	✓	✓		✓	✓	✓	✓	✓	

HDPE, Zhang et al. [9]	✓	✓		✓	✓		✓		
HDPE, Meng et al. [10]	✓	✓		✓	✓	✓	✓	✓	
HDPE, Zhao, et al. [11]	✓	✓	✓		✓	✓	✓	✓	✓
PP, Khare, et al. [5]	✓	✓	✓	✓	✓		✓	✓	✓
PP, Zheng et al. [12]	✓	✓		✓	✓	✓	✓		
PP, Luo et al. [18]	✓	✓	✓		✓	✓	✓	✓	
PP, You and Li [19]	✓	✓	✓	✓	✓		✓	✓	
PP, Luo et al. [20]	✓	✓		✓	✓		✓	✓	
PE, Kou et al. [21,22]	✓	✓			✓				
LLDPE, Touloupidis et al. [14]	✓	✓			✓		✓		
LLDPE, Kashani at el. [23]	✓	✓			✓		✓		

We conclude this section, noting two points.

(1) Not all production targets are fully independent of each other. As an example, MI typically depends on MWW for most polyolefins, and depends on atactic fraction (ATFRAC) for PP. In our simulation, we use a FORTRAN ("Calculator") block to calculate the MI based on a correlation developed from past plant data using MWW and compare the calculated MI value with the current plant data. If the resulting deviation between the calculated and measured MI values is not acceptable, we would

fine-tune the simulation parameters for better MWW predictions, and possibly update the MI-MWW correlation with new plant data.

(2) Not all suggested production targets in reported modeling studies have the relevant plant data for model validation. Depending on the intended purposes for using the resulting simulation model and the accuracy requirements of model predictions, the model developers must decide if they wish to make a serious effort to collect plant data of certain production targets for validating the simulation model. Alternatively, they could use available data of relevant process variables or the values of simulation output variables as independent variables to develop soft sensors or inferential models (such as those based on neural networks [24]) for production targets (e.g., MI and ATFRAC) that are not routinely measured.

5.5 Methodology for Polyolefin Kinetic Estimation

Table 5.3 summarizes the important commercial production targets that we have considered for kinetic parameter estimation. The number of targets that can be used for estimation depends on the data availability. In our strategy estimating kinetic parameters, we first try to match some production targets in a single catalyst site model, and we fit the remaining targets after converting the single-site model into a multisite model. In this procedure, we consider the rate constants for all the reactions involved in the ZN polyolefin kinetics, including catalyst activation, initiation, propagation, chain transfer, deactivation and other polymer-specific reactions. The kinetic rate constants follow the Arrhenius form given in Eq. (5.1). As mentioned in Section 4.4.8, for polyolefin reactors operating in a small temperature range, we only estimate the pre-exponential factor k_o and keep the activation energy E constant with values from the literature. Our methodology for kinetic parameter estimation does allow us to estimate the activation energy if necessary.

Table 5.3 Production targets for single-site and multisite models

Single-Site Targets	**Multisite Targets**
Production Rate	PDI of polymer
MWN overall	MWN produced at catalyst site
Monomer Conversion	Mass fraction for polymer produced at each site
Comonomer Conversion or SFRAC	Atactic fraction ATFRAC for each site for PP
Polymer solution density	Catalyst site inhibition fraction CISFRAC for each site for HDPE
Residence time	Rho /Polymer pellet density
Atactic fraction ATFRAC for PP	

5.5.1 Efficient Use of Software Tool: Data Fit

We develop models using Aspen Polymers and fit the kinetic parameters to plant data using the data fit tool, previously introduced in Chapter 3. Data fit is an efficient nonlinear regression tool that allows the user to determine statistically acceptable, kinetic parameters from constant, time-varying, or temperature-dependent laboratory measurements, or from matching the process simulation to plant targets. We can use point data or time-profile data for regression. We need to define the data with reconciled input variables and a standard deviation. We estimate the model parameters using the data within the specified range. We refer the reader to Section 3.8 for more discussion of the principle of data fit and will illustrate its application in Section 5.5.2.1 below.

5.5.2 Flowchart of the Methodology for Kinetic Parameter Estimation

Figure 5.9a shows our methodology for estimating kinetic parameters for polyolefin process models from plant data using simulation software tools, and Figure 5.9b shows an expanded version of the methodology. In the following, we discuss the details of the algorithm and present illustrative applications to commercial polyolefin processes. We also give some useful suggestions based on our experiences in guiding practicing engineers to apply the methodology to several dozen commercial HDPE, PP, LLDPE and EPDM processes in the Asia-Pacific.

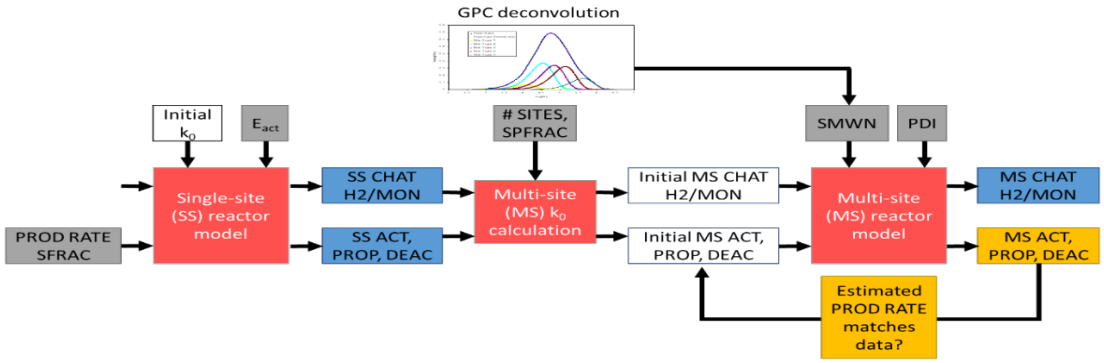

Figure 5.9a. The methodology for kinetic parameter estimation for polyolefin process models from plant data using simulation software tools.

Single-Site

Use data fit to regress reaction rate constants for ACT-SPON, ACT-COCAT, ACT-H2, PROPAGATION, and DEACT-SPON to match production rate, monomer and comonomer conversions, and monomer mole fraction in the copolymer product (SFRAC). Adjust max. sites parameter to match production rate if needed.

Multi-Site

GPC deconvolution to calculate n, SPFRAC and SMWN

Calculate the values of the multi-site reaction rate constants for ACT-SPON, ACT-COCAT, ACT-H2, CHAIN-INI, PROPAGATION, CHAT-MON, CHAT-H2 and FSINH-H2 and RFINH-H2 from single-site and deconvolution results using equations (5.6) to (5.9). Assume the same rate constant values for DEACT-SPON for the multi-sites as calculated from single site.

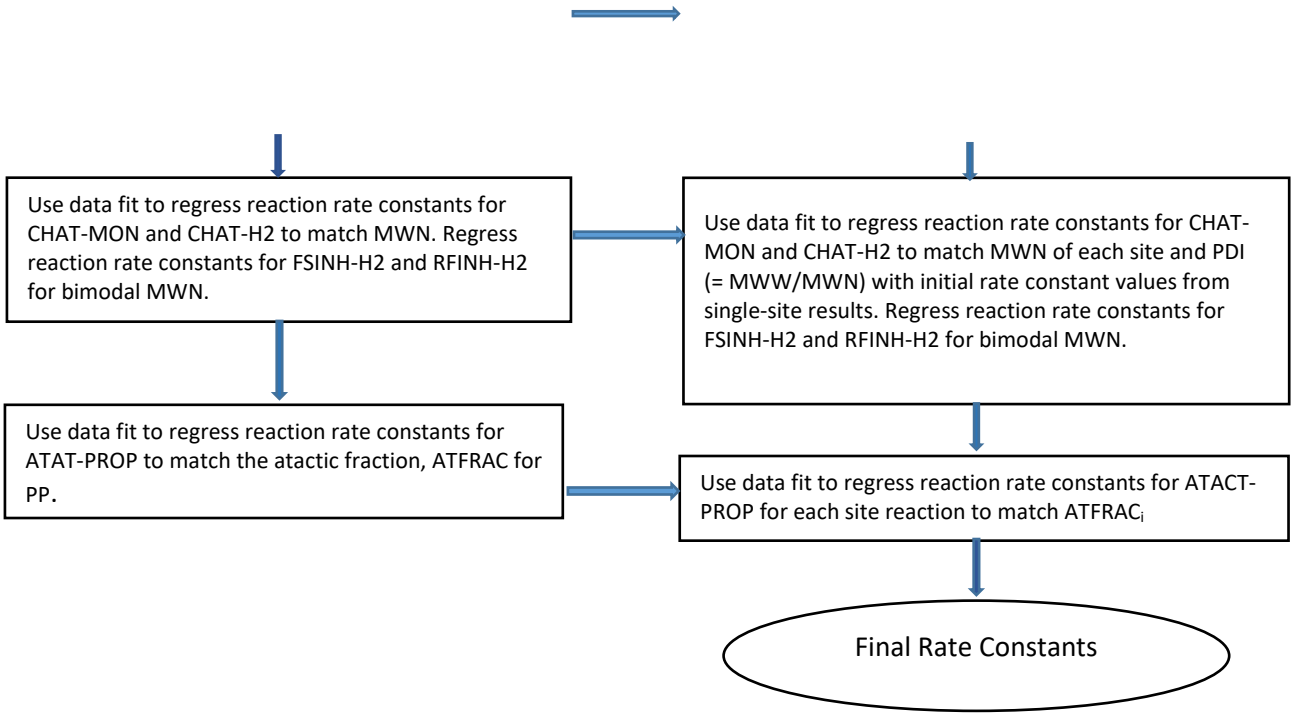

Figure 5.9b. An expanded version of the methodology for kinetic parameter estimation for polyolefin process models from plant data using simulation software tools.

5.5.2.1 Multiple Product Grades and Single Active Catalyst Sites

We first make a single-site model and try to estimate the kinetic parameters based on single-site production targets for multiple product grades. Using the production rate data for multiple grades, the data fit tool enables us to *simultaneously* regress the reaction rate constants for catalyst activation (ACT-SPON, ACT-COCAT, and ACT-H2), propagation (PROPAGATION) reactions for monomer, and deactivation (DEAC-SPON) reactions, and any inhibition (FSINH-H2 and RSINH-H2) reactions if considered. This is different from most of the previous studies, including our previous work [4,5], which *sequentially* estimate these reaction rate constants.

Before matching the production rates, we must ensure that the residence time matches plant data. We can adjust the PC-SAFT thermodynamic parameters and change the mixing model equation to adjust the polymer solution density. The residence time of the reactor depends on the solution density.

We estimate the rate constants for propagation (PROPAGATION) reactions for the monomer using the production rate for the homopolymer and monomer conversion. We use the production rate for the copolymer and the ratio of the reaction rates of comonomer to monomer (SFRAC) or conversion of comonomer to estimate the rate constants of the propagation reactions for the comonomer.

For PP, we need to ensure that the isotacticity of the homopolymer matches the plant data. We do so by including the atactic propagation (ATACT-PROP) reaction and estimate the rate constant using the atactic fraction (ATFRAC), which is the ratio of the atactic polymer formed over the total polymer. We want the calculated ATFRAC to be close to [1 – isotacticity/100].

For HDPE, we also consider the inhibition of the catalyst because of the polymers since the rate of polymerization decreases with hydrogen concentration for ethylene-based polymer reactions. We usually estimate the forward inhibition and backward inhibition (FSINH-H2 and RSINH-H2) reactions using the MWN. In the single-site model, we can also match the weight-average molecular weights and use them to estimate the rate constants of chain transfer to hydrogen and monomer/comonomer.

Depending on data available, the melt index of polymer is also useful in matching the molecular weight of polymer. Melt index is usually a function of weight-average molecular weight (MWW), but for the case of polypropylene homopolymer, it is also a function of atactic fraction (ATFRAC). Section Section 2.10.1.

In case SFRAC and comonomer content data are not available, we may use the final polymer pellet density to estimate the comonomer propagation rate constants, as the polymer density depends on the SCB and comonomer content.

Table 5.4 shows the major kinetic parameters that significantly affect the single-site production targets.

Table 5.4. Major kinetic parameters affecting the single-site production target

Single-Site Target	**Major Kinetic Parameters Affecting the Target**
Production Rate	Max sites parameter, propagation rate constant, catalyst activation, inhibition reaction
MWN overall	Chain transfer reactions –monomer and H2
Monomer conversion	Monomer propagation rate constant
Comonomer conversion or SFRAC	Comonomer propagation rate constant
Reactor residence time	Polymer solution density and thermodynamic property parameters
ATFRAC	Atactic propagation rate constant
Melt Index	Chain transfer reactions and ATFRAC
Polymer pellet density	Comonomer content/comonomer propagation rate constants

We illustrate the application of the methodology to estimating the kinetic parameters for modeling a commercial Mitsui HYPOL PP process. ***Supplement 5.1*** [3] gives details of six polyolefin process

modeling examples, including the process description, polymerization reactions, production targets, estimated rate constants, sensitivity analysis, model validations, etc.

We demonstrate below the efficient use of data fit tool for the *simultaneous* estimation of kinetic parameters.

Table 5.5 lists the plant data for single-site modeling for a commercial Mitsui HYPOL PP process of Figure 5.5, and Figure 5.10 shows an Aspen Polymers simulation flowsheet of the process with the addition of one more fluidized-bed reactor, D204.

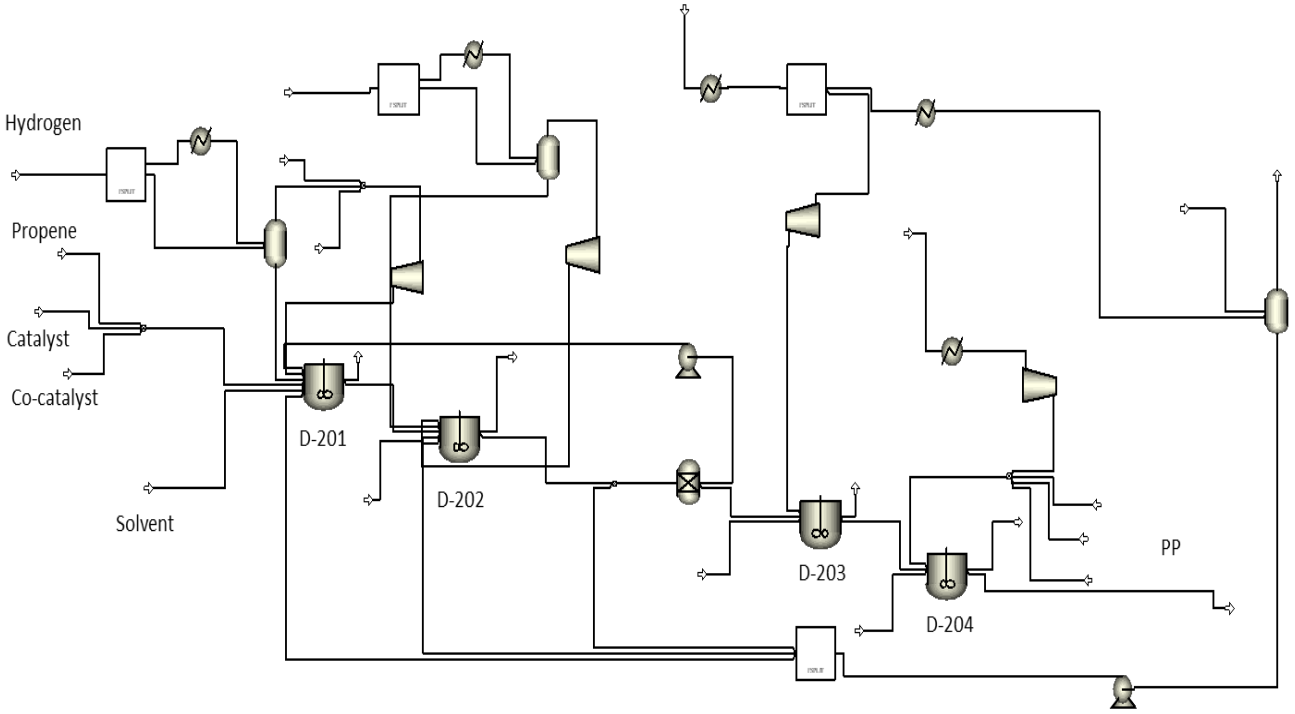

Figure 5.10 An Aspen Polymers simulation flowsheet of the Mitsui HYPOL PP process.

Table 5.5 Plant data for kinetic modeling a commercial Mitsui HYPOL PP process [33]

			Grade 1	Grade 2
Dataset	**Process parameters**	**Reactor**	**Production target**	Production target
PROD123	Polymer production rate (kg/hr)	D-201	1560	1560
		D-202	3120	3120
		D-203	6240	6240
PROD4		D-204	8600	8600

MWN123	Number-average molecular weight (MWN)	D-201	60000	76000
		D-202	63000	83000
		D-203	77000	88000
MWN4		D-204	80000	96000
SFRAC4	Ethylene content in copolymer, mole fraction	D-204	0.145	0.15
PDI	Polydispersity index	D-201	5.50	5.60
		D-202	5.52	5.70
		D-203	5.54	5.80
		D-204	6.00	6.20
H2/C3H6 mole ratio x 10E3	H2/monomer mole ratio in reactor overhead	D-201	188	17
		D-202	209	9.3
		D-203	15	1.7

To simplify the kinetic parameter estimation, we begin by setting some kinetic parameters to be equal. For example, we make the pre-exponential factors for propagation (PRPRE-EXP) from ethylene segment (C2-SEG) and from propylene segment (C3-SEG) to ethylene comonomer (C2H4) equal. Therefore, we use a Calculator (FORTRAN block) to make PRPRE-EXP PROPAGATION (C2-SEG/C2H4) equal to PRPRE-EXP PROPAGATION (C3-SEG/C2H4). ***Supplement 5.1a*** gives additional details about this simplification.

Our data fit application includes the *simultaneous* execution of two regression runs for the first three reactors D201 to D203, and a regression run for the fourth reactor, D204 that focuses on copolymer production. First, *regression run RPROD123* varies the pre-exponential factors for spontaneous site activation (ACT-SPON), catalyst activation by cocatalyst (ACT-COCAT), propagation (PROPAGATION) reactions for monomer, and deactivation (DEAC-SPON) reactions, to match dataset *PROD123* listed in Table 5.6. Next, *regression RMWN123* varies the pre-exponential factors for chain transfer of propylene segment and of ethylene segment to H2 and to propylene monomer to match dataset *MWN123.* Lastly, *regression RD204* varies the pre-exponential factors for chain propagation of propylene segment and from ethylene segment to comonomer C2H4, and chain transfer from propylene segment and from ethylene segment to comonomer C2H4, to match the datasets *PROD4, MWN4 and SFRAC4*.

Table 5.6 demonstrates that the data fit tool enables us to accurately estimate the kinetic parameters for the single-site model that have the most impacts on specific production targets (see Table 5.4) for the Mitsui HYPOL PP process. The comparison between model predictions and production targets shows minimum errors of 0.37% to 3.22%.

Table 5.6. Comparison of single-site model predictions with production targets obtained by data fit

	Grade one			**Grade two**		
Polymer production, kg/hr	**D201**	**D202**	**D203**	**D201**	**D202**	**D203**
Plant data	1560	3120	6240	1560	3120	6240
Prediction	1541	3153	6151	1538	3211	6236
% Error	1.18%	0.76%	0.83%	2.17%	2.39%	0.37%
0.37%	**D201**	**D202**	**D203**	**D201**	**D202**	**D203**
Plant data	60000	63000	70000	80000	83000	88000
Prediction	61797	61511	68598	80547	82693	85167
% Error	3.06%	2.36%	2.00%	0.68%	0.37%	3.22%
	D204 Production, kg/hr	**D204 MWN**	**D204 SFRAC, mole fraction**	**D204 Production, kg/hr**	**D204 MWN**	**D204 SFRAC, mole fraction**
Plant data	8600	80000	0.145	8600	96000	0.150
Prediction	8812	78004	0.142	8730	95099	0.152
%Error	2.45%	2.49%	1.80%	1.51%	0.94%	1.60%

5.5.2.2 Multisite Model and Deconvolution Analysis

We now convert our single-site model into a multisite model by changing the specified number of sites in the model. We then make use of the gel permeation chromatography (GPC) analysis of the polymer samples.

Using the GPC characterization data, we apply the deconvolution procedure first presented by Soares and Hamielec [34]. We deconvolute the MWD to determine the most probable chain length distribution (CLD) for each active catalyst site. We assume that the CLD of the polyolefins produced by each active site of ZN catalyst follows the Flory distribution.

We represent the instantaneous weight chain length distribution (WCLD) by averaging the distribution of each catalyst site in Eq. (5.5)

$$\mathrm{W[logM]} = \sum_{i=1}^{n} w_i (2.30268 \times M^2 \, \tau_i{}^2 e^{-M \tau_i}) \qquad (5.5)$$

In the equation, $\mathrm{W[logM]}$ is the mass fraction of the chains of polymer having molecular weight M in logarithmic scale; *n* is the total number of active sites; w_i is the mass fraction of polymer formed at each site *i*; τ_i is the fitting parameter for each site *i,* which is equal to the inverse of the number-average molecular weight of polymer formed at each site, that is, τ_i = 1/MWN$_i$. Here, w_i and MWN$_i$ are equivalent to the production targets SPFRAC and SMWN defined previously.

5.5.2.3 GPC Data and Deconvolution Analysis to Estimate the Number of Active Catalyst Sites

Gel permeation chromatography is a method of characterization used to determine the molecular weight distribution of a polymer. A polymer sample travels down a tube containing a porous gel. The longer polymer chains reach the end of the tube relatively quickly, while the shorter chains take longer because they become trapped in the pores of the gel. Data collection consists of time of elution versus molecular weight. These data yield a curve for the molecular weight distribution.

We fit the model in equation (5.5) to the experimental GPC data and estimate the parameters by minimizing the difference between the model and experimental values. We estimate the minimum number of Flory distributions, *n*, required to describe the experimental MWD, which in turn gives the minimum number of active catalyst sites. We also estimate the MWN of polymer produced at each active catalyst site, MWN$_i$ and the mass fraction of polymer produced at each active site, w_i.

Supplement 5.2, "An Illustration of Using Deconvolution Excel Spreadsheet", gives an Excel spreadsheet and a detailed illustrative example for implementing the deconvolution of GPC data of MWD that our readers may download for use in their polyolefin processes. This supplement illustrates the procedure to develop the deconvolution results summarized in Table 5.7 from a homopolymer MWD from a UNIPOL LLDPE process. ***Supplement 5.1e*** presents details of our kinetic model and kinetic parameter estimation, including the reaction rate constants chosen and their initial values for this slurry HDPE process. Section 5.8.5 gives another example of using the deconvolution Excel spreadsheet to determine the number of active catalysts for sites from GPC data from a commercial LLDPE process.

Figure 5.11 plots the weight chain length distribution as given in equation (5.5) for the example of Table 5.7. The figure shows the weight chain length distribution for each catalyst active site and distribution of

the plant data. The sum of the three individual distributions of the catalyst site weighted with the mass fraction of polymer formed for each site predicts the chain length distribution of the polymer.

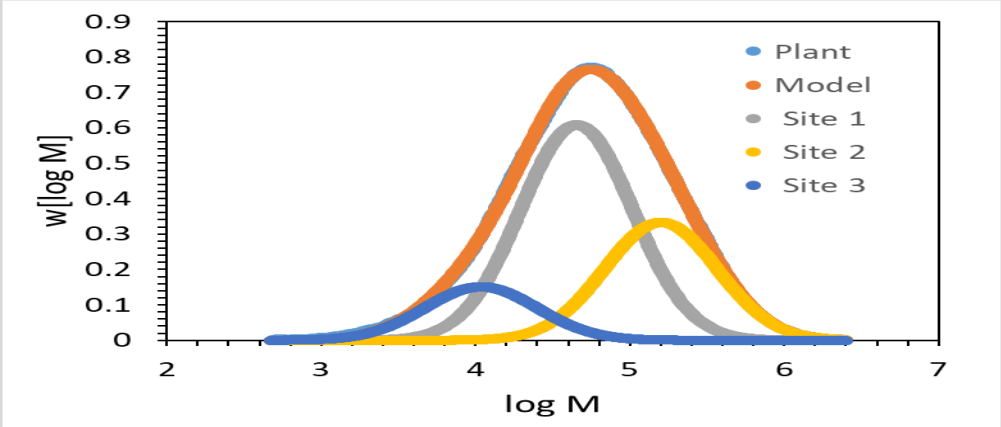

Figure 5.11. GPC deconvolution of a homopolymer sample from a UNIPOL LLDPE process

We use the rate constants from single-site modeling and the deconvolution results of Table 5.8 to further calculate the rate constants for the multi-site kinetics. We calculate the pre-exponential factors for catalyst activation reactions (ACT-SPON, ACT-COCAT and ACT-H2) at each site k_{ai} from the single-site value k_a,

$$k_{ai} = \frac{k_a}{n} \tag{5.6}$$

Eq. (5.6) results from the fact that the concentration of potential catalyst sites is identical for both single-site and multisite models, but the concentration of vacant catalyst sites must be divided by the number of site types, *n*. We resolve this issue by dividing the pre-exponential factors for catalyst activation reactions by the number of catalyst site types, *n* [3].

We estimate the pre-exponential factor for the chain initiation reaction (CHAIN-INI) at each site by

$$k_{ii} = k_i * w_i * n \tag{5.7}$$

We calculate the pre-exponential factor for the propagation reaction (PROPAGATION) at each site by

$$k_{pi} = k_p * w_i * n \tag{5.8}$$

Equations (5.6) to (5.8) give the actual values of the activation, chain initiation and propagation rate constants for the multisite model directly. Based on our modeling experience with polyolefin processes, we find that further data fit runs that vary these reaction constants, obtained from applying equations

(5.6) to (5.8), to match the relevant datasets for production rate, MWN, SFRAC, etc. within the multisite model, would produce only minimum or no changes to the reaction rate constant values.

We calculate the initial value for pre-exponential factor for the chain transfer reaction (CHAT-MON and CHAT-H2) at each site by

$$k_{ci} = k_c * w_i * n \tag{5.9}$$

It is important to maintain the same relative contributions of chain transfer to hydrogen (CHAT-H2) and to monomer (CHAT-MON) from the same single-site model in the multisite model, to preserve the sensitivity of these reactions to the concentrations of hydrogen and monomer [3]. We do this by using a Calculator (FORTRAN block) in Aspen Polymers.

To estimate the rate constants for chain transfer to H2 and to monomer for each site, we regress the PDI and MWN data for the polymer stream exiting each reactor, along with the SMWN results from GPC analysis. For more accurate estimates of these kinetic parameters, it is helpful to have these data obtained with varying H2 and monomer flow rates. In the example presented in Tables 5.5 and 5.8, we use the measured PDI and MWN data for the polymer stream exiting each reactor to estimates the chain transfer rate constants. We should also make sure that measured MWD matches the model MWD by matching the SMWN and SFRAC values obtained from GPC analysis.

The other rate constants, such as the deactivation rate constants (DEACT-ACT and DEACT-TCA), and inhibition reactions (FSINH-H2 and RSING-H2), are all identical to those of the single-site model. If we consider the catalyst inhibition reactions (FSINH-H2 and RSING-H2), we must ensure that the total CISFRAC for the multisite model is the sum of $CISFRAC_i$ for all single sites. Also, for the PP model, the ATFRAC considered should be the same for each site and matching the plant data. After updating all the rate constants, the multisite model matches all the targets.

We continue to demonstrate our methodology for kinetic parameter estimation for multi-site model for the Mitsui HYPOL PP process of Figure 5.5 and ***Supplement 5.1a*** that we presented previously in Tables 5.5 and 5.6 in Section 5.6.2.1. In the supplement, we see that the deconvolution analysis of GPC data gives 4 active catalyst sites for the process.

To simplify the kinetic parameter estimation, we begin by setting some kinetic parameters to be equal. We make the pre-exponential factors for chain transfer (CTPRE-EXP) from ethylene segment (C2-SEG) and from propylene segment (C3-SEG) to propylene monomer (C3H6) and to ethylene comonomer

(C2H4) equal. Therefore, we use a Calculator (FORTRAN block) to make PRPRE-EXP CHAT-MON (C2-SEG/C3H6) equal to PRPRE-EXP CHAT-MON (C3-SEG/C3H6) and make PRPRE-EXP CHAT-MON (C2-SEG/C2H4) equal to PRPRE-EXP CHAT-MON (C3-SEG/C2H4). We can see the pre-exponential factor and activation energy values for these reaction rate constants in Section A6 of ***Supplement 5.1a***.

We apply data fit to execute a *regression run RPDI* that varies the reaction rate constants for chain transfer to hydrogen (CHAT-H2) and to monomer C3H6 and comonomer C2H4 (CHAT-MON) in order to match the dataset *PDI* (and hence the MWW data) given in Table 5.5 from reactors D201 to D204 for two grades with different H2/C3H6 ratios in the reactor overheads. Section A6 of **Supplement 5.1a** shows the resulting reaction rate constants for the multisite model, and we note that the resulting pre-exponential factors for chain transfer to hydrogen and to monomer are indeed different. Table 5.8 compares minimum errors between the model predictions and plant data for PDIs. We note the percent errors between our model predictions and plant data in Table 5.6 (0.37% to 3.06%) and Table 5.8 (0.25% to 1.84%) are equivalent to or smaller than those in reported modeling studies for polyolefin processes (approximately 5% in our previous work for HDPE [2] and for PP [3]).

Table 5.8. Comparison of multi-site model predictions with production targets obtained by data fit

	Grade one				**Grade two**			
PDI	D-201	D-202	D-203	D-204	D-201	D-202	D-203	D-204
Plant data	5.50	5.52	5.54	6.00	5.60	5.70	5.80	6.20
Model Prediction	5.48	5.50	5.64	5.95	5.62	5.67	5.76	6.26
Error %	0.25%	0.37%	1.84%	0.67%	0.33%	1.42%	0.68%	1.03%

Table 5.9 shows the different reaction constants that have the major effect on the production targets in a multisite model. We can use sensitivity analysis as described in Section 5.6.3 to quantify the effect of varying kinetic parameters on the simulation targets.

Table 5.9. Major kinetic parameters affecting the multi-site simulation targets

Multisite Targets	**Major Affecting Kinetic Parameters**
1. PDI of polymer	Chain transfer reaction rate constant

2. MWN produced at catalyst site and overall MWN	Chain transfer reaction rate constant for each site
3. Mass fraction for polymer produced at each site and overall production rate	Propagation reactions for each site
4. ATFRAC for each site	Atactic propagation reaction rate constant
5. Polymer solution density	Comonomer rate constants

5.5.3 Efficient Use of Software Tools: Sensitivity Analysis

Sensitivity analysis enables us to quantify the dependence of the production targets on the reaction kinetic parameters. The analysis helps us in deciding which directions to vary the operating conditions to match the production targets. Sensitivity analysis also helps in validating the kinetic estimation procedure for polyolefins. We illustrate below some examples of sensitivity analysis of the different polyolefin processes that we have modeled and estimated kinetics using our procedure.

Supplement 5.1e gives details of our kinetic model and kinetic parameter estimation, including the reaction rate constants chosen and their initial values for the Unipol LLDPE process of Figure 5.8. Applying the sensitivity analysis, we illustrate in Figure 5.12a how varying the reaction rate constant for chain transfer to hydrogen, $k_{th,i}$ of just one of the three active site affects the final LLDPE polymer properties, including the polydispersity index PDI, the number-average molecular weight at the chosen catalyst site SMWN, and the overall MWN. As we increase the reaction rate constant for chain transfer to hydrogen, both the SMWN and MWN decreases, while the PDI increases gradually. In other words, we can vary the hydrogen flow rate to change the rate of chain transfer reaction to achieve the desired MWN and PDI.

As another example, for the Mitsui Hypol PP process of Figure 5.5 and ***Supplement 5.1a***, Figure 5.12b illustrates that varying the reaction rate constant for chain transfer to monomer, $k_{tm,i}$ results in similar trends of changes in PDI, SMWN and MWN, as with the chain transfer to hydrogen. The similar trends observed in Figures 5.12a and 5.12b and in Figures 5.13a-5.13b and Figure 5.14a-5.14b below, support our approach of applying the same methodology for kinetic parameter estimation for modeling different commercial polyolefin processes from plant data.

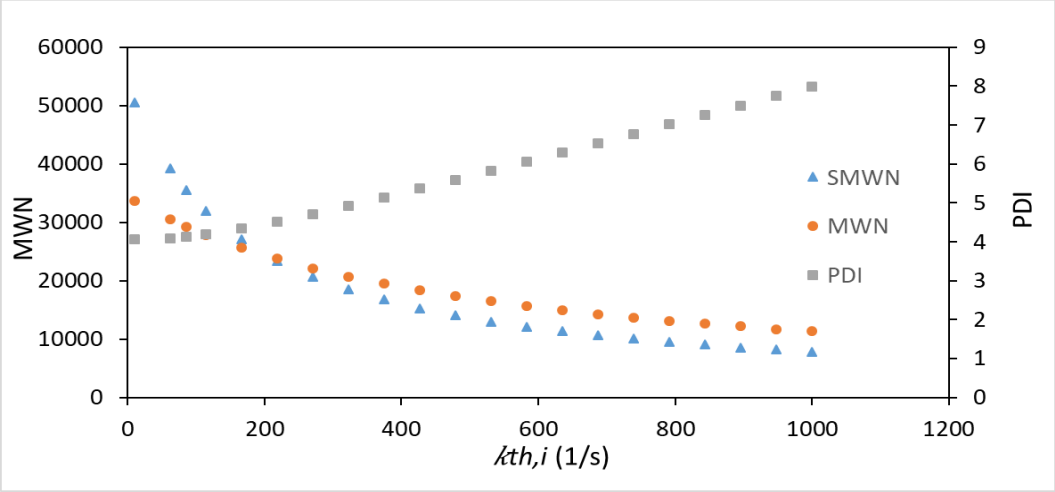

(a)

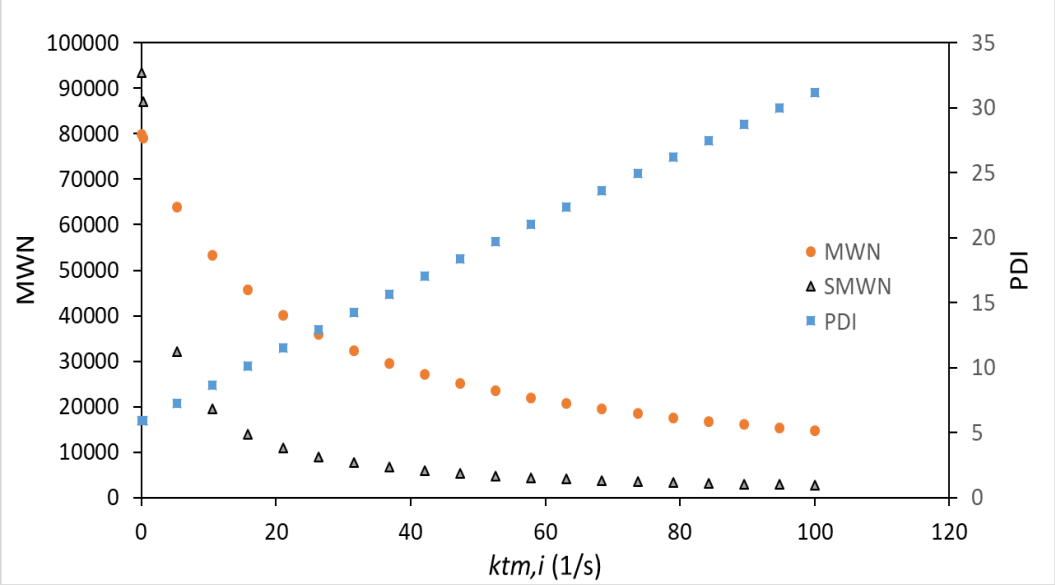

(b)

Figure 5.12. Sensitivity of the PDI, MWN and SMWN for the Unipol LLDPE process on the pre-exponential factor of the reaction rate constant for (a) chain transfer to hydrogen, and (b) chain transfer to monomer.

We demonstrate the further use of sensitivity analysis for the Unipol LLDPE process of Figure 5.8 and ***Supplement 5.1e***. Figure 5.13a shows how increasing the per-exponential factor of the propagation rate constant, $k_{p,i}$ for one of the three active sites increases the production rate and mass fraction of polymer produced at that site (SPFRAC).

Supplement 5.1d gives details of our kinetic model and kinetic parameter estimation, including the reaction rate constants chosen and their initial values for the Basell Spheripol PP process of Figure 5.6. In Figure 5.13b, we show how increasing the atactic propagation rate constant increases the atactic fraction, ATFRAC, for the Spheripol PP process.

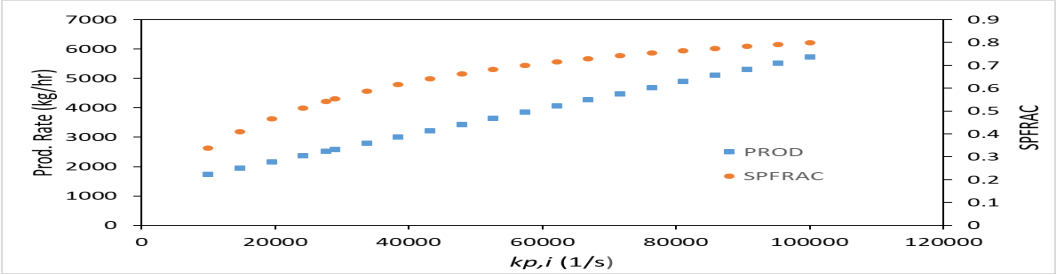

(a)

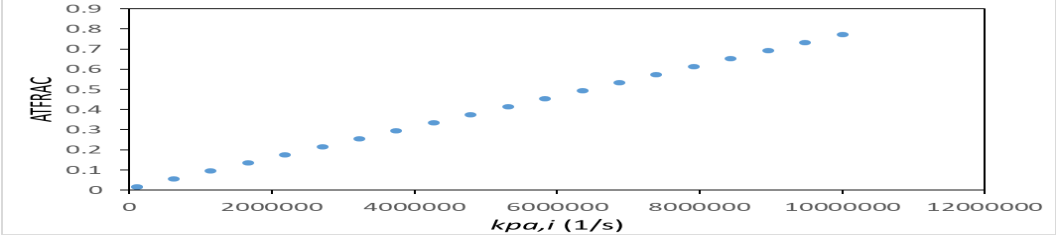

(b)

Figure 5.13. (a). The sensitivity of the production rate and SPFRAC for the Unipol LLDPE process to changes in the propagation reaction rate constant; (b). The sensitivity of the atactic fraction ATFRAC to changes in the atactic propagation reaction rate constant for the Spheripol PP process.

For the Mitsui slurry HDPE process with serial reactor configuration of Figure 5.3 and ***Supplement 5.1b***, we show in Figure 5.14a and Figure 5.14b the sensitivity of the polymer production rate to changes in the reaction rate constants for catalysts activation by cocatalyst, $k_{act,i}$, and for spontaneous catalyst deactivation $k_{ds,i}$ for one of the five active catalyst sites.

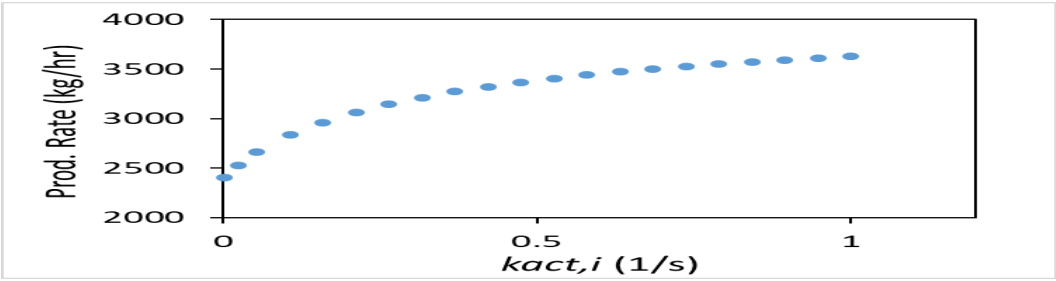

(a)

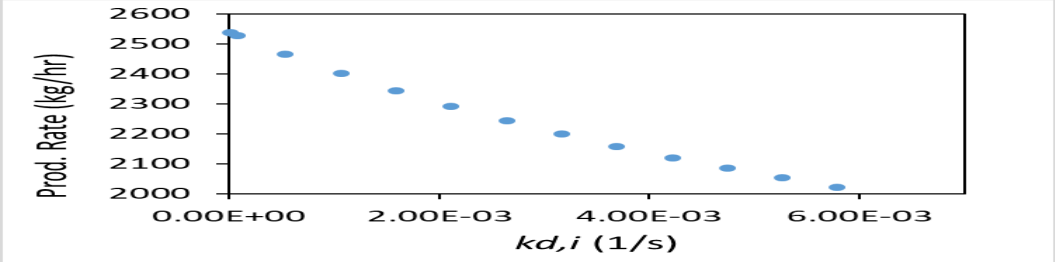

(b)

Figure 5.14. The sensitivity of the production rate for the slurry HDPE process to changes in the reaction rate constant for (a) catalyst activation by cocatalyst, and (b) spontaneous catalyst deactivation.

Figure 5.15 illustrates the sensitivity of the MWD from a Mitsui slurry HDPE process of Figure 5.3 and ***Supplement 5.1b*** to changes in the reaction rate constant for forward catalyst inhibition by hydrogen, $k_{finh,i}$, for two different of the five active catalyst sites. The MWD of the HDPE produced from a single reactor can change from unimodal to bimodal. This happens since the difference in the rate of inhibition for different catalyst sites.

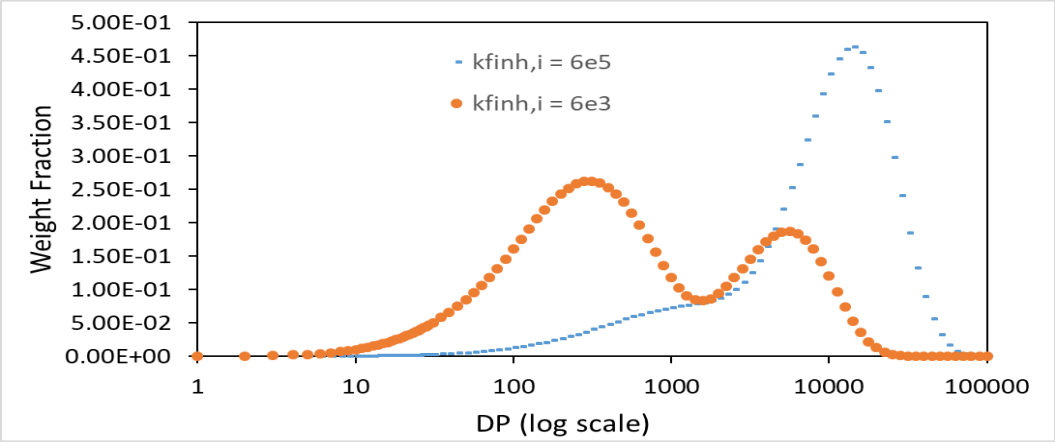

Figure 5.15. Sensitivity of the MWD from a Mitsui slurry HDPE process to changes in the reaction rate constant for catalyst inhibition for two different of the five active catalyst sites.

Figure 5.16 shows the effect on the production rates for the two horizontal bed reactors (represented as P1, P2 in the figure) in the Innovene gas-phase PP process of Figure 5.7 by varying the pre-exponential rate constant of propagation reaction for a particular active site. The details of the process are available in ***Supplement 5.1c.***

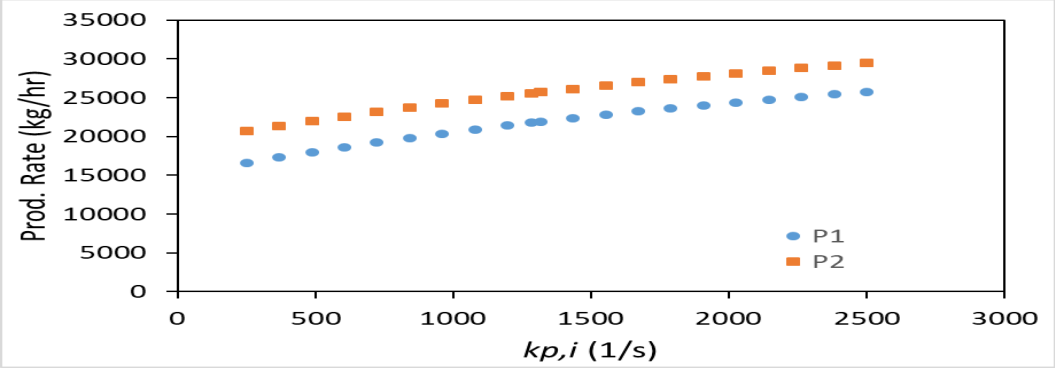

Figure 5.16. The sensitivity of the production rate from an Innovene gas-phase PP process to changes in the propagation reaction rate constant.

5.5.4 Efficient Use of Software Tools: Design Specification

Design specification (design spec) is an important tool that supports process modeling and kinetic estimation. While sensitivity analysis quantifies an increasing or a decreasing trend of a production target when varying a reaction rate constant within a chosen range of values, applying the design spec enables us to identify the reaction rate constant value within the chosen range to reach a specific production target.

Design spec is particularly useful in converging models of polyolefin processes having recycle loops. We can fix a particular ratio of components in a recycle stream and the model can vary input flow rates to maintain the ratio. As an illustration, in the Spheripol PP process of Figure 5.6 and ***Supplement 5.1d***, we can use a design spec to maintain the ratio of ethylene to propylene in a recycle stream into the fluidized-bed reactor where the stream is a combination of the overall recycle stream and a feed of ethylene and hydrogen. Design spec varies the flow rates of ethylene (comonomer) and the hydrogen to maintain the desired ratio of ethylene and propylene in the recycle stream. Similarly, we can use another design spec for the recycle flow into the loop reactor by varying the flow of the propylene and hydrogen in the feed stream. Figure 5.17 show a flowsheet of the Spheripol PP process with the design specs [35].

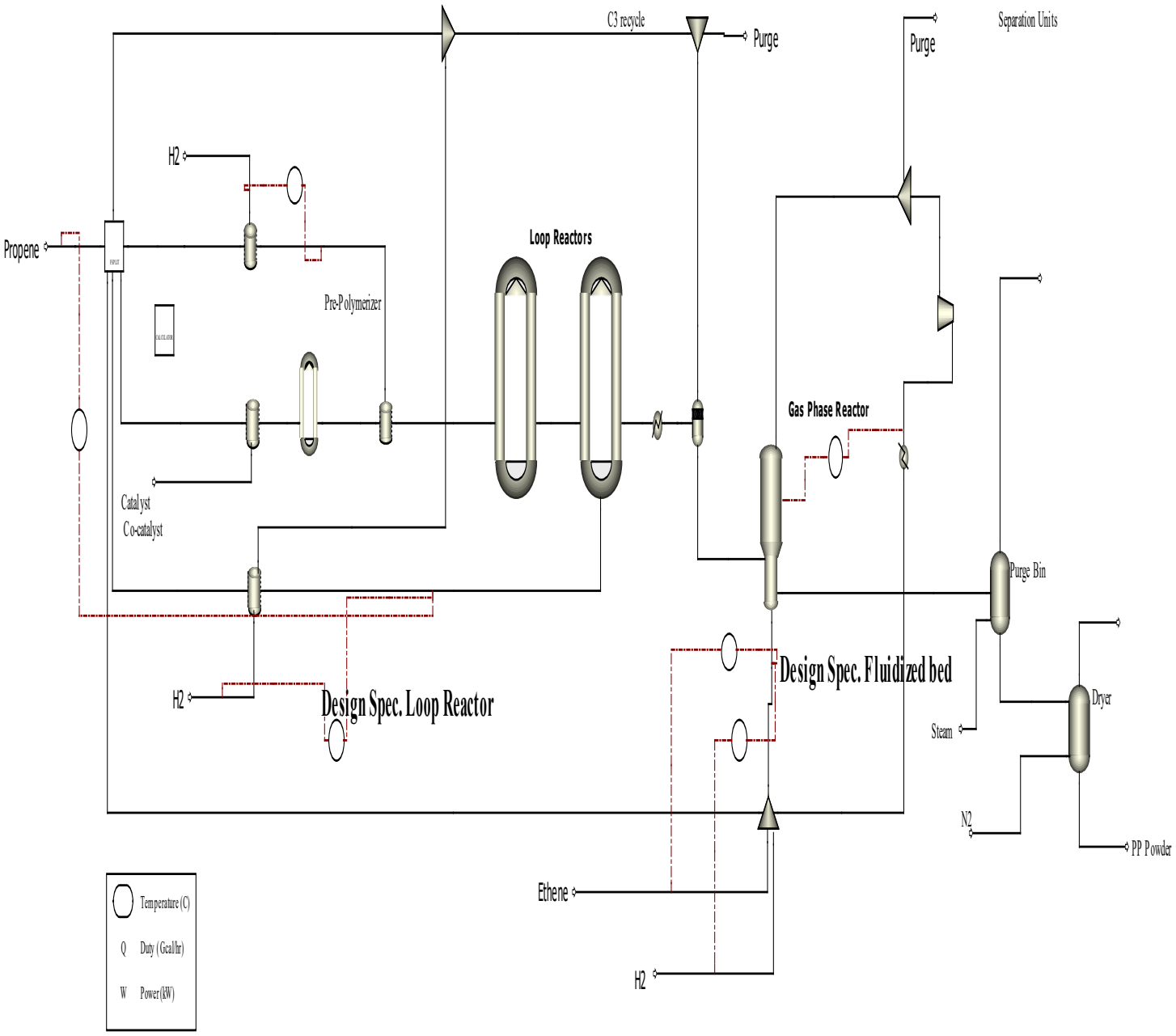

Figure 5.17 Spheripol PP process flowsheet indicating the design specification

Specifically, for the Spheripol PP model, we define the design specs as follows:

1) Design specification for the hydrogen mass fraction in the recycle stream entering the loop reactor, while the manipulated variable is the make-up hydrogen flow rate

2) Design specification for ratio of propene to ethylene in the recycle stream entering the fluidized-bed reactor, while the manipulated variable is the flow rate of ethane.

Table 5.10 shows the design spec results.

Table 5.10: Design specification for the Spheripol PP process

Design specification	**Target Value**	**Model Result**	**Initial Vary (kg/hr)**	**Final Vary (kg/hr)**	**Range set (kg/hr)**
1	4 e-5	3.9e-5	0.1	0.16	0.01 -10
2	0.5	0.48	1000	3250	5- 1000

5.5.5 Model Applications

A polyolefin process model validated by plant data can have many useful applications. The model will be helpful for the capacity expansion of the current plant. The model will also be useful in the process development stage for a new plant. We can use the validated model to study the effect of changes in process variables on production targets.

We can use the model to change certain production target, while maintaining the same value for other targets. As an example, we can vary certain process conditions to make polymer grades of different MWNs for the same throughput as shown in Figure 5.18. It shows a sensitivity analysis for the effect of changes in hydrogen flow rates on MWN, while the production rate remains same for the UNIPOL LLDPE process.

In another application of the model, we can increase the throughput, while keeping the same MWN using design specification and we demonstrate this on the UNIPOL LLDPE process as well. We use design specification to vary the hydrogen flow rate to keep the same MWN at around 29000, while increasing the production rate of LLDPE from 2400 to 3200 kg/hr. Table 5.11 summarizes the results of the UNIPOL process design specification. Lastly, when combined with process control and optimization techniques, a validated model can be useful for polymer quality control and effective polymer grade changes.

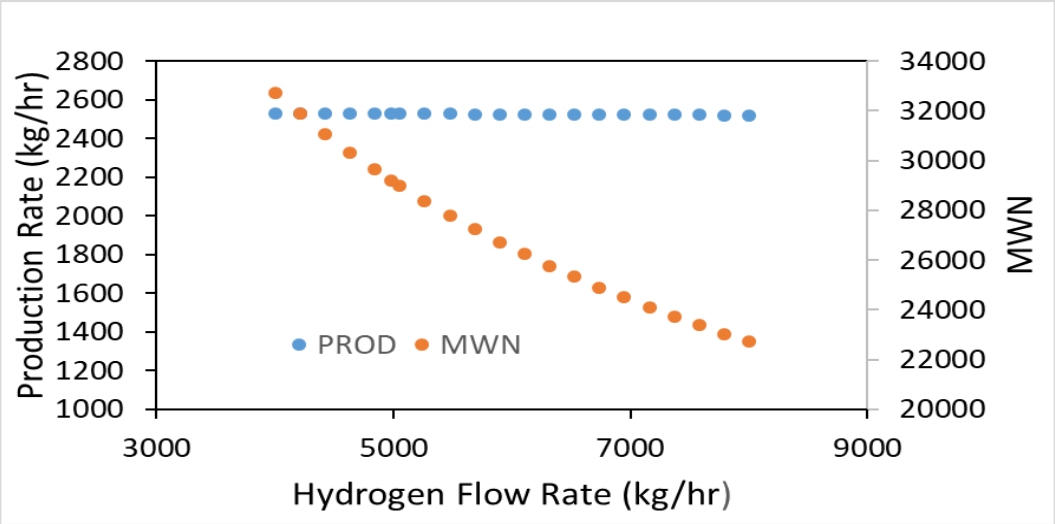

Figure 5.18. Sensitivity Analysis of the MWN and production rate on changes in hydrogen flow rates on the Unipol LLDPE process

Table 5.11. Design specification for the UNIPOL LLDPE process

Target MWN	**Model MWN**	**Initial H2 flow (kg/hr)**	**Final H2 flow (kg/hr)**	**Range set (kg/hr)**
29194	29217	4938	7515	3000-9000

5.6 Workshop WS 5.1: Simulation of a Slurry HDPE Process

5.6.1 Objective

In this workshop, we simulate a slurry HDPE process [1]. The process consists of two CSTRs in series. The workshop is based on HDPE production process of a petrochemical company in the Asia-Pacific region. We simulate a simplified open-loop flowsheet of the plant, focusing more on the Ziegler-Natta reaction part. In this workshop, the kinetic rate constants and the minimum number of active catalyst sites are available. So, the focus is on building a HDPE process model and not estimating kinetic parameters. We also convert our simple open-loop model to a closed-loop plant model and perform sensitivity analysis

5.6.2 Process Flowsheet

Figure 5.19 shows a simulation flowsheet of a complete process, and Figure 5.20 displays a simplified simulation flowsheet for the current workshop. In Figure 5.20, D201 and D221 are CSTRs, and 201F and

221F are flash units. We save the simulation file for Figure 5.20 as ***WS5.1a HDPE_Open Loop.bkp,*** and continue the current workshop with this file.

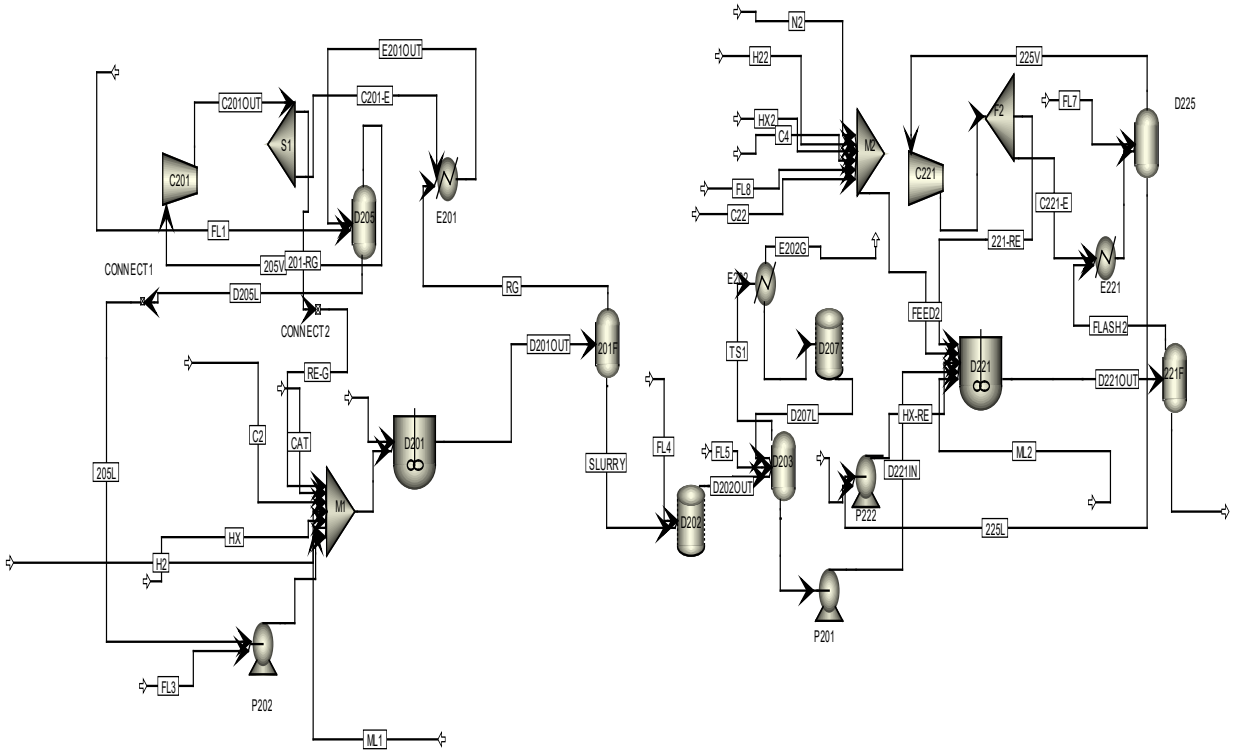

Figure 5.19 A complete simulation flowsheet of a slurry HDPE process in a series configuration.

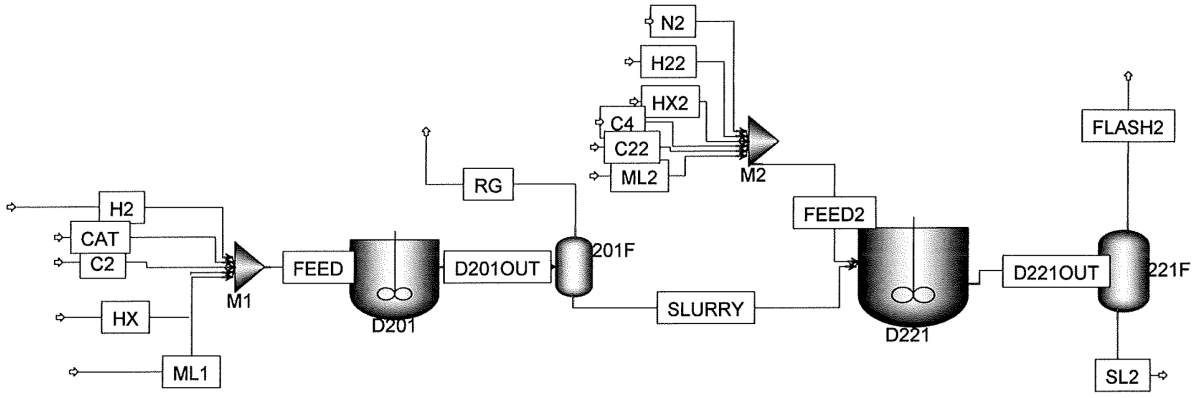

Figure 5.20 A simplified open-looped simulation flowsheet of a slurry HDPE process in a series configuration for workshop WS10-1a.

5.6.3 Unit System, Components, Characterization of Oligomer, Polymer and Site-Based Species

We use METCBAR unit system for this process. Figures 5.21a and 5.21b show the components used in the simulation of the slurry HDPE process, and the associated enterprise databases chosen.

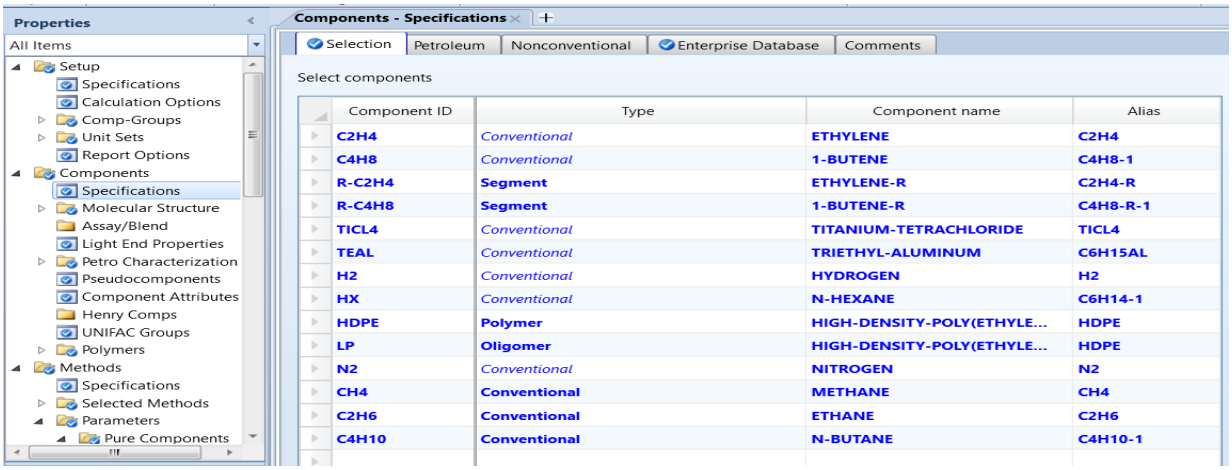

Figure 5.21a Component specifications

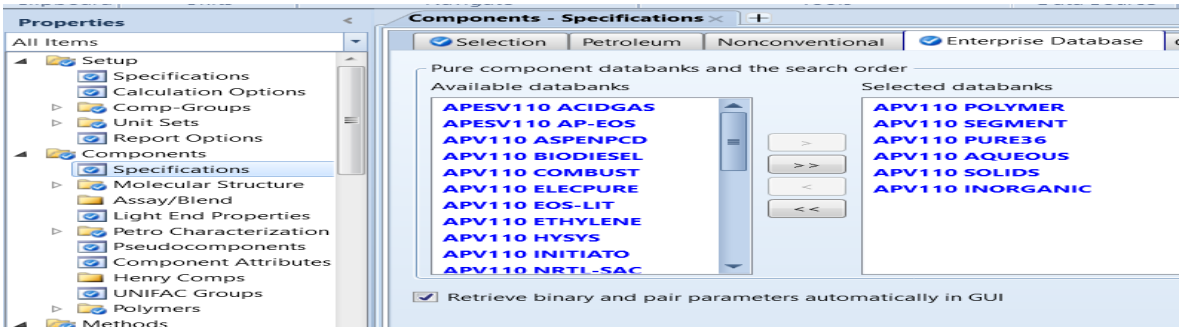

Figure 5.21b. Enterprise databases chosen.

Ethylene and 1-butene are monomer and comonomer, respectively, with each having a repeated segment; and we assume the oligomer, LP, contains 19 repeated ethylene segments (Figure 5.22). TICl4 is catalyst, and TEAL (triethyl aluminum) is cocatalyst. Hydrogen is chain transfer agent, and hexane is solvent. Nitrogen is a purge gas, and CH4, C2H6 and C4H10 are impurities.

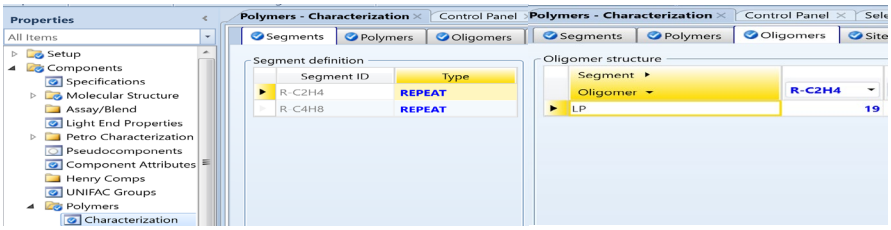

Figure 5.22 Definition of segments and representation of oligomer LP.

To characterize the polymer, HDPE, we choose the default attributes for Ziegler-Natta selection. See Figure 5.23.

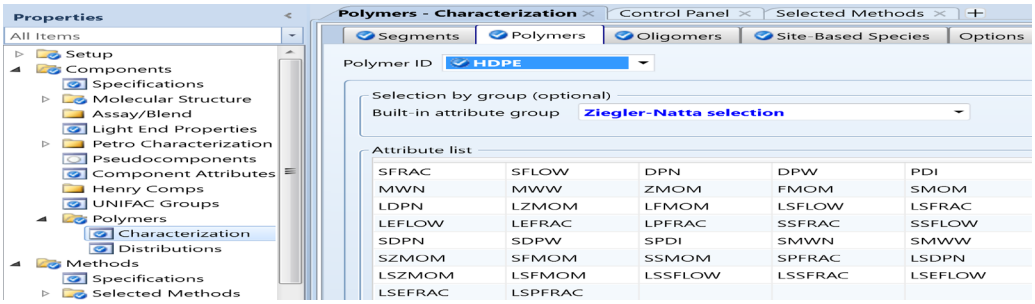

Figure 5.23 Characterization of Ziegler-Natta polymer attributes.

Figure 5.24 shows the characterization of the ZN catalyst, TiCl4, under site-based species. To understand the meanings of the attributes, click on one of the attribute names and you will see a table of attribute selection on the right of the figure, explaining each attribute.

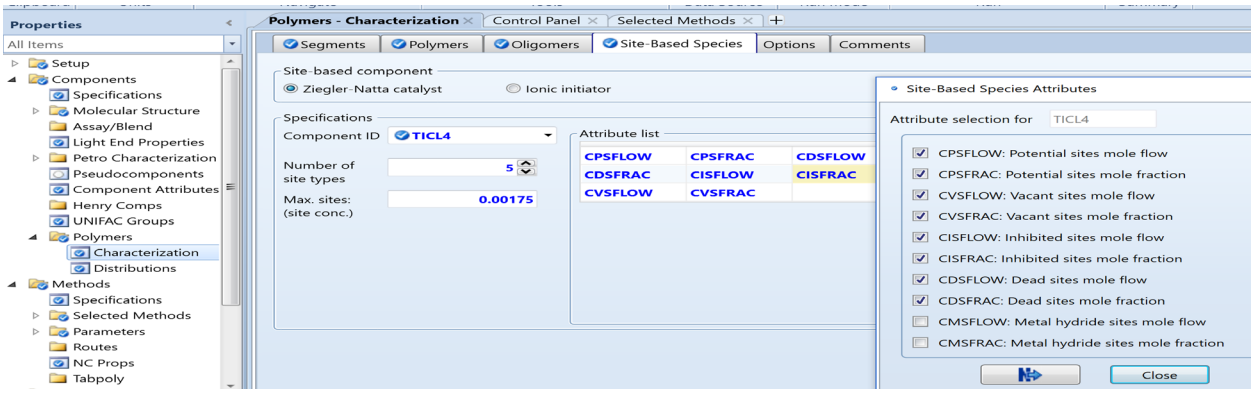

Figure 5.24 Characterization of ZN catalyst and attribute selection

5.6.4 The Role of Solid Polymer in Phase-Equilibrium Calculations

In the reactor, ethylene molecules react to form long polymer chains. In the slurry process, the reactor temperature (70 to 85 °C) is below the melting point of the polymer (140 °C). The polymer molecules solidify upon formation, creating a slurry system.

In the actual process, the solid polymer does not interact thermodynamically with the other components in the reactor. Our primary assumption in phase calculations is that *the polymer is dissolved in the liquid phase with the solvent*, as would be the case in solution polymerization of ethylene, where the reactor temperature would be above the melting point of the polymer. Although this modeling simplification does not represent the physical picture of what is happening in the slurry

polymerization of ethylene, the effect of it in the thermodynamic modeling is relatively small. Figure 5.25 illustrates the difference between the actual conditions and the modeling assumption [4].

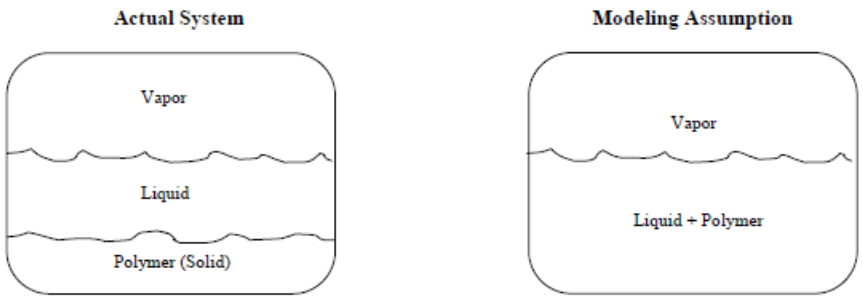

Figure 5.25 A comparison between the actual slurry system and the modeling assumption that the polymer is dissolved in the liquid phase with the solvent.

In reference [4], we have presented quantitative evidence to demonstrate that we can make this assumption without undermining the robustness of the reactor model.

5.6.5 Thermodynamic Model and Parameters

We use the polymer Sanchez-Lacombe equation of state (POLYSL), presented previously in Section 2.6, for the slurry HDPE process [2]. The model is given by:

$$\bar{\rho}^2 + \bar{P} + \bar{T}\left[\ln(1-\bar{\rho}) + \left(1 - \frac{1}{r}\right)\bar{\rho}\right] = 0 \qquad (5.10)$$

where

$$\bar{\rho} = \frac{\rho}{\rho^*}, \quad \bar{P} = \frac{P}{P^*}, \quad \bar{T} = \frac{T}{T^*} \qquad (5.11)$$

are the reduced density, pressure, and temperature, respectively; and ρ*, P* and T* are the scale factors that completely characterize each pure fluid. They correspond to pure component (unary) parameters SLRSTR, SLPSTR and SLTSTR within Aspen Polymers. See Figure 5.26 for entering the parameter values according to the online help for “Sanchez-Lacombe unary parameters” in Aspen Polymers.

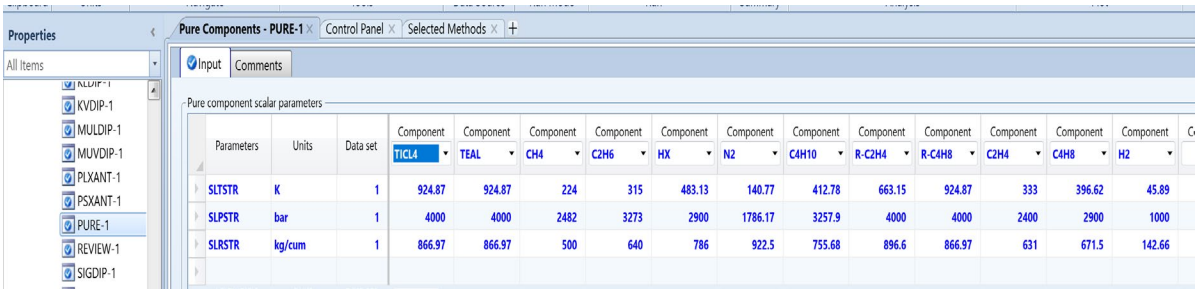

Figure 5.26 Pure component parameters for POLYSL thermodynamic model: Properties->Methods -> Parameters -> Pure Components -> PURE-1

To model the copolymer production, we include binary interaction parameters. Through the online help for "Sanchez-Lacombe binary parameters" in Aspen Polymers, we see the temperature-dependent expressions for two binary interaction parameters:

$$k_{ij} = a_{ij} + b_{ij}/T_r + c_{ij} \ln T_r + d_{ij} T_r + e_{ij} T_r^2 \tag{5.12}$$

$$\eta_{ij} = a'_{ij} + b'_{ij}/T_r + c'_{ij} \ln T_r + d'_{ij} T_r + e'_{ij} T_r^2 \tag{5.13}$$

where T_r is the reduced temperature defined by T/T_{ref}, and the default value of reference temperature T_{ref} is 298.15 K. We enter the parameter values of these two equations (see Tables 5 and 6 in [2]) in Aspen Polymers following the path: Properties->Methods -> Parameters -> Binary Interaction -> SLKIJ-1 and SLETIJ-1. See Figures 5.27.

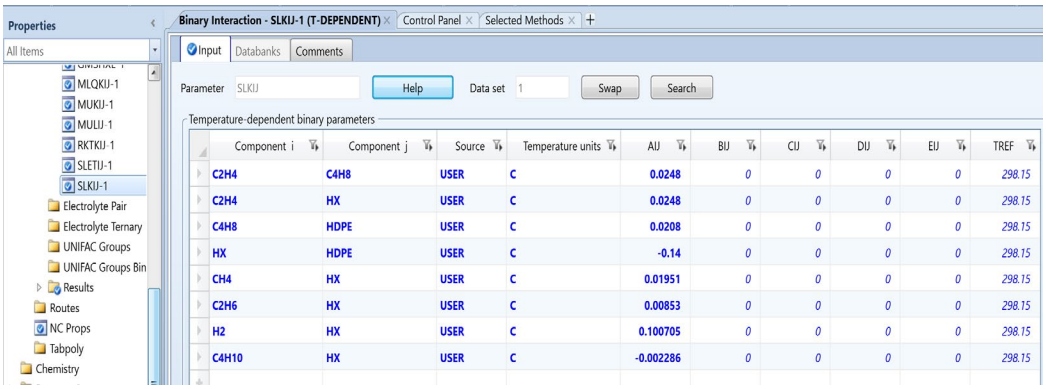

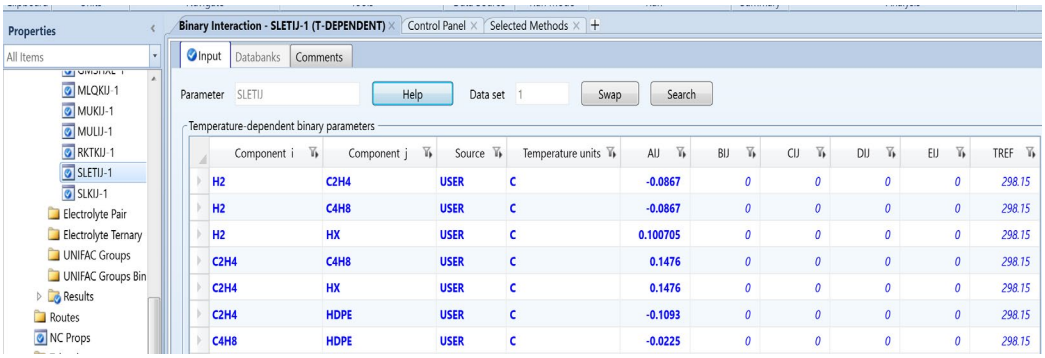

Figure 5.27 Binary interaction parameters for POLYSL thermodynamic model [2].

5.6.5 Pure-Component Parameters

To extract the property parameters for pure components from the Aspen Polymers databanks, we follow the path: Properties -> Components ->Specifications -> Review (see Figure 5.28):

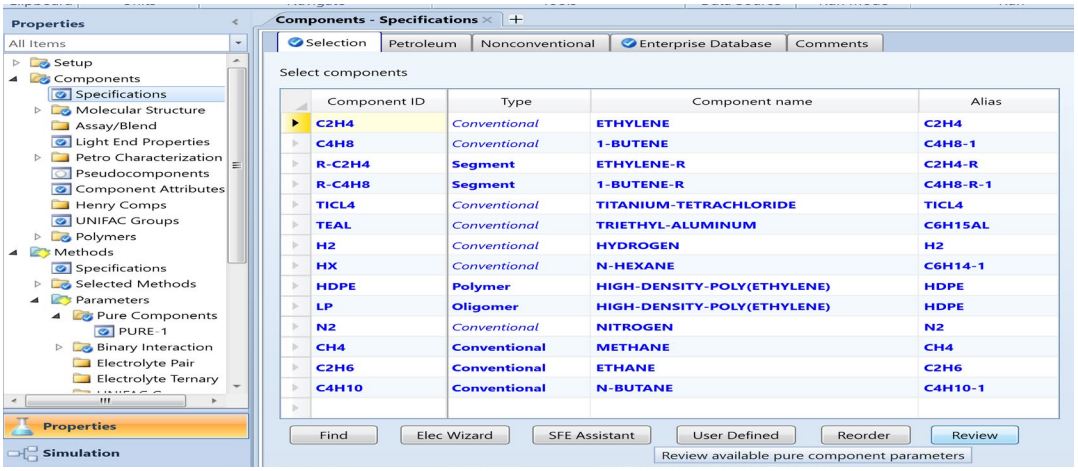

Figure 5.28 Review of property parameters for pure components

We then see the listing of parameter values by following the path: Properties -> Methods -> Parameters -> Pure Components -> Review-1. See Figure 5.29.

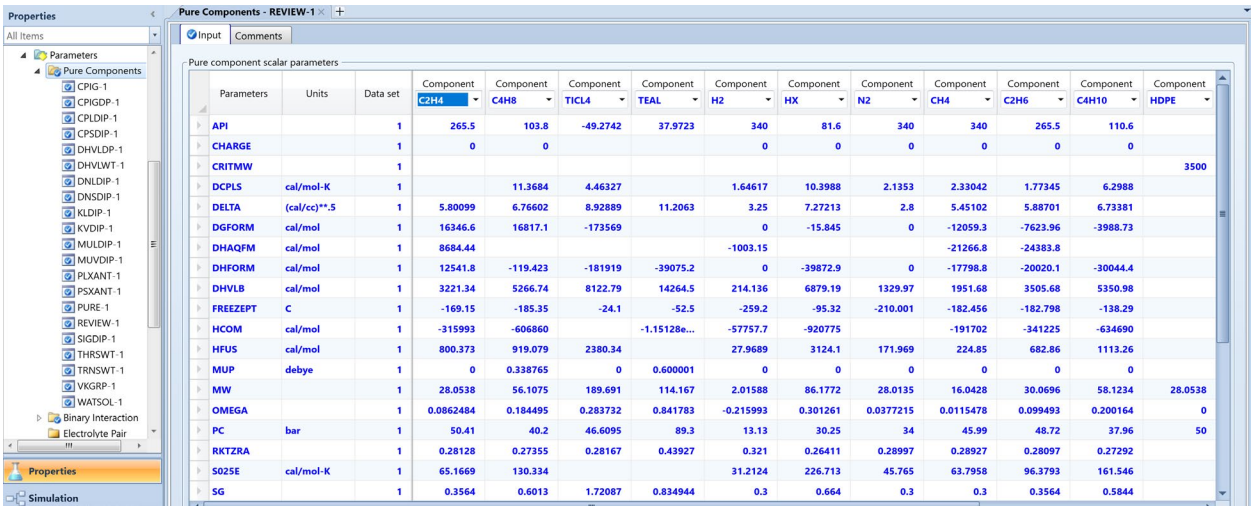

Parameters	Units	Data set	Component C2H4	Component C4H8	Component TICL4	Component TEAL	Component H2	Component HX	Component N2	Component CH4	Component C2H6	Component C4H10	Component HDPE
API		1	265.5	103.8	-49.2742	37.9723	340	81.6	340	340	265.5	110.6	
CHARGE		1	0	0			0	0	0	0	0	0	
CRITMW		1											3500
DCPLS	cal/mol-K	1		11.3684	4.46327		1.64617	10.3988	2.1353	2.33042	1.77345	6.2988	
DELTA	(cal/cc)**.5	1	5.80099	6.76602	8.92889	11.2063	3.25	7.27213	2.8	5.45102	5.88701	6.73381	
DGFORM	cal/mol	1	16346.6	16817.1	-173569		0	-15.845	0	-12059.3	-7623.96	-3988.73	
DHAQFM	cal/mol	1	8684.44				-1003.15			-21266.8	-24383.8		
DHFORM	cal/mol	1	12541.8	-119.423	-181919	-39075.2	0	-39872.9	0	-17798.8	-20020.1	-30044.4	
DHVLB	cal/mol	1	3221.34	5266.74	8122.79	14264.5	214.136	6879.19	1329.97	1951.68	3505.68	5350.98	
FREEZEPT	C	1	-169.15	-185.35	-24.1	-52.5	-259.2	-95.32	-210.001	-182.456	-182.798	-138.29	
HCOM	cal/mol	1	-315993	-606860		-1.15128e...	-57757.7	-920775		-191702	-341225	-634690	
HFUS	cal/mol	1	800.373	919.079	2380.34		27.9689	3124.1	171.969	224.85	682.86	1113.26	
MUP	debye	1	0	0.338765	0	0.600001	0	0	0	0	0	0	
MW		1	28.0538	56.1075	189.691	114.167	2.01588	86.1772	28.0135	16.0428	30.0696	58.1234	28.0538
OMEGA		1	0.0862484	0.184495	0.283732	0.841783	-0.215993	0.301261	0.0377215	0.0115478	0.099493	0.200164	0
PC	bar	1	50.41	40.2	46.6095	89.3	13.13	30.25	34	45.99	48.72	37.96	50
RKTZRA		1	0.28128	0.27355	0.28167	0.43927	0.321	0.26411	0.28997	0.28927	0.28097	0.27292	
S025E	cal/mol-K	1	65.1669	130.334			31.2124	226.713	45.765	63.7958	96.3793	161.546	
SG		1	0.3564	0.6013	1.72087	0.834944	0.3	0.664	0.3	0.3	0.3564	0.5844	

Figure 5.29 Extraction of pure-component property values from Aspen Polymers databanks.

We need to input several other scalar and temperature-dependent parameters for pure components. First, we enter the estimated or literature values of scalar pure-component parameters that are not available within Aspen Polymer databanks: Properties->Parameters ->Pure Components ->New -> Scalar -> Enter parameter name and value. Figure 5.30 shows the assumed values of critical temperature (TC) and critical pressure (PC) for our catalysts.

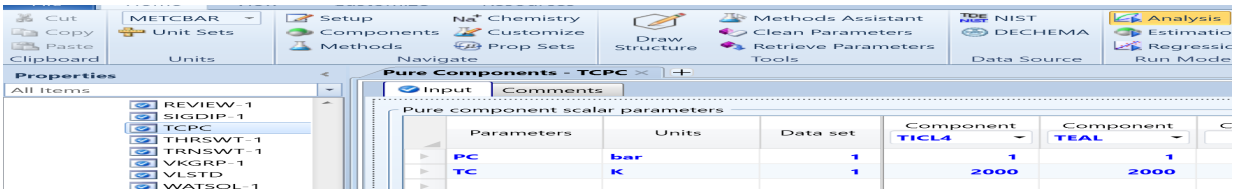

Parameters	Units	Data set	Component TICL4	Component TEAL
PC	bar	1	1	1
TC	K	1	2000	2000

Figure 5.30 Assumed values of critical pressure PC and critical temperature TC for ZN catalyst TiCl4 and cocatalyst triethyl aluminum (TEAL).

We also enter the estimates the critical parameters for the oligomer LP: Properties -> Parameters ->Pure Components ->New -> Scalar -> Name: LPCrit ->Enter parameter name, unit and value (see Figure 5.31).

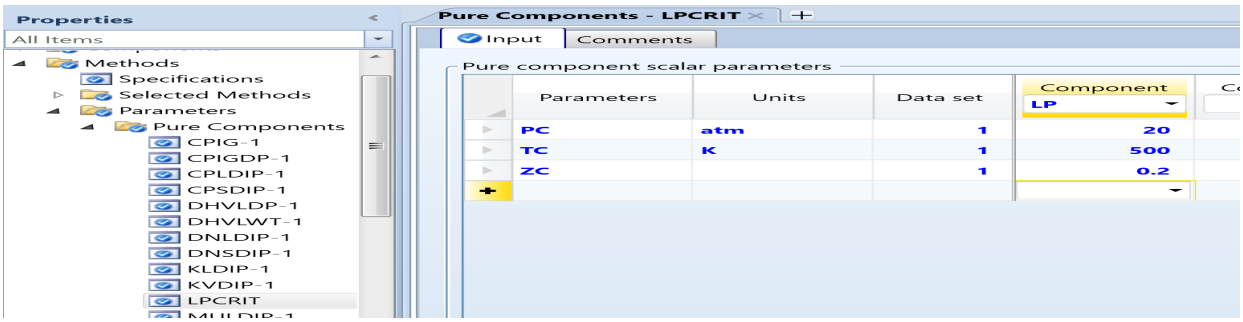

Parameters	Units	Data set	Component LP
PC	atm	1	20
TC	K	1	500
ZC		1	0.2

Figure 5.31 Assumed values of critical prrssure PC, critical temperature TC and compressibility factor ZC for oligomer LP.

Next, to ensure that polymer HDPE, oligomer LP, and catalysts TiCl4 and TEAL do not valorize, we can specify the first parameter in the T-dependent liquid vapor pressure correlation PLXANT-1 to a large

negative number like -40. This will make the vapor pressure of these four components extremely small (4.24 E-23 Bar) [36]. See Figure 5.32.

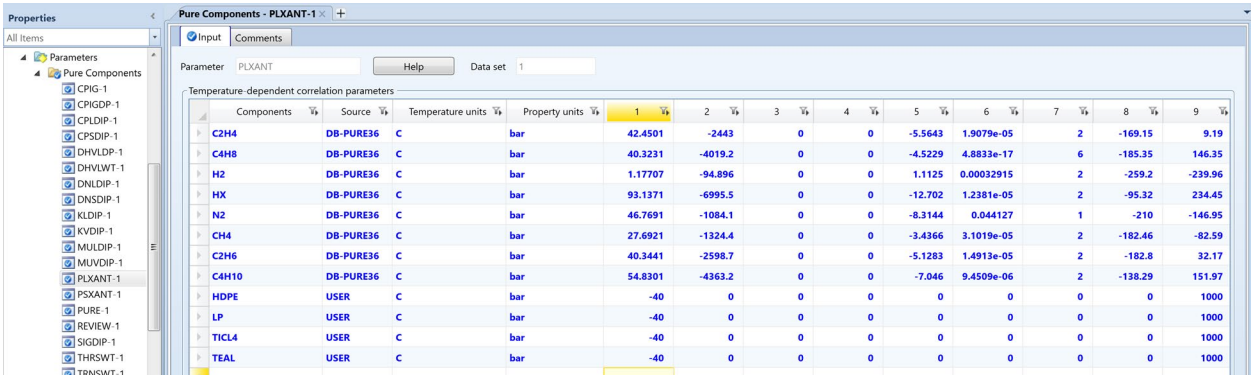

Figure 5.32 Setting the first parameter of the T-dependent liquid vapor pressure correlation PLXANT-1 to a large negative number of -40 to ensure the selected components remaining in the liquid phase.

Lastly, it is important that we compare the predictions of thermophysical properties of components using the POLYSL thermodynamic method with the reported experimental data in order the validate our selection of POLYSL as an accurate thermodynamic method for the slurry HDPE process simulation [4]. We refer the reader to ***WS 2.3***, Section 2.7 for this validation.

5.6.6 Feed Streams

The feed to the first reactor consists of the ethylene monomer feed (C2), catalyst (CAT), solvent (HX), hydrogen (H2), oligomer stream recycled from the separation section(ML1), which are combined in a mixer (M1) before entering the first reactor (D201) in series.

The feed to the second reactor (D221) consist of the outlet from the first reactor and the commoner butane (C4), ethylene monomer (C2), hydrogen(H2), solvent (HX), and oligomer (ML2) streams.

We input the essential data for these feed streams specified in Table 5.12 under Simulation -> Streams:

Table 5.12 Specifications of feed streams

Stream	T(C)	P(bar)	Flow	Mass Fraction
C2	40	13	5588 kg/hr	C2H4 = 0.9998; C2H6 =0.0001;CH4=0.0001,H2=1E-6
CAT	20	7	255 kg/hr	TiCl4 = 0.005;TEAL = 0.005; HX = 0.99
H2	25	1.0125	36 cum/hr	H2 = 0.9773 ;CH4 = 0.0227
HX	40	14	3500 kg/hr	HX = 1
ML1	67	14.5	5300 kg/hr	LP = 0.05 ; HX = 0.95
C4	116	13.4	96 kg/hr	C4H8 =0.983 ; C4H10 = 0.017

C22	40	13	5412 kg/hr	C2H4 = 0.9998; C2H6 =0.0001;CH4=0.0001,H2=1E-6
H22	25	1.0125	8.68 cum/hr	H2 = 0.9773; CH4 = 0.0227
HX2	40	14	2000 kg/hr	HX = 1
ML2	240	1.45e6	8780 kg/hr	LP = 0.05 ; HX = 0.95
N2	20	8	20 kg/hr	N2 = 1

	C2H4	C4H8	TEAL	HX	LP	N2	C2H6
ML1	2.27	4.53	0.19	5023.31	267.862	0.70	1.14
ML2	3.77	7.52	0.32	8320.55	444.752	1.19	1.9
Unit: kg/hr Both ML1 and ML2 at 67 C, 14.5 bar Total mass flow: ML1=5300 kg/hr; ML2 =8780 kg/hr							

Referring to Figure 5.24 where we define the site-based species attributes for catalyst TiCl4, we show below how to enter the initial attribute values for stream CAT. See Figures 5.33 and 5.34.

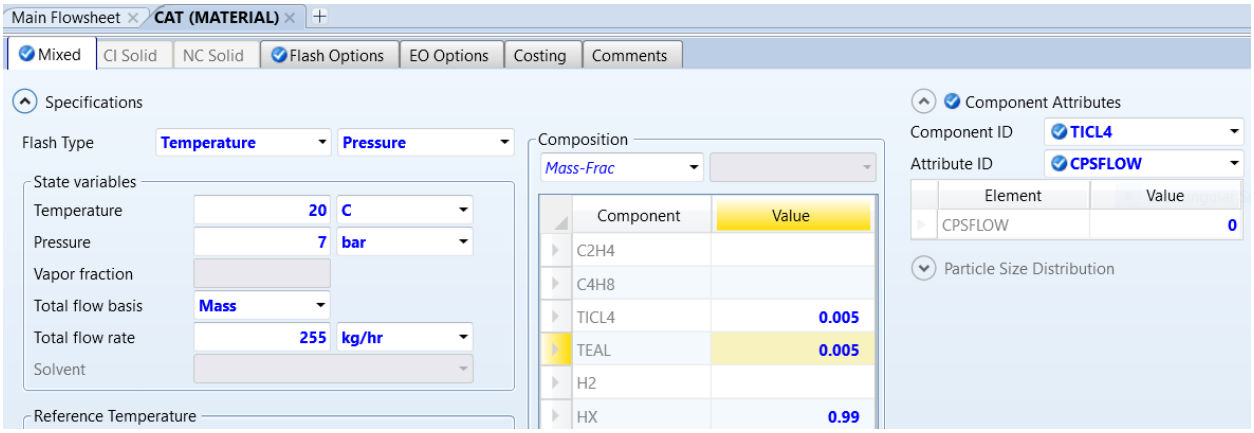

Figure 5.33 Specification of initial site-based species attributes for CAT stream: Setting potential site mole flow (CPSFLOW) to zero. Do the same for potential site mole fraction (CPSFRAC), dead site mole flow (CDSFLOW) and dead site mole fraction (CDSFRAC).

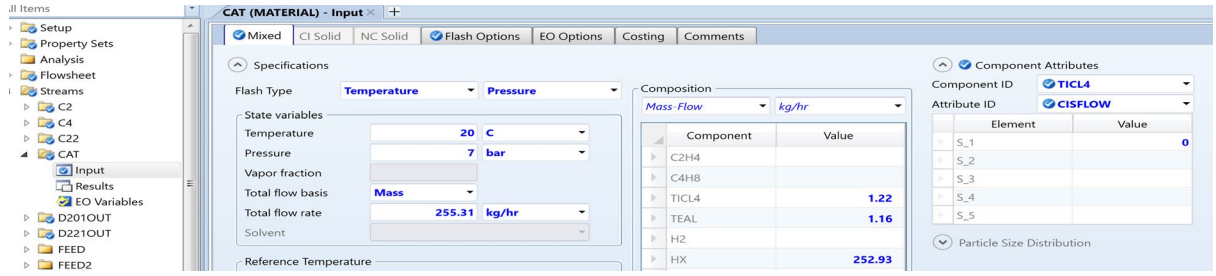

Figure 5.34 Specification of initial site-based species attributes for CAT stream: Setting the mole flow of the first inhibited site S_1 (CISFLOW) to zero. Do the same for the mole fraction of first inhibited site S_1

(CPSFRAC), mole flow of the first vacant site S_1 (CVSFLOW) and mole fraction of the first vacant site S_1 (CVSFRAC).

5.6.7 Ziegler-Natta Kinetics Specifications

We create a Z-N reaction set, named ZN: Reactions ->New-> ID = ZN, Reaction type= Ziegler-Nat -> Species (see Figure 5.35):

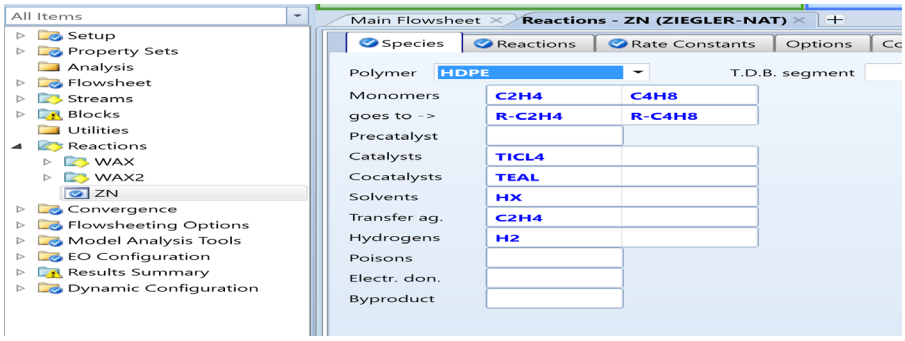

Figure 5.35 ZN kinetics reaction species specification

We have previously specified in Figure 5.24 the number of active catalyst sites as 5. We generate the reactions by including:

(1) 5 catalyst site activation by cocatalyst reactions (ACT-COACT), with one reaction per active catalyst site;
(2) 10 chain initiation reactions by monomer C2H4 and by comonomer C4H8, with two reactions per active catalyst site;
(3) 20 chain propagation reactions (PROP) of reacting polymer chain P_n[C2H4] with C2H4 and C4H8, and reacting polymer chain P_n[C4H8] with C2H4 and C4H8, totaling 4 reactions per active catalyst site;
(4) 10 reactions of chain transfer to hydrogen (CHAT-H2) by reacting polymer chain Pn[C2H4] with H2, and reacting polymer chain Pn[C4H8] with H2, with two reactions per active catalyst site; and
(5) 5 spontaneous catalyst deactivation reactions (DEACT-SPON), with one reaction per active catalyst site type; and (6) 5 forward and 5 reverse catalyst inhibitions by hydrogen (FSINH-H2 and RFINH-H2), with one reaction per active catalyst site type. Figures 5.36a to 5.36b show the 60 reactions generated.

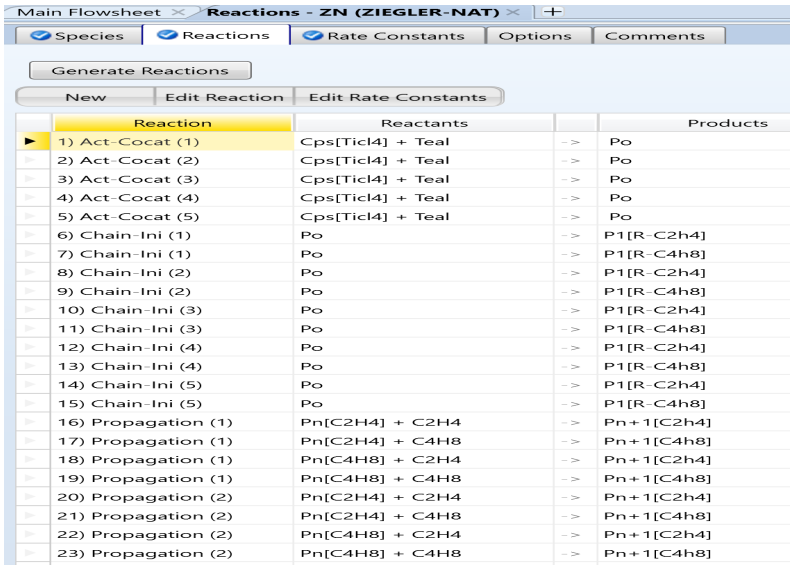

Reaction	Reactants		Products
1) Act-Cocat (1)	Cps[Ticl4] + Teal	->	Po
2) Act-Cocat (2)	Cps[Ticl4] + Teal	->	Po
3) Act-Cocat (3)	Cps[Ticl4] + Teal	->	Po
4) Act-Cocat (4)	Cps[Ticl4] + Teal	->	Po
5) Act-Cocat (5)	Cps[Ticl4] + Teal	->	Po
6) Chain-Ini (1)	Po	->	P1[R-C2h4]
7) Chain-Ini (1)	Po	->	P1[R-C4h8]
8) Chain-Ini (2)	Po	->	P1[R-C2h4]
9) Chain-Ini (2)	Po	->	P1[R-C4h8]
10) Chain-Ini (3)	Po	->	P1[R-C2h4]
11) Chain-Ini (3)	Po	->	P1[R-C4h8]
12) Chain-Ini (4)	Po	->	P1[R-C2h4]
13) Chain-Ini (4)	Po	->	P1[R-C4h8]
14) Chain-Ini (5)	Po	->	P1[R-C2h4]
15) Chain-Ini (5)	Po	->	P1[R-C4h8]
16) Propagation (1)	Pn[C2H4] + C2H4	->	Pn+1[C2h4]
17) Propagation (1)	Pn[C2H4] + C4H8	->	Pn+1[C4h8]
18) Propagation (1)	Pn[C4H8] + C2H4	->	Pn+1[C2h4]
19) Propagation (1)	Pn[C4H8] + C4H8	->	Pn+1[C4h8]
20) Propagation (2)	Pn[C2H4] + C2H4	->	Pn+1[C2h4]
21) Propagation (2)	Pn[C2H4] + C4H8	->	Pn+1[C4h8]
22) Propagation (2)	Pn[C4H8] + C2H4	->	Pn+1[C2h4]
23) Propagation (2)	Pn[C4H8] + C4H8	->	Pn+1[C4h8]

Figure 5.36a Z-N reactions for HDPE - part 1.

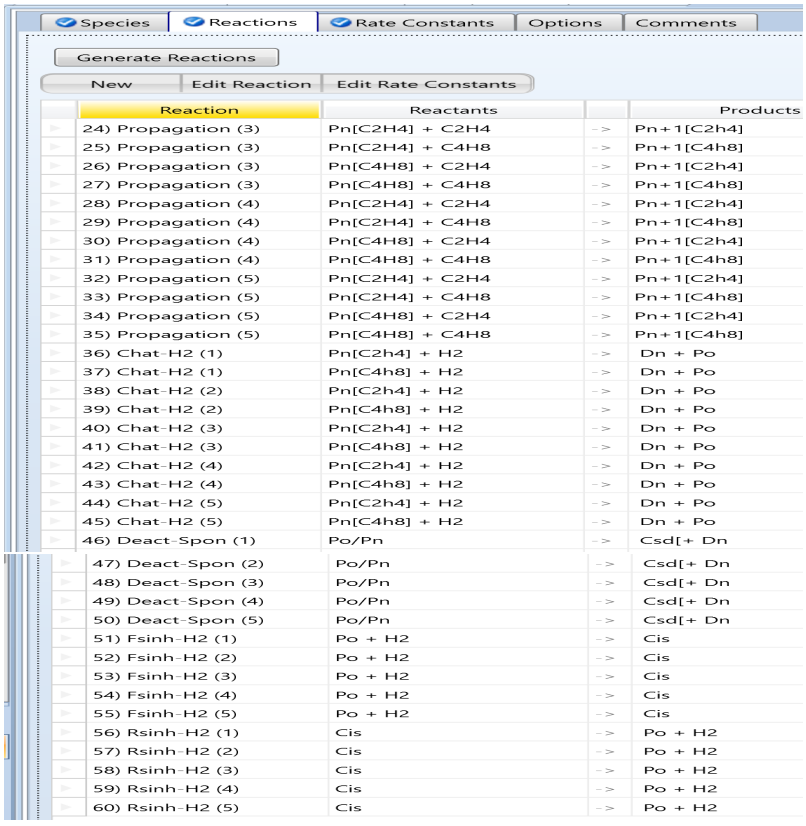

Reaction	Reactants		Products
24) Propagation (3)	Pn[C2H4] + C2H4	->	Pn+1[C2h4]
25) Propagation (3)	Pn[C2H4] + C4H8	->	Pn+1[C4h8]
26) Propagation (3)	Pn[C4H8] + C2H4	->	Pn+1[C2h4]
27) Propagation (3)	Pn[C4H8] + C4H8	->	Pn+1[C4h8]
28) Propagation (4)	Pn[C2H4] + C2H4	->	Pn+1[C2h4]
29) Propagation (4)	Pn[C2H4] + C4H8	->	Pn+1[C4h8]
30) Propagation (4)	Pn[C4H8] + C2H4	->	Pn+1[C2h4]
31) Propagation (4)	Pn[C4H8] + C4H8	->	Pn+1[C4h8]
32) Propagation (5)	Pn[C2H4] + C2H4	->	Pn+1[C2h4]
33) Propagation (5)	Pn[C2H4] + C4H8	->	Pn+1[C4h8]
34) Propagation (5)	Pn[C4H8] + C2H4	->	Pn+1[C2h4]
35) Propagation (5)	Pn[C4H8] + C4H8	->	Pn+1[C4h8]
36) Chat-H2 (1)	Pn[C2h4] + H2	->	Dn + Po
37) Chat-H2 (1)	Pn[C4h8] + H2	->	Dn + Po
38) Chat-H2 (2)	Pn[C2h4] + H2	->	Dn + Po
39) Chat-H2 (2)	Pn[C4h8] + H2	->	Dn + Po
40) Chat-H2 (3)	Pn[C2h4] + H2	->	Dn + Po
41) Chat-H2 (3)	Pn[C4h8] + H2	->	Dn + Po
42) Chat-H2 (4)	Pn[C2h4] + H2	->	Dn + Po
43) Chat-H2 (4)	Pn[C4h8] + H2	->	Dn + Po
44) Chat-H2 (5)	Pn[C2h4] + H2	->	Dn + Po
45) Chat-H2 (5)	Pn[C4h8] + H2	->	Dn + Po
46) Deact-Spon (1)	Po/Pn	->	Csd[+ Dn
47) Deact-Spon (2)	Po/Pn	->	Csd[+ Dn
48) Deact-Spon (3)	Po/Pn	->	Csd[+ Dn
49) Deact-Spon (4)	Po/Pn	->	Csd[+ Dn
50) Deact-Spon (5)	Po/Pn	->	Csd[+ Dn
51) Fsinh-H2 (1)	Po + H2	->	Cis
52) Fsinh-H2 (2)	Po + H2	->	Cis
53) Fsinh-H2 (3)	Po + H2	->	Cis
54) Fsinh-H2 (4)	Po + H2	->	Cis
55) Fsinh-H2 (5)	Po + H2	->	Cis
56) Rsinh-H2 (1)	Cis	->	Po + H2
57) Rsinh-H2 (2)	Cis	->	Po + H2
58) Rsinh-H2 (3)	Cis	->	Po + H2
59) Rsinh-H2 (4)	Cis	->	Po + H2
60) Rsinh-H2 (5)	Cis	->	Po + H2

Figure 5.36b Z-N reactions for HDPE - part 2.

To specify the reaction rate constants, we follow the standard Arrhenius form, Eq. (5.1). ***Supplement WS5.1a*** gives the numerical values of the pre-exponential factor k_0 and the activation energy *E* for each reaction.

In [2], we developed the oligomer reactions for both reactors D201 and D221 based on plant data. We include the same empirical reaction in the current simulation. See Figures 5.37a to 5.37b:

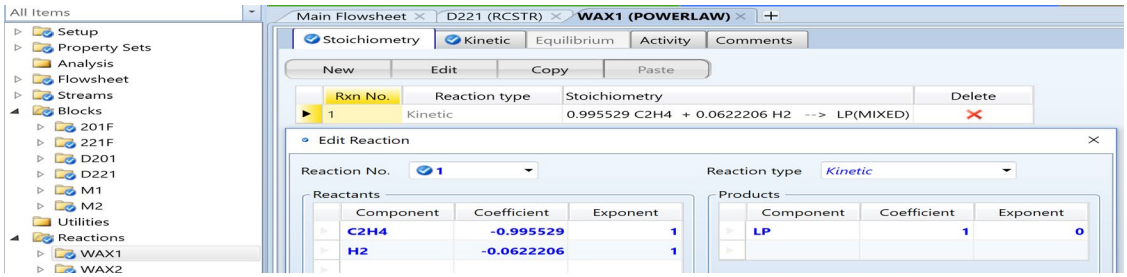

Figure 5.37a Stoichiometry for oligomer reaction WAX1 for first reactor D201 and for oligomer reaction WAX2 for second reactor D221.

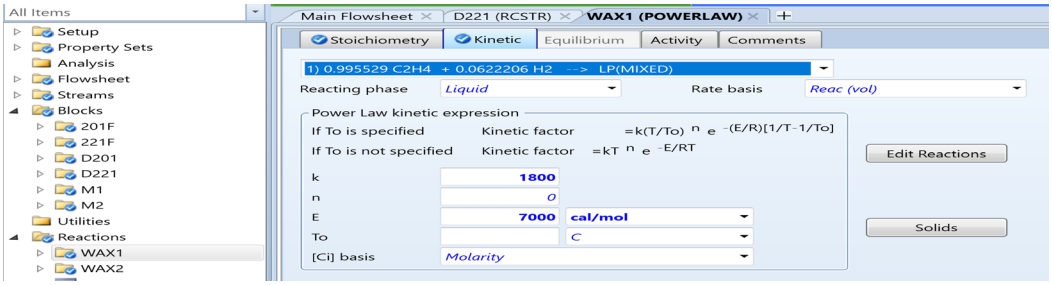

Figure 5.37B. Specification of kinetic parameters for oligomer reaction WAX1. For oligomer reaction WAX2, k = 4.2, and E = 1.6172 cal/mol.

5.6.8 Specifications of unit operations and chemical reactor blocks

5.6.8.1 Mixers (Figure 5.38)

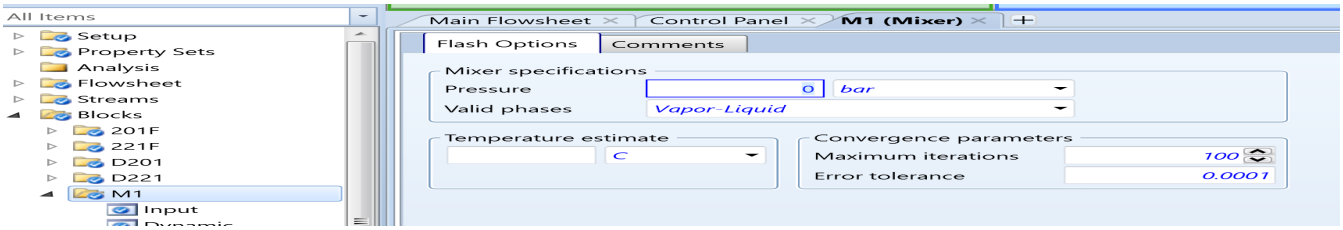

Figure 5.38 Specification of no pressure drop for mixer M1. Same specification for mixer M2.

5.6.8.2 Reactors (Figures 5.39 to 5.42)

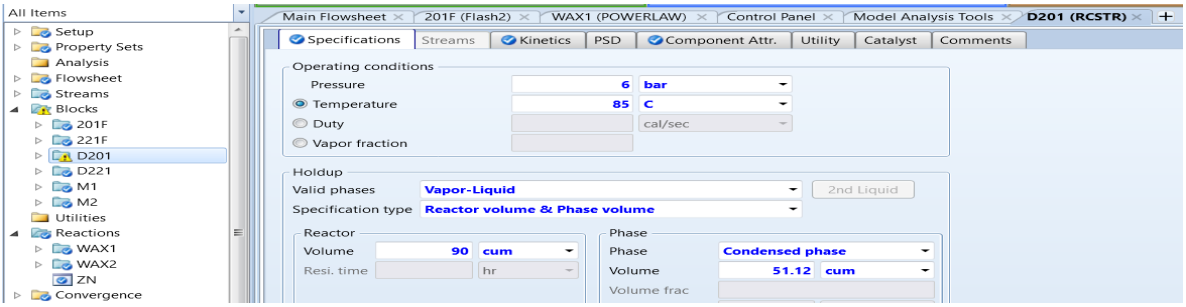

Figure 5.39 Specification of the first reactor D201. For second reactor D221, change pressure to 3.5 bar, and temperature to 80 C.

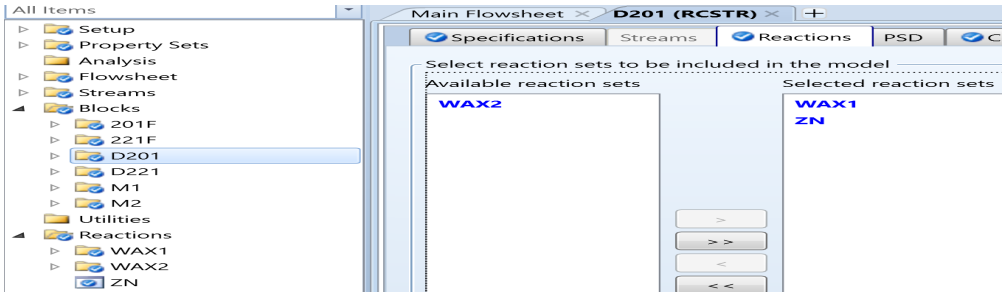

Figure 5.40 Specification of reactions R1 and WAX1 for the first reactor D201. For second reactor D221, replace reaction WAX1 by reaction WAX2.

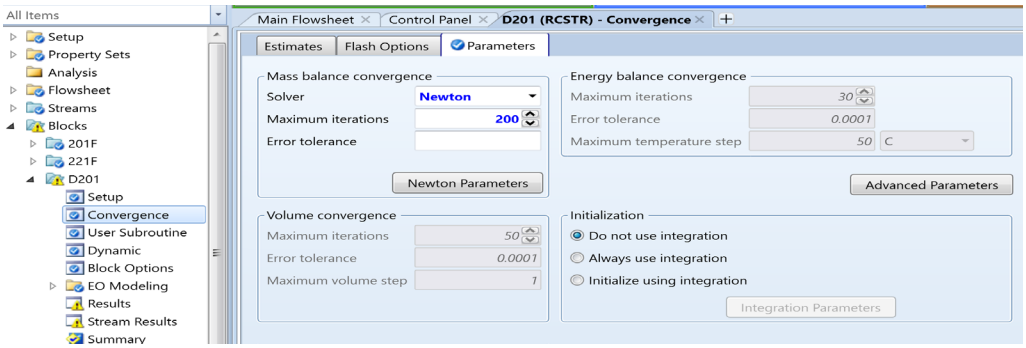

Figure 5.41 Specification of mass-balance convergence scheme (Newton) and number of maximum iterations (200) for both reactors D201 and D221.

5.6.8.3 Specification of flash drums (Figure 5.42)

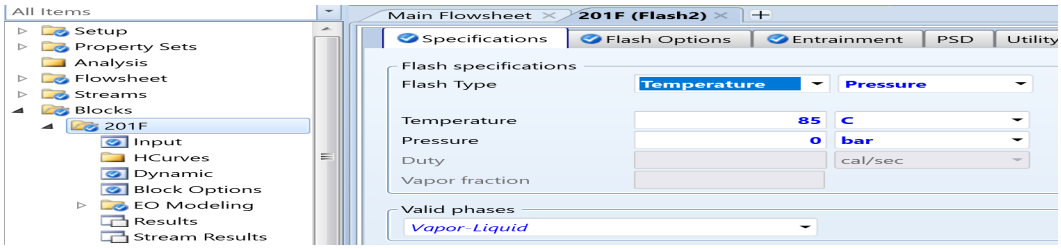

Figure 5.42 Specification of flash drum 201F. For flash drum 221F, change temperature to 80 C.

5.6.9 Simulation results

Table 5.13 shows the simulation results. For Aspen Polymers to show the computed component attributes such as MWW and PDI, and display the flow rate in mass unit, we follow the path: stream summary -> display option -> full option (showing component attributes) -> flow: mass, composition: mass.

Table 5.13 Simulation results from the open-loop HPDE flowsheet of Figure 5.20

Mass flow, kg/hr	Feed	D201OUT	Slurry	Feed2	D221OUT

Total stream, kg/hr	14646.3	14646.3	14646.3	16308.8	30927.6
Selected component, kg/hr					
C2H4	5589.15	14.6007	12.2919	5414.68	35.982
C4H8	4.53	4.53	4.32593	101.945	106.271
HDPE	0	5374.93	5374.93	0	10574.9
LP	267.862	470.17	470.17	444.752	1006.66
HX	8776.24	8776.24	8752.46	10320.6	19073
Component attribute					
MWN		7769.51			15038.7
MWW		110123			80781.1
PDI		14.1737			53.7154
Mass flow, kg/hr	Feed	D201OUT	Slurry	Feed2	D221OUT
*Ethylene conversion to HDPE = 10574.9/(5589.15 +5414.68) = 96.10%					

We use the mass-balance results of Table 5.13 to share a tip to speed up the convergence of some reactor simulations. Previously, we demonstrated in Figure 5.43 to increase the number of maximum iterations to 200. On the same convergence input form of Figure 5.43, we see the "estimate" folder. Based on the mass flow rate of FEED stream to the first reactor D201, and the total mass flow rate of D201OUT and Feed2 entering the second reactor D221, and assuming a C2H4 conversion of 97% to HDPE and a negligible vaporization of HX within the reactor, we can estimate the key component mass flows exiting both reactors in streams D201OUT and D221OUT. See Figure 5.43.

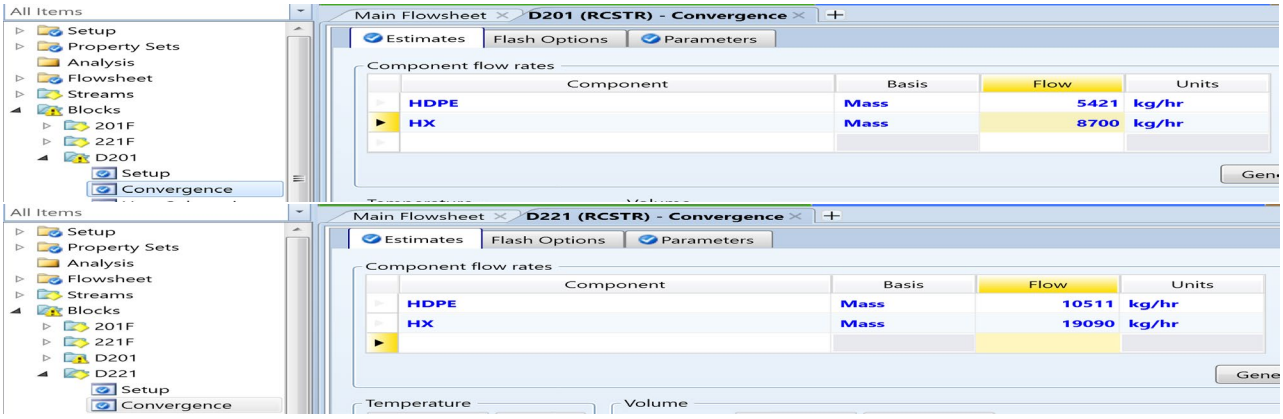

Figure 5.43 Estimate of key component mass flow rates exiting reactors D201 and D221 to speed up convergence of reactor simulations

For the current workshop, we find that adding this mass flow estimates is not necessary, but for more difficult reactor simulation problems (such as the closed-loop simulations below), this approach could speed up the convergence of reactor simulation.

5.6.10 Sensitivity Analysis

We vary the hydrogen flow rate to the second reactor, D221, and investigate its effects on the MWN, MWW and mass flow rate of the HDPE product. See Figures 5.44a to 5.44e. As expected, increasing the hydrogen mass flow rate results in increase in the chair-transfer reactions, and smaller molecular weights MWN and MWW, and HDPE production rate.

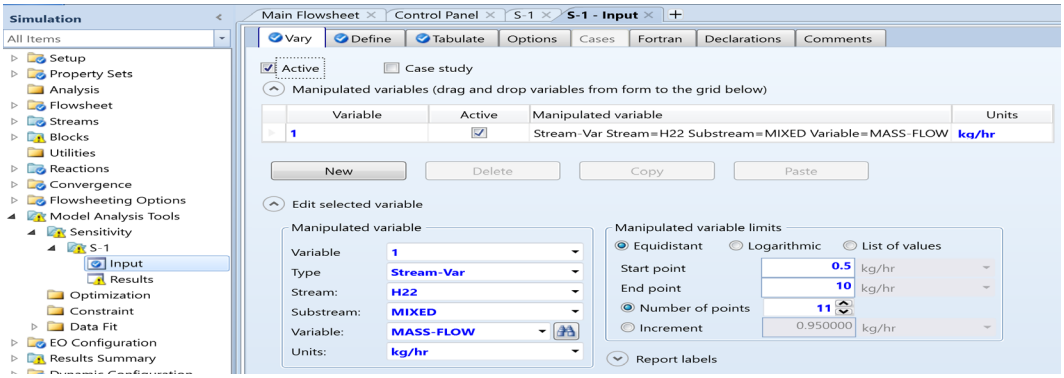

Figure 5.44a Define the independent variable for sensitivity analysis S-1.

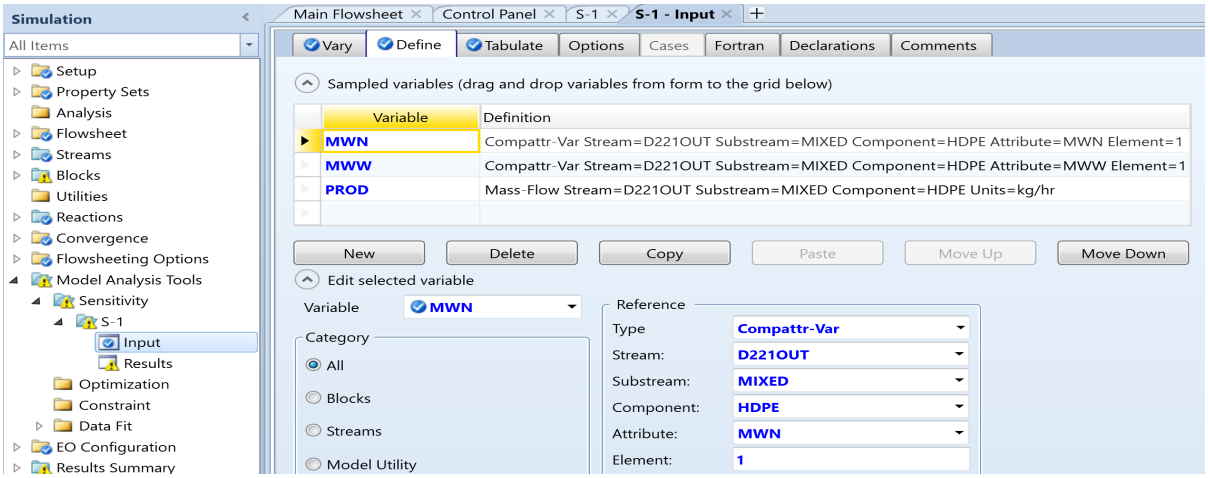

Figure 5.44b Define the dependent variables for sensitivity analysis S-1.

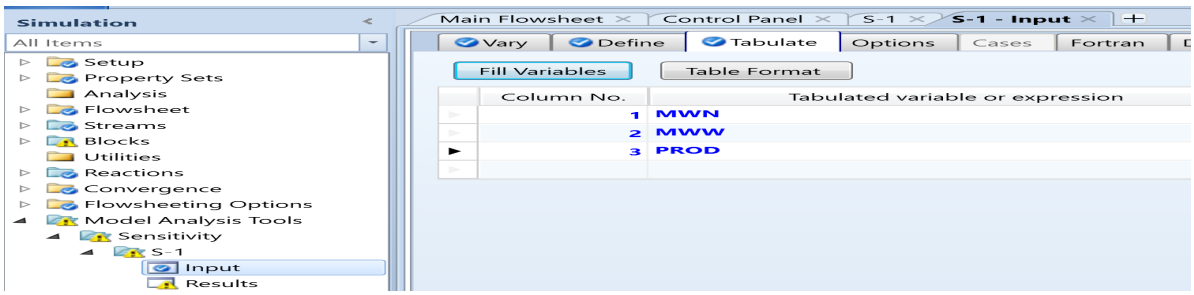

Figure 5.44c Define the display variables for sensitivity analysis S-1.

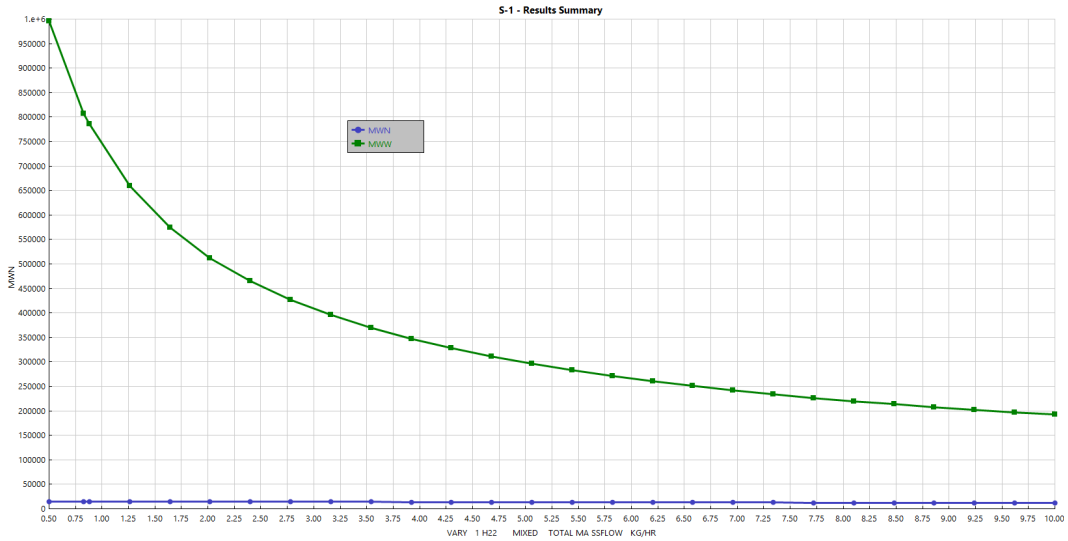

Figure 5.44d Effect of hydrogen inlet flow rate to reactor D221 on the product molecular weights.

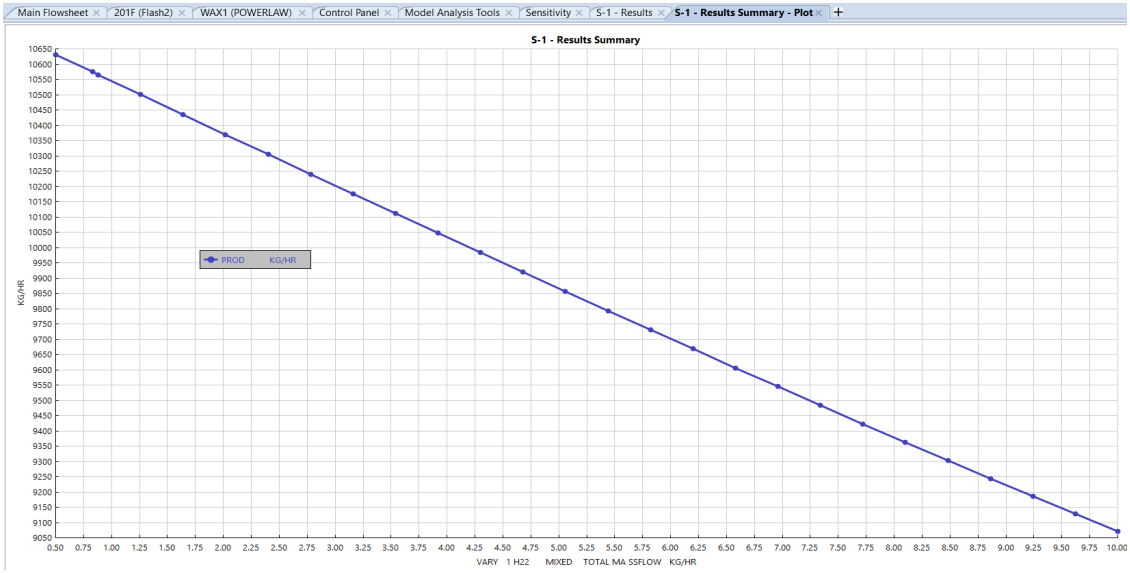

Figure 5.44e Effect of hydrogen inlet flow rate to reactor D221 on the HDPE product mass flow.

5.6.11 Closing the Recycle Loops

We first save the open-loop simulation file, ***WS5.1a Open Loop HDPE.bkp*** as ***WS5.1b Closed Loop HDPE.bkp***, and begin to modify the flowsheet. Specifically, we add two essentially identical recycle loops. This loop includes coolers (exchangers E201 and E221), flash drums (D205 and D225), compressors (C201 and C221), stream splitters (S1 and S2), pumps (P201 and P202), plus makeup hexane steams HX1 and HX4 to flash drums, and HX3 and HX5 to pumps. Figure 5.45 shows the closed-loop flowsheet.

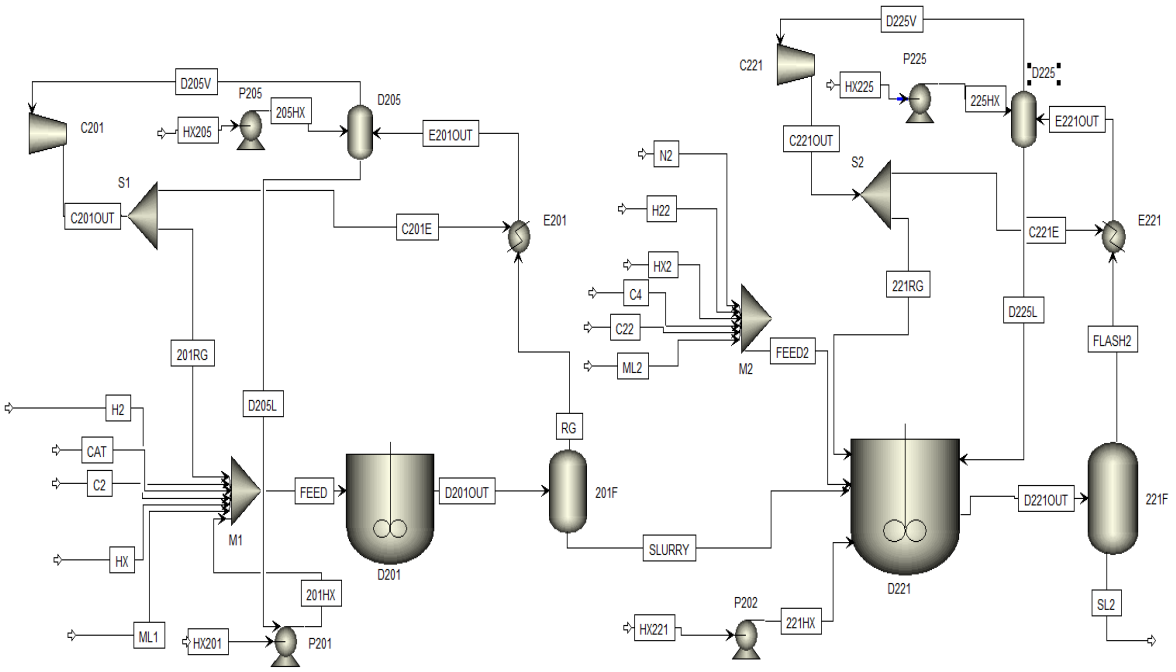

Figure 5.45 A closed-loop flowsheet of the slurry HDPE process.

Table 5.14 specifies the new unit operation blocks. All the HX nakeup streams have a mass fraction of hexane (HX) of 1.0. The mass flow rates are: HX201 - 440 kg/hr, HX205 - 584 kg/hr, HX221 - 115 kg/hr, and HX225- 120 kg/hr (all for HX makeup streams are at 40°C and 1 bar).

Table 5.14 Specifications of unit operations

Equipment	Block names	Specifications
Compressor	C201, C221	Isentropic, discharge pressure =5.8 Bar (C201); 4.37 Bar (C221); isentropic efficiency = 0.8, mechanical efficiency =0.9
Flow splitter	S1, S2	Flow fraction = 0.635 (201RG); 0.5625 (221RG)
Flash drum	D205, D225, 201F,221F	D205: Output temperature= 80°C, 5.8 Bar; D225: 80°C,3.3 Bar. 201F:85°C,3.5 Bar; 221F: 80°C,3.5 Bar
Recycle cooler	E201, E221	Exit temperature = 32°C, Pressure = -0.2 Bar (pressure drop)
Pump	P201,P202,P205, P225	Discharge pressure = 6Bar (P201);3.5 Bar (P202); 5.8 Bar (P205); 3.3 Bar (P225); pump efficiency = 0.6, driver efficiency = 0.9

To speed up the simulation convergence, we follow Figure 5.43 and enter the estimates of key component mass flow rates exiting reactors D201 and D221. We change the flash options of recycle coolers E201 and E221 following Figure 5.46.

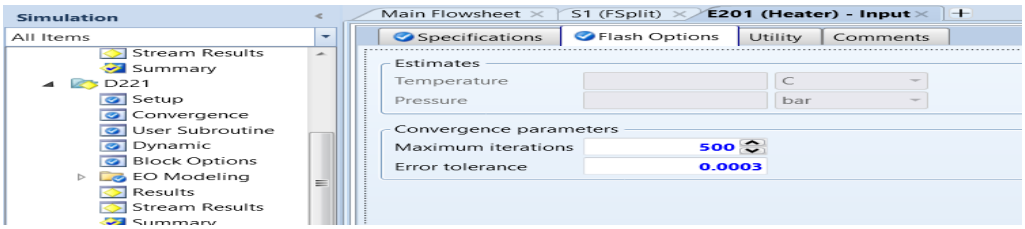

Figure 5.46 Flash option input for recycle cooler E201 (and E221).

We also change the method for tear convergence to Broyden. See Figure 5.47.

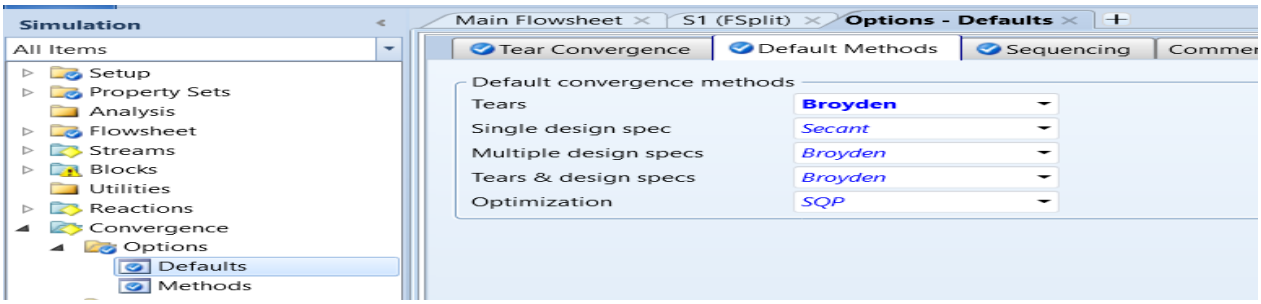

Figure 5.47 Setting the method for tear convergence to Broyden method.

We then run the simulation, which does converge. We save the simulation file as ***WS5.1b HDPE Closed Loop.bkp***. Table 5.15 shows the resulting mass balance of key components and their attributes.

Table 5.15 Simulation results from the closed-loop HDPE flowsheet of Figure 5.45

Stream Name	**Feed**	**Feed2**	**Slurry**	**SL2**
C2H4	5589.14	5414.68	8.442203	66.0835
C4H8	4.53	101.945	4.53	101.761
HDPE	0	0	5028.21	10178.8
LP	267.862	444.752	823.494	1444.41
MWN			25550	51106.9
MWW			214919	291821
PDI			8.41171	57.1002
*Ethylene conversion to HDPE = 10178.8/ (5089.14 +5414.68) = 92.5%				

The resulting ethylene conversion is slightly low. However, this workshop does not involve further validation with plant data to fine-tune the model parameters, such as kinetic parameters, to improve the simulation results.

5.7 Workshop WS5.2: Simulation of Stirred-Bed Gas-Phase PP Process

5.7.1 Objective

The objective of this workshop is to demonstrate how to develop a simulation model for a gas-phase polypropylene using stirred-bed reactors. We model the process based on publically available process patents [37 to 41] and research articles [5,42 to 47]. Unlike slurry and solution processes, no liquid phase is present in the reactors, and only vapor and solids are present. There is also no solvent or liquid

monomer to separate from the polymer, purify and recycle. We show how to develop both open-loop and closed-loop processes.

5.7.2 Process Description

Figure 5.48 shows a simplified diagram of a gas-phase PP process using a stirred-bed reactor [44]. Polymerization takes place in a horizontal stirred-bed reactor that operates between 66 and 75 °C and between 20 and 25 bar [44]. Reactor offgas is condensed, flashed, and returned to the reactor. The vapor recycle enters at various points along the bottom of the bed at a sufficiently low flow rate to avoid bed fluidization. The liquid recycle is sprayed at various locations along the top of the reactor. The vaporizing liquid absorbs most of the exothermic heat of polymerization, allowing for 10 to 15% conversion per pass to maintain a constant reactor temperature [44]. Fresh propylene enters the process at the overhead flash unit. Ethylene also enters here, for copolymerization processes. Fresh hydrogen, used for molecular weight control (chain-transfer agent), enters at the vapor recycle stream. Catalyst deactivation agents may enter the vapor recycle stream also. A small portion of the vapor recycle stream is vented to remove propane and ethane that accumulate in the recycle loop.

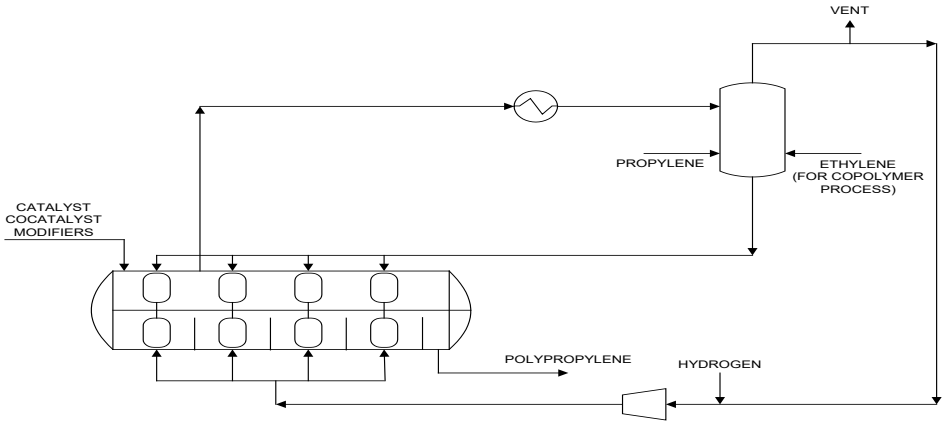

Figure 5.48 A simplified diagram of a gas-phase PP process using a stirred-bed reactor for making a homopolymer [44].

The PP process uses a titanium-based catalyst and an aluminum-alkyl-based cocatalyst. Examples are titanium tetrachloride (TiCl4) and triethyl aluminum [Al-$(C2H5)_3$], respectively [49]. Silane-based tacticity control agents, such as diisobytyldimethoxysilane (DIBDMS) [41], fed with the catalyst, are commonly used to increase the isotactic content of the polypropylene.

The reactor is horizontal and cylindrical and contains several zones that are sometimes separated by weirs. [44] The polymer exists as a powder, given that the reactor temperature remains well below the polypropylene melting point of 157 °C [50]. Paddles connected to a rotating shaft mildly agitate the powder such that there is essentially no backmixing [44]. For the impact polymer process, two reactors are configured in series, and the second reactor incorporates the comonomer. Figure 5.49 shows a simplified diagram of a two-reactor system [5].

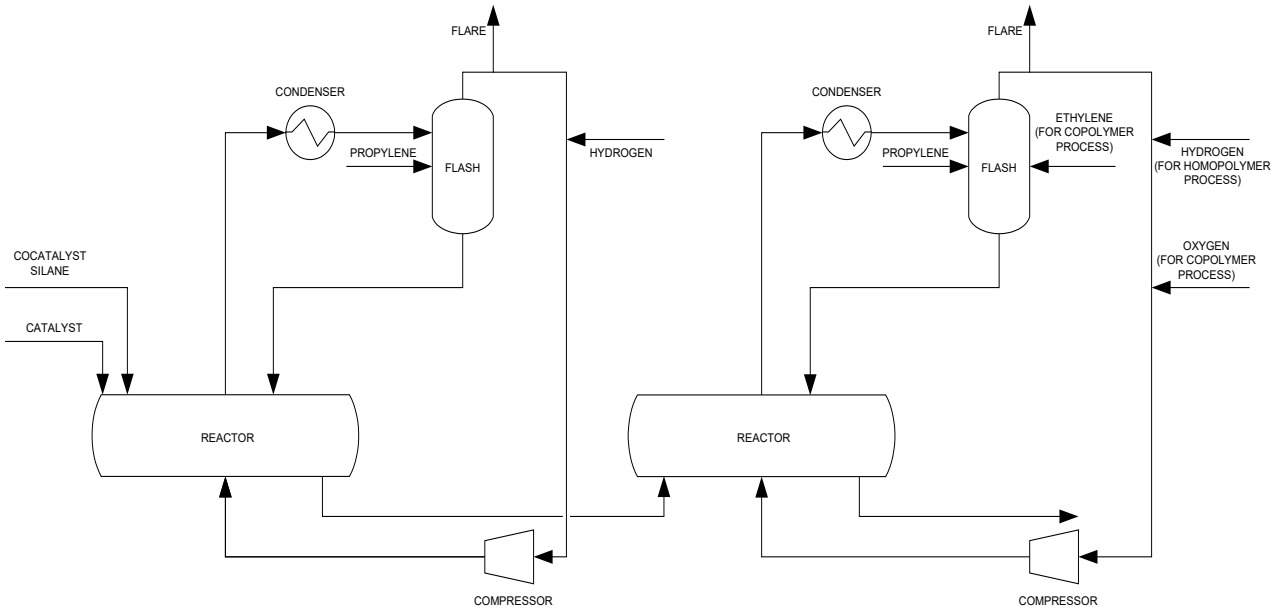

Figure 5.49 A simplified diagram of a gas-phase PP process using two stirred-bed reactors in series for making an impact polymer [5].

5.7.3 Modeling the Stirred-Bed Reactor

During steady-state operation, the polymer level remains constant along the reactor length. The paddles along the reactor agitate the polymer only mildly, and the solids are not fluidized [44]. The polymer phase essentially experiences plug flow conditions along the reactor length. We can simulate the plug flow situation by using several continuous stirred-tank reactors (CSTRs) configured in series. Experimental studies on the residence-time distribution (RTD) of polymers produced in horizontal stirred-bed reactors suggest that the polymer RTD is equivalent to that produced by three to five CSTRs [44]. Figure 5.50 compares the actual reactor to this modeling assumption. In our model, we use four CSTRs to represent the stirred-bed reactor. Other modelers have used this approach as well [45]. Each CSTR receives liquid and vapor recycled from the overhead condenser, which includes fresh monomer and hydrogen. Only the first CSTR receives fresh catalyst and cocatalyst. The temperature and pressure are the same for all zones.

The concept of residence time is significantly different between this situation and that for multiple CSTRs in series. Furthermore, a residence-time calculation requires knowledge of the volumetric holdup in the reactor. We cannot measure the volume holdup very accurately because the paddles are always agitating the polymer and there is a void fraction associated with the solid phase. Therefore, we do not use residence time as a simulation target in the model and instead use reactor mass holdup. In the simulation, we constrain the CSTRs to the same polymer mass to maintain the same level along the bed length. This results in monotonically decreasing residence times for the four CSTRs corresponding to a given stirred-bed reactor, which conforms to reported experimental results [44].

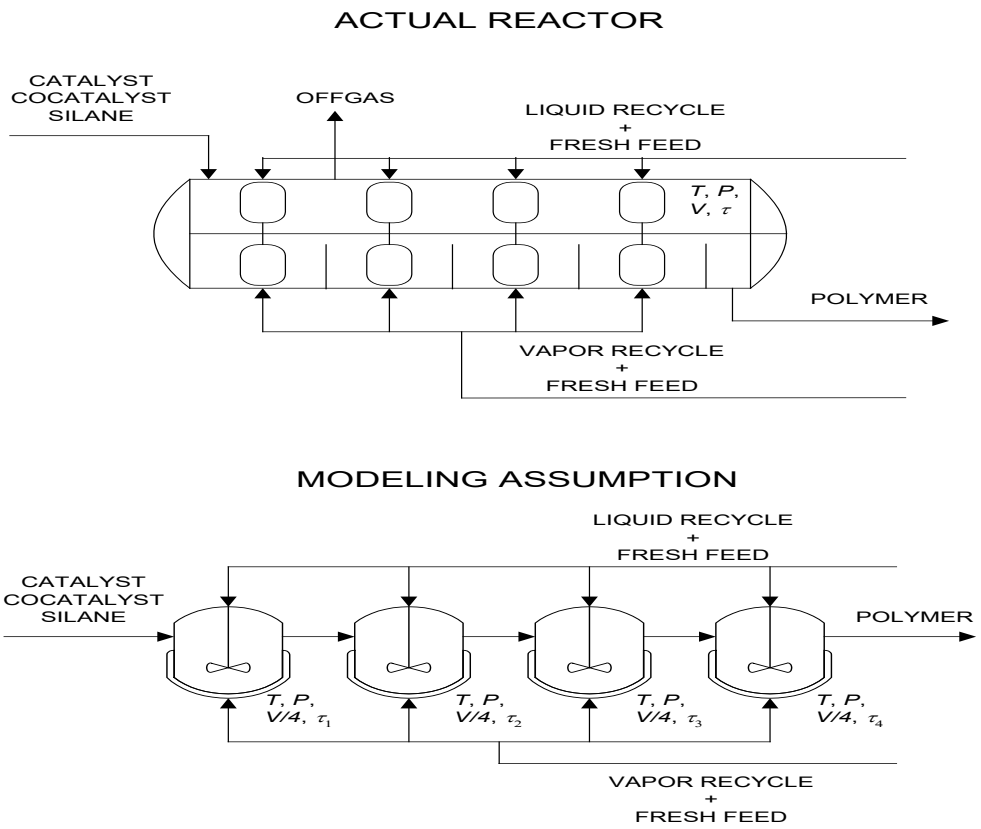

Figure 5.50 Comparison of the actual reactor with the modeling assumption of four CSTRs in series [5].

The relationship between mass holdup and residence time is

Reactor mass holdup =

(Outlet mass flow rate of condensed phase) x (Condensed-phase residence time) (5.11)

We apply this calculation to the final CSTR of each set of four CSTRs to determine the mass holdup for a given stirred-bed reactor.

5.7.4 Process Flowsheet

Figure 5.51a and Figure 51b show the first and second stirred-bed reactors of a two-reactor system for producing a gas-phase PP polymer. These two figures represent an expanded version of Figure 5.49. To close the recycle loops, streams 5 and 5A in Figure 5.51a together with streams 54 and 54a in Figure 5.51b would become a single stream, steam 5 and stream 54, respectively.

In the flowsheets, C1 and C2 are compressors, COND1 and COND2 are condensers, FL1 and FL2 are flash drums, MIC1 to MIX8 are mixers, P1 and P2 are pumps, RSPLT1, RSPLT1, and SPT1 to SPT10 are flow splitters. We save the simulation file for Figure 5.51a and Figure 5.51b as ***WS5.2 PP_Open Loop.bkp***, and go through the current workshop with this file.

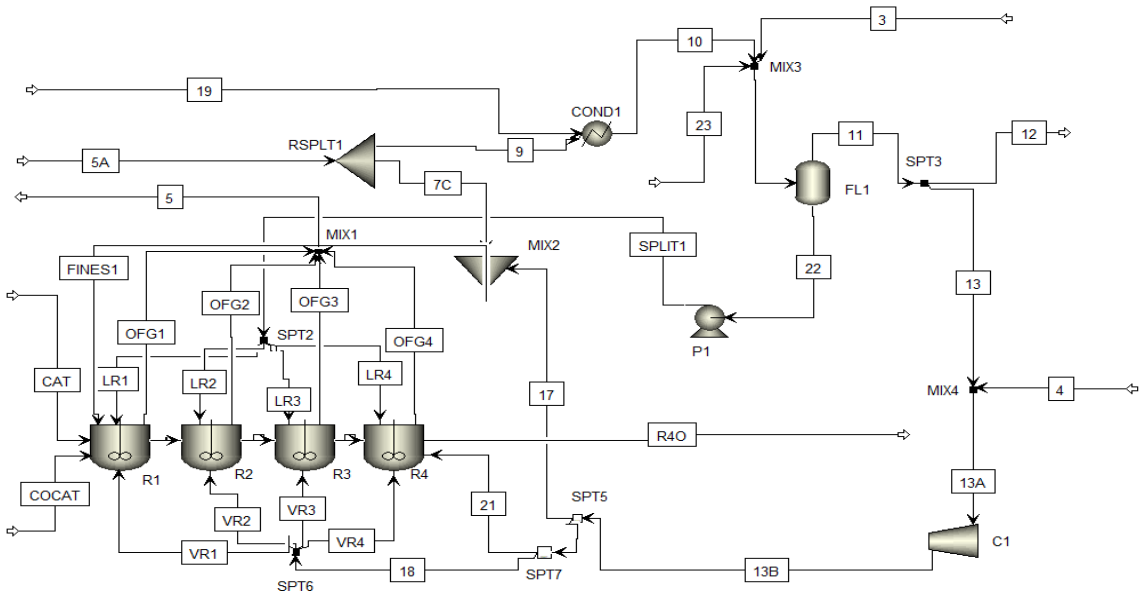

Figure 5.51a The front end of a two-reactor system for producing gas-phase PP polymer using stirred-bed reactors (open-loop).

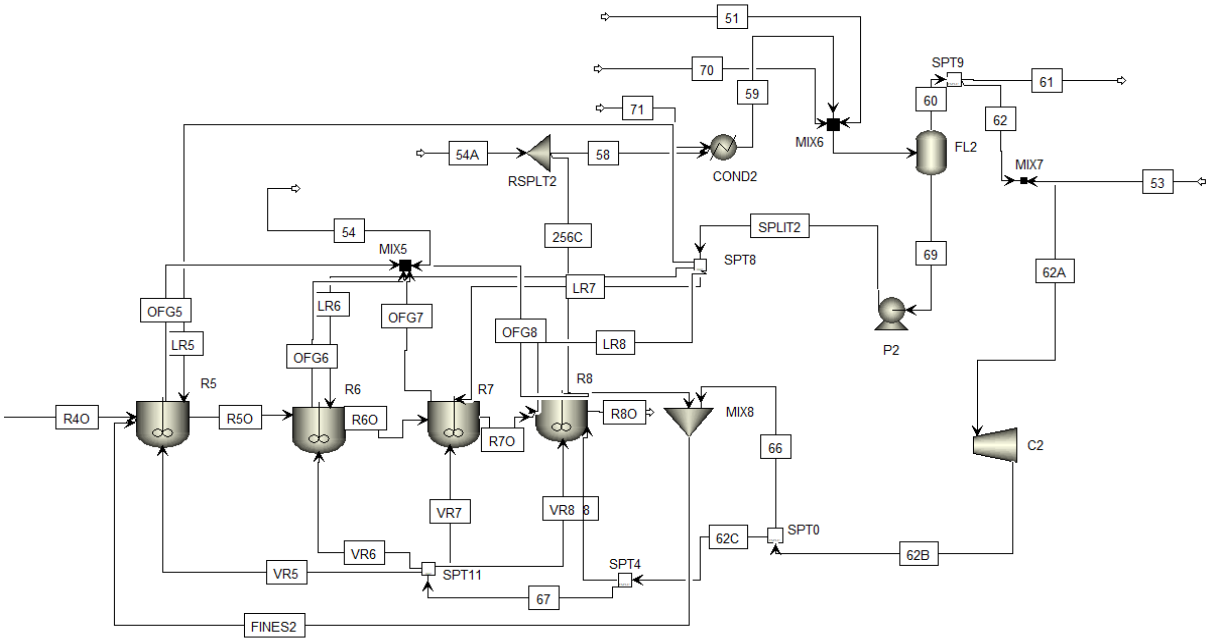

Figure 5.51b The rear end of a two-reactor system for producing gas-phase PP polymer using stirred-bed reactors (open-loop).

5.7.3 Unit System, Components, Characterization of Polymer and Site-Based Species

We use METCBAR unit system for this workshop. Figures 5.52a and 5.52b show the components involved in the gas-phase PP process, and the corresponding enterprise databases selected.

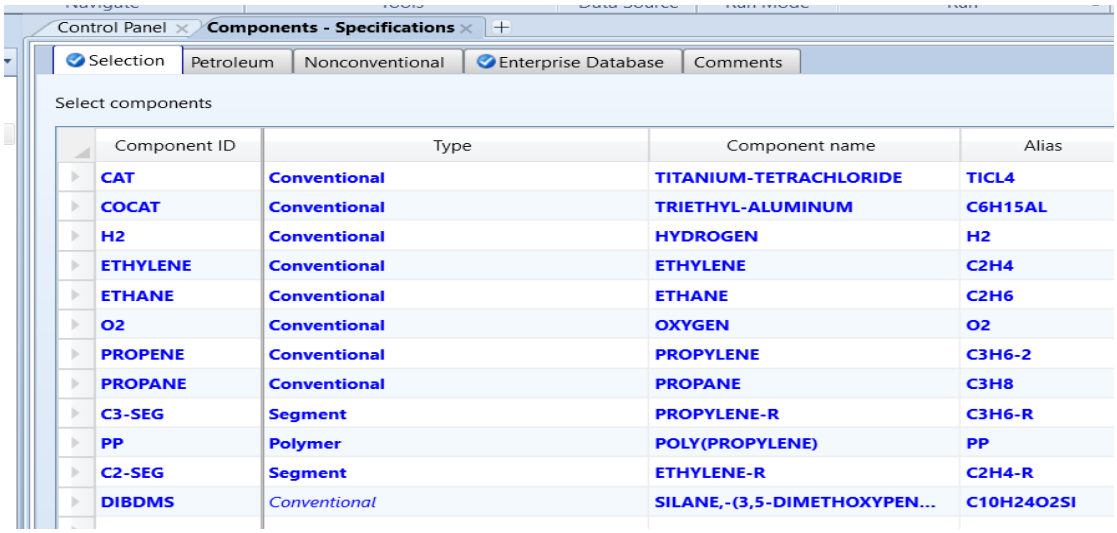

Component ID	Type	Component name	Alias
CAT	Conventional	TITANIUM-TETRACHLORIDE	TICL4
COCAT	Conventional	TRIETHYL-ALUMINUM	C6H15AL
H2	Conventional	HYDROGEN	H2
ETHYLENE	Conventional	ETHYLENE	C2H4
ETHANE	Conventional	ETHANE	C2H6
O2	Conventional	OXYGEN	O2
PROPENE	Conventional	PROPYLENE	C3H6-2
PROPANE	Conventional	PROPANE	C3H8
C3-SEG	Segment	PROPYLENE-R	C3H6-R
PP	Polymer	POLY(PROPYLENE)	PP
C2-SEG	Segment	ETHYLENE-R	C2H4-R
DIBDMS	*Conventional*	SILANE,-(3,5-DIMETHOXYPEN...	C10H24O2SI

Figure 5.52a Component specifications

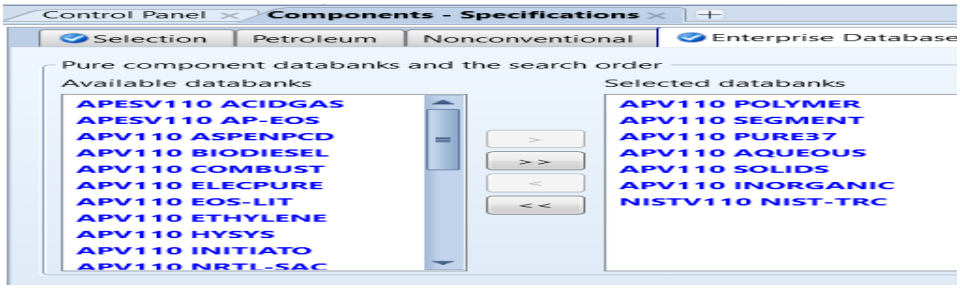

Figure 5.52b Enterprises databases selected.

Propene (propylene) and ethylene are monomer and comonomer, respectively, with each having a repeated segment. TICl4 is catalyst, and TEAL (triethyl aluminum) is cocatalyst. Hydrogen is chain transfer agent, and oxygen is a purge gas. Ethane and propane are impurities. DIBDMS (diisobutyldimethoxysilane) is a tacticity control agent [41]. A search on Chemical Book website (www.chemicalbook.com) gives the molecular structure file, ***17980-32-4.mol***. We import the structure of DIBDMS into our simulation file by following the path: Properties -> Components ->Molecular Structure -> DIBDMS -> Structure and Functional Group -> Structure -> Draw/Import/Edit ->Import -> ***17980-32-4.mol.*** We also define the molecular by its connectivity according to Figure 5.53, which is needed for estimating unknown physical properties. We define the repeated segments of ethylene (R-C2H4) and propene (R-C3H6) following Figure 5.22 and characterize the attributes for Ziegler-Natta polymerization according to Figure 5.23.

To characterize our catalyst following Figure 5.24, we assume four active catalyst sites with a concentration of 0.0012 moles of sites per gm of catalyst [5] that are determined separately from our

deconvolution of GC data according to Section 5.5.2.3 and ***Supplement 5.2.*** We follow Section 5.5.2.2 to do deconvolution analysis and will show the deconvolution results in Section 5.7.6.

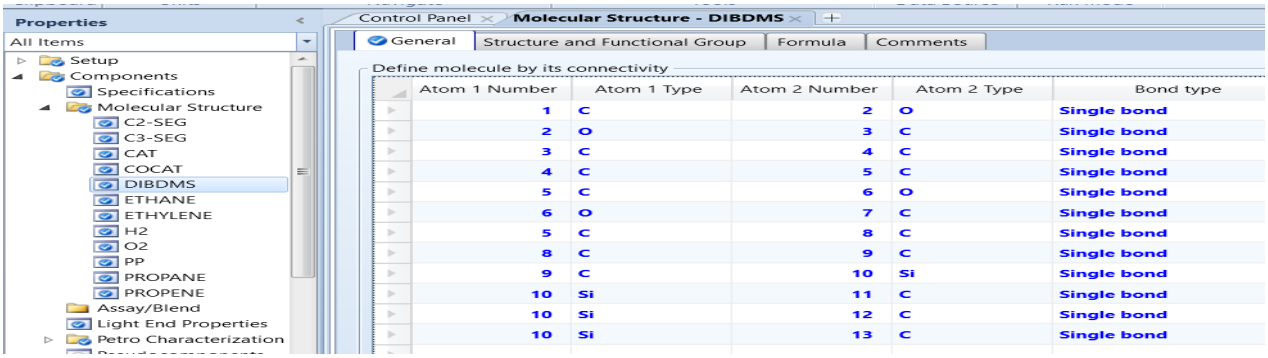

Figure 5.53 Defining structure of DIBDMS (diisobutyldimethoxysilane).

5.7.4 Thermodynamic Model and Parameters

Following the LDPE example in Section 4.5.4, we choose polymer perturbed-chain statistical fluid theory (POLYPCSF) equation of state (Section 2.8) as our thermodynamic method. Based on the original references for POLYPCSF [51,52], the Aspen Polymers Spheripol high impact PP copolymer example [35], our previous article [5], and a search of Aspen Polymers online help on "Parameters (POLYPCSF)", we input the pure component parameters: Properties -> Methods-> Parameters-> Pure Components ->New -> Scalar -> Change name from Pure-1 to PCSAFT -> Enter values as in Figure 5.54.

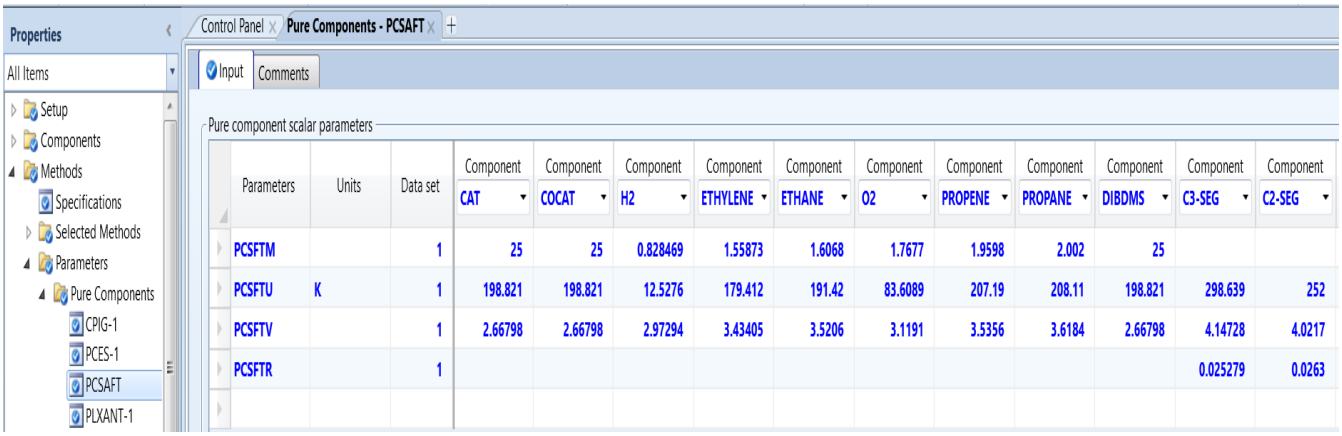

Figure 5.54 POLYPCSF pure component parameters.

Specifically, PCSFTU is the segment energy parameter (K), PCSFTV is the segment diameter (Å), and PCSFTM is the segment number, and PCSFTR, is a ratio parameter reserved for polymers that is equal to PCSFTM (m) divided by the molecular weight of the monomer (M), or m/M. When these parameters are not readily available, Aspen Polymers online help recommends the following default values: (1) PCSFTU = 269.67 K, (2) PCSFTV = 4.072 Å, (3) PCSFTM =0.02434, and (4) PCSFTR = 0.02434*M; M is the molecular weight.

Figure 5.55 shows the parameters for the ideal gas heat capacity, CPIG-1. These parameter values came from references [5,35]. The parameter values for DIBDMS result from applying the estimation tool,

based on the structure of Figure 5.53 by following the path: Properties -> Estimation ->Input -> Setup -> -> Estimation option -> Estimate all missing parameters. After obtaining the estimated parameter values as shown by R-PCES for DIBDMS in Figure 5.55, we change the estimation option to “Do not estimate any parameters”.

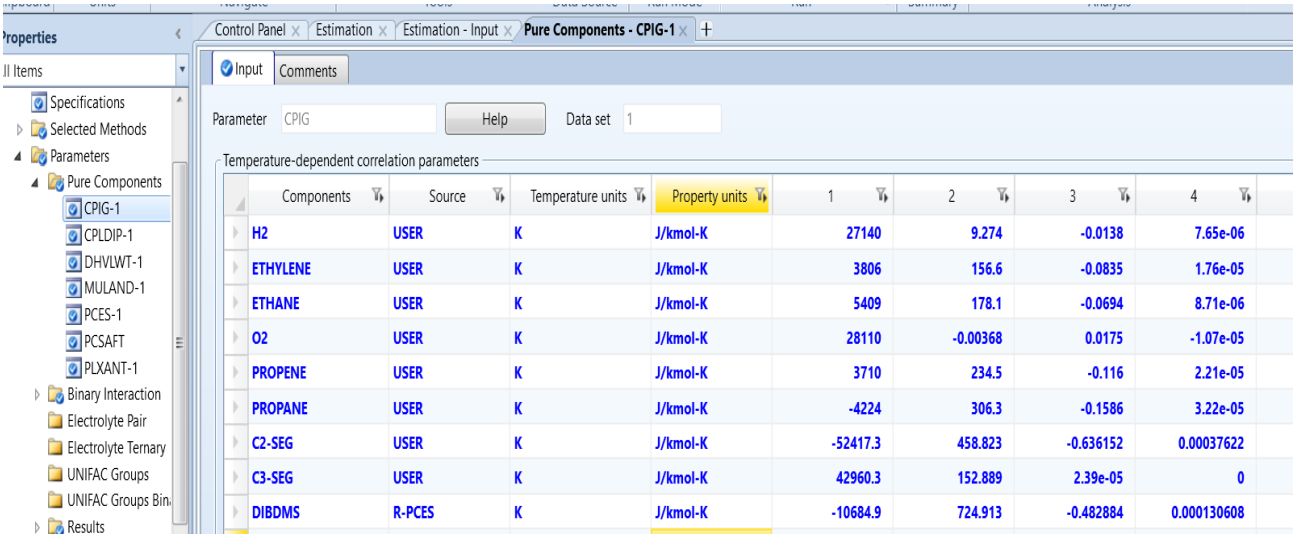

Components	Source	Temperature units	Property units	1	2	3	4
H2	USER	K	J/kmol-K	27140	9.274	-0.0138	7.65e-06
ETHYLENE	USER	K	J/kmol-K	3806	156.6	-0.0835	1.76e-05
ETHANE	USER	K	J/kmol-K	5409	178.1	-0.0694	8.71e-06
O2	USER	K	J/kmol-K	28110	-0.00368	0.0175	-1.07e-05
PROPENE	USER	K	J/kmol-K	3710	234.5	-0.116	2.21e-05
PROPANE	USER	K	J/kmol-K	-4224	306.3	-0.1586	3.22e-05
C2-SEG	USER	K	J/kmol-K	-52417.3	458.823	-0.636152	0.00037622
C3-SEG	USER	K	J/kmol-K	42960.3	152.889	2.39e-05	0
DIBDMS	R-PCES	K	J/kmol-K	-10684.9	724.913	-0.482884	0.000130608

Figure 5.55 User and estimated parameters of ideal gas heat capacity.

Figures 5.56 to Figure 5.58 show the estimated parameters for: (1) the liquid-phase heat capacity (CPLDIP-1) of PP based on the temperature-dependent correlation of the Design Institute for Physical Property Research (DIPPR); (2) Watson heat of vaporization (DHVLWT-1) of PP; and (3) Andrade liquid viscosity (MULAND-1) of PP. By clicking on the “Help” button, we can see the explicit temperature-dependent correlation for each parameter.

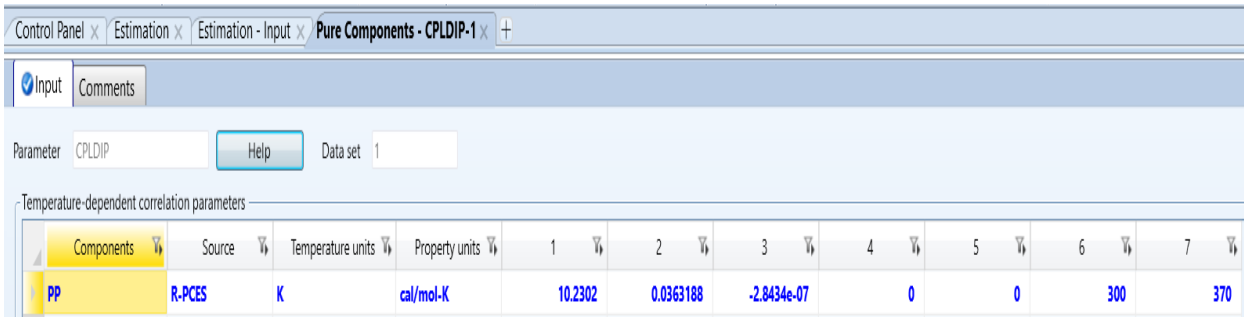

Components	Source	Temperature units	Property units	1	2	3	4	5	6	7
PP	R-PCES	K	cal/mol-K	10.2302	0.0363188	-2.8434e-07	0	0	300	370

Figure 5.56 Estimated parameters of liquid-phase heat capacity of PP.

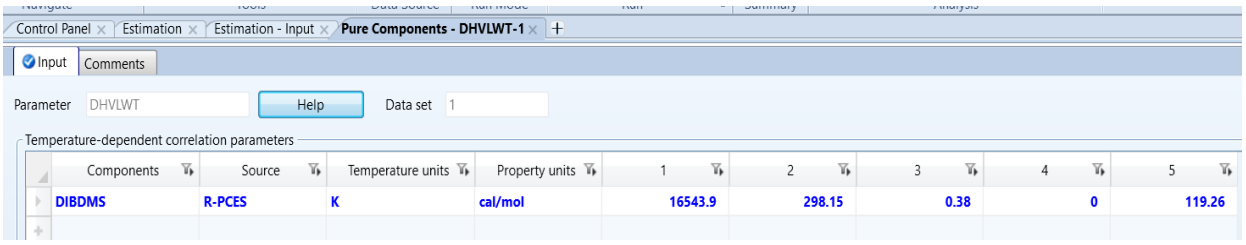

Components	Source	Temperature units	Property units	1	2	3	4	5
DIBDMS	R-PCES	K	cal/mol	16543.9	298.15	0.38	0	119.26

Figure 5.57 Estimated parameters of Watson heat of vaporization of PP.

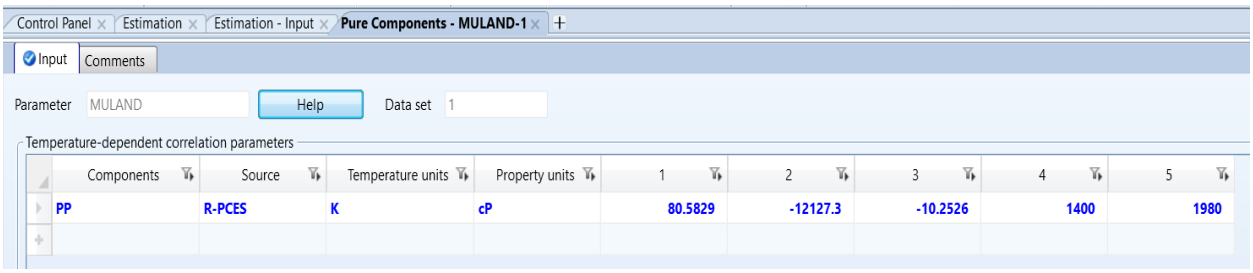

Figure 5.58 Estimated parameters of Andrade liquid viscosity of PP.

Figure 5.59 shows the estimated pure component parameters for DIBDMS and PP.

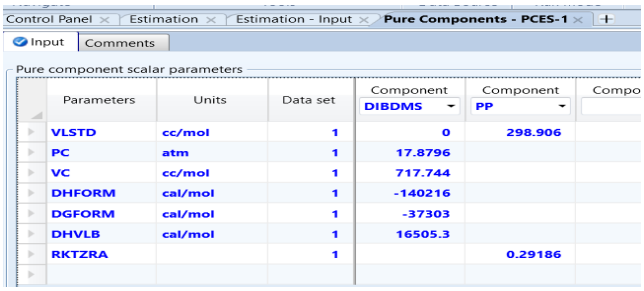

Figure 5.59 Estimated pure component parameters of DIBDMS and PP.

Lastly, following Figure 5.32, we set the first parameter in the T-dependent liquid vapor pressure correlation PLXANT-1 for catalyst TiCl4, and cocatalyst TEAL, and tacticity control agent DIBDMS to a large negative number like -40. This ensures that these three components do not vaporize [36].

5.7.5 Feed Streams

Table 5.16 specifies the feeds to the front end of a two-reactor flowsheet of Figure 5.51a. The last column in the table gives the total mass flows of monomers entering the process in the front end, excluding those through the tear stream 5A.

Table 5.16 Feed streams entering the front-end of the process shown in Figure 5.51a.

Stream	CAT	COCAT	3	4	5A	19	23	Total (excluding 5A)
T(°C)	32	32	32.22	32.22	66.001	129.71	32.22	
P(bar)	26.2	26.2	30.3371	26.545	22	24.4559	30.3371	
Mass flow, kg/hr	1341.9 (total)	344.496	17155.7	0.34	186472	7955.55	359	
CAT	1.7 kg/hr							
COCAT		41.6						
H2			0.34	0.34	12.2083	0.15		
Propene	1333.5	338.5			171191	7485.9	371.119	19375.739
Propane	6.7	1.7			15268.7	469.5	1.88054	569.647
DIBDMS		0.136						

Table 5.17 specifies the feeds to the rear end of a two-reactor flowsheet of Figure 5.51b. The last column in the table gives the total mass flows of monomers entering the process in the front end, excluding those through the tear stream 54A.

Table 5.17 Feed streams entering the rear-end of the process shown in Figure 5.51b.

Stream	**51**	**53**	**54a**	**70**	**71**	**Total**
T(°C)	32	32	66.0009	32	78	(excluding 54a)
P(bar)	30	26	22	30	24	
Mass Flow, kg/hr	6619					
(total)	0.51	116819	226	4010		
H2		0.51 kg/hr	6.68323	0.34	0.267647	
Propene	6584.33		102144	224.816	3471.94	10551.086

We must also specify the site-based species attributes for CAT streams, following Figures 5.33 and 5.34. Figure 5.60 shows our specifications of the site-based attributes for catalyst CAT.

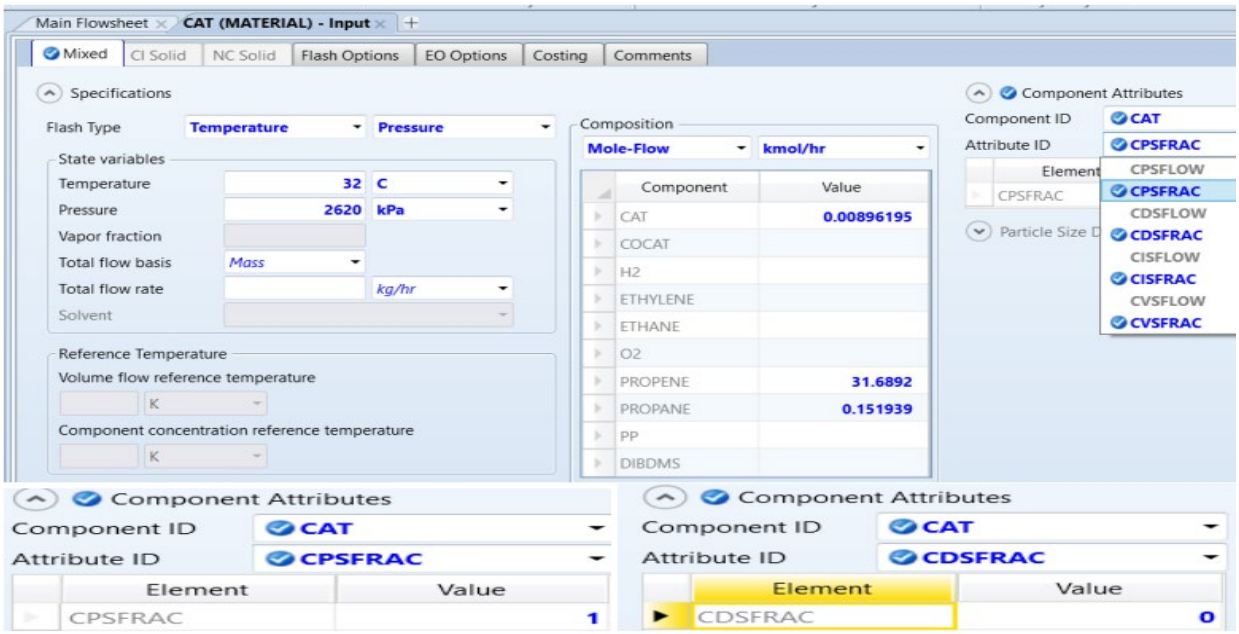

Figure 5.60 Specification of site-based species attributes for CAT stream: Setting potential site mole fraction (CPSFRAC) to one, and the dead site mole fraction(CDSFRAC) to zero. Set the mole fractions for the four inhibited sites (CISFRAC) (S_1 to S_4) to zero, and do the same for the four dead sites (CDSFRAC) (S_1 to S_4).

5.7.6 Ziegler-Natta Kinetics Specifications

Following Figure 5.35, we create a Z-N reaction set, named ZN-PP. Figure 5.61 shows the species specifications of the ZN reactions.

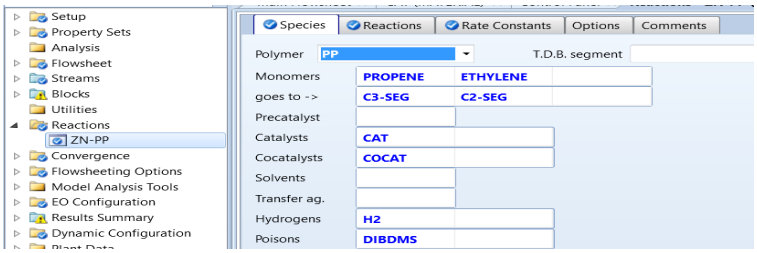

Figure 5.61 Species specifications of ZN-PP reaction set.

Based on deconvolution of GPC data for this process, we specify previously in Section 5.7.3 that the number of active catalysts as 4. ***Supplement 5.2*** gives the details of these 72 reactions, together with the relevant kinetic parameters. These reactions include:

(1) 4 spontaneous catalyst site activation reactions (ACT-SPON), with one reaction per active catalyst site;
(2) 4 catalyst activation reactions (ACT-H2) by hydrogen [53] with one reaction per active catalyst site;
(3) 8 chain initiation reactions by monomer C3H6 and by comonomer C2H4, with two reactions per active catalyst site;
(4) 16 chain propagation reactions (PROP) of reacting polymer chain Pn[C3H6] with C3H6 and C2H4, and reacting polymer chain Pn[C2H4] with C3H6 and C2H4, totaling 4 reactions per active catalyst site;
(5) 16 reactions of chain transfer to monomer (CHAT-MON) by reacting polymer chain Pn[C3H6] with C3H6 and C2H4, and by reacting polymer chain Pn[C2H4] with C3H6 and C2H4, totaling 4 reactions per active catalyst site;
(6) 8 reactions of chain transfer to hydrogen (CHAT-H2) by reacting polymer chain Pn[C3H6] with H2, and by reacting polymer chain Pn[C2H4] with H2, with two reactions per active catalyst site;
(7) 4 spontaneous catalyst deactivation reactions (DEACT-SPON), with one reaction per active catalyst site type;
(8) 8 reactions of deactivation by tacticity control agent DIBDMS by reacting an activated catalyst site $P_{0,i}$ with DIBDMS and by reacting a live polymer chain containing n segments attached to catalyst site i, $P_{n,i}$, with DIBDMS, with i=1 to 4 for four active sites. (Because of the lack of deactivation reaction by agent [DEACT-AGENT] within Aspen Polymers, we use deactivation reaction by poison [DEACT-POISON] to represent these 8 reactions); and
(9) 4 reactions of atactic propagation (ATACT-PROP) with one reaction per active catalyst site.

To specify the reaction rate constants according to the Arrhenius form, Eq. (5.1), we follow the pre-exponential factors k_0 and the activation energy E for each reaction given in ***Supplement 5.3*.**

5.7.7 Specifications of unit operation and chemical reactor blocks

5.7.7.1 Mixers MIX1 to MIX8 (Figure 5.62)

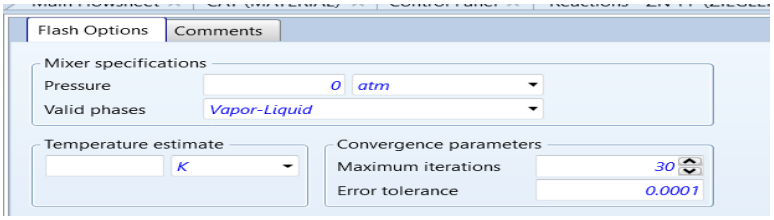

Figure 5.62 Specification of no pressure drop, maximum iterations and error tolerance for MIX1 to MIX8.

5.7.7.2 Reactors R1 to R8 (Figures 5.63 and 5.64)

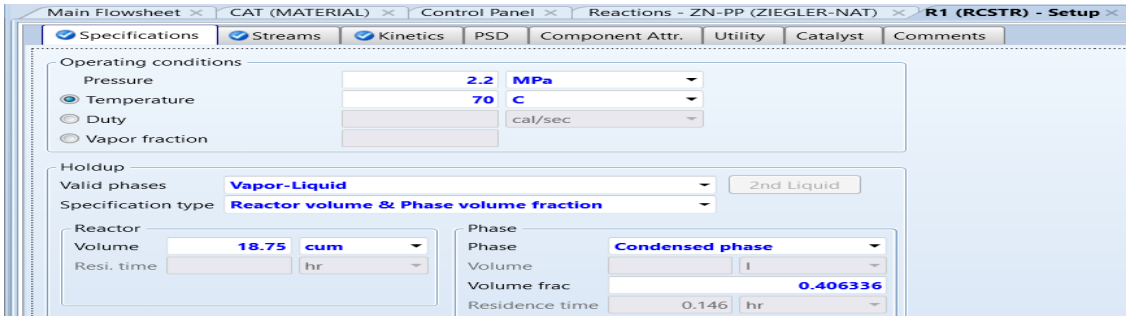

Figure 5.63 Specifications of reactors R1 to R8. For R5 to R8, change the condensed phase volume fraction to 0.408138.

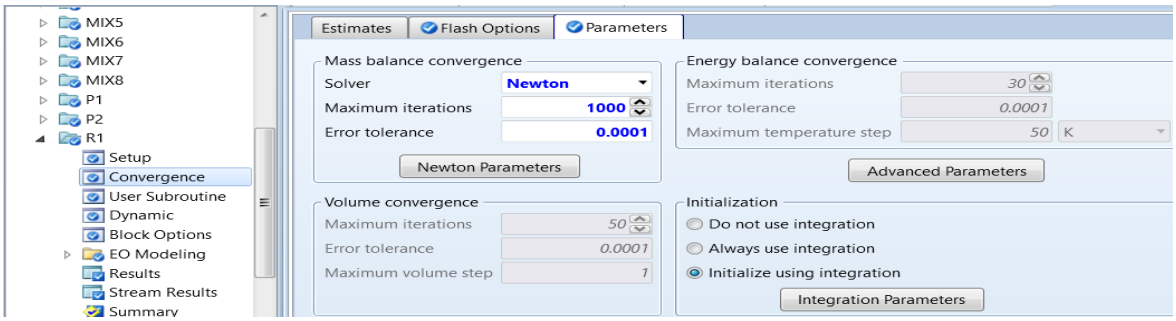

Figure 5.64 Specification of convergence parameters for reactors.

As illustrated in Figure 5.64, we further click on “Newton Parameters”, and specify “Line-Search” under Other (stabilization strategy), as recommended by Aspen Polymers online help for RCSTR convergence.

5.7.7.3 Other Blocks

For flash units, FL1 and FL2, we specify the pressure at 2.04 MPa, and the heat duty at 0 cal/sec (adiabatic). For pumps P1 and P2, we specify a discharge pressure of 2.8 MPa, a pump efficiency of 0.6 and a driver efficiency of 0.9. For compressors C1 and C2, we specify an isentropic operation with a discharge pressure of 2.68 MPa, an isentropic efficiency of 0.8 and a machanucal efficiency of 0.9. For condensers COND1 and COND2, we assume a zero pressure drop; for COND1, we assume an exit temperature of 51.6°C, and for COND2, we specify an exit temperature of 43.5°C. For flow splitters RSPLT1 and RSPT2, we specify the mass flow of stream 7C as 1031.9 kg/hr, and of stream 56C as 984 kg/hr. Table 5.18 specifies the mole split fractions to various streams for flow splitters SPT0 to SPT10.

Table 5.18 Flow splitter specifications.

Flow splitter	Mole split fraction	Stream(s)
SPT1	0.223807	66
SPT2	0.367147, 0.204109, 0.201312	LR1, LR2, LR3
SPT3	0.9999	13
SPT4	0.038	68
SPT5	0.192527	17
SPT6	0.359248, 0.204293, 0.02972	VR1, VR2, VR3
SPT7	0.03859	21
SPT8	0.462916, 0.168904, 0.232728	LR5, LR6, LR7
SPT9	0.9999	62
SPT10	0.204768, 0.232443, 0.230056	VR5, VR6, VR7

5.7.7.4 Convergence blocks

Figure 5.65 specifies the convergence methods under: Convergence ->Options ->Default Methods.

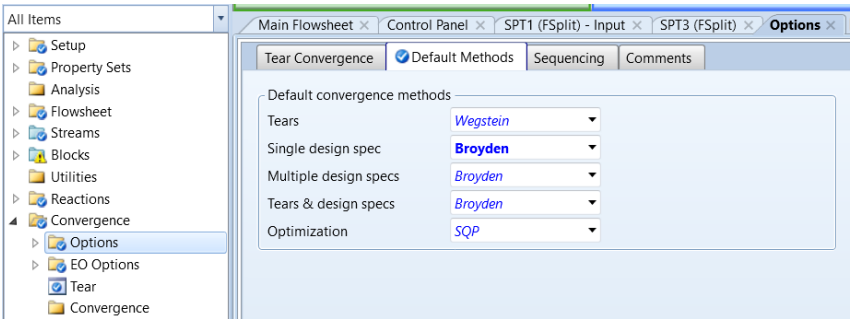

Figure 5.65 Selected convergence methods.

We also fix the number of maximum flowsheet evaluations under: Convergence ->Options -> Methods -> Wegstein -> Maximum flowsheet evaluations= 800.

5.7.8 Open-Loop Simulation Results and Closing the Loop

We run the open-loop simulation, and the simulation converges. Table 5.19 shows the key results of the assumed tear streams 5A and 54A, compute tear streams 5 and 54, and PP product stream R8O in the open-loop flowsheet. We save the converged open-loop simulation file as ***WS5.2 PP_Open-Loop-Converged.bkp.***

Table 5.19 Comparison of assumed and computed tear streams, and result of PP product stream R8O

	5A(assumed)	5(computed)	54A(assumed)	54(computed)	R8O
Temperature, °C	339.151	343.15	339.151	343.15	343.15
Pressure, MPa	21.7123	21.7123	21.7123	21.7123	21.7123
Mass flow, kg/hr					
Propene	171,191	171,616	102,144	104,293	5292.11
Propane	15268.7	15464.7	14668	14827.8	787.452

H2	12.2083	11.9805	6.68323	7,22583	0.0095
PP	0	0	0	0	28,996.8
PP, ATFRAC					0.0384897
MWN					58861.4
MWW					322,183
PDI					5.4736

Based on the last columns of Tables 5.16 and 5.17, we see that the total amounts of propene and propane entering the process are 29,286.83 and 1108.625 kg/hr, which sum together to give the total monomer mass flow of 30,395.455 kg/hr. When compared to the PP production of 28,996.8 kg/hr for stream R8O in Table 5.19, this gives a monomer conversion of 95.398% for the open-loop simulation.

Referring to the open-loop flowsheets of Figures 5.51a and 5.51b, we close the loop by deleting the assumed tear stream 5A entering the flow splitter RSPLIT1 and replacing it by the computed tear stream 5 in Figure 5.51a. We also delete the assumed tear stream 54A entering the flow splitter RSPLIT2 and replace it by the computed tear stream 54 in Figure 5.51b. The resulting closed-loop flowsheets appear in Figures 5.66a and 5.66b.

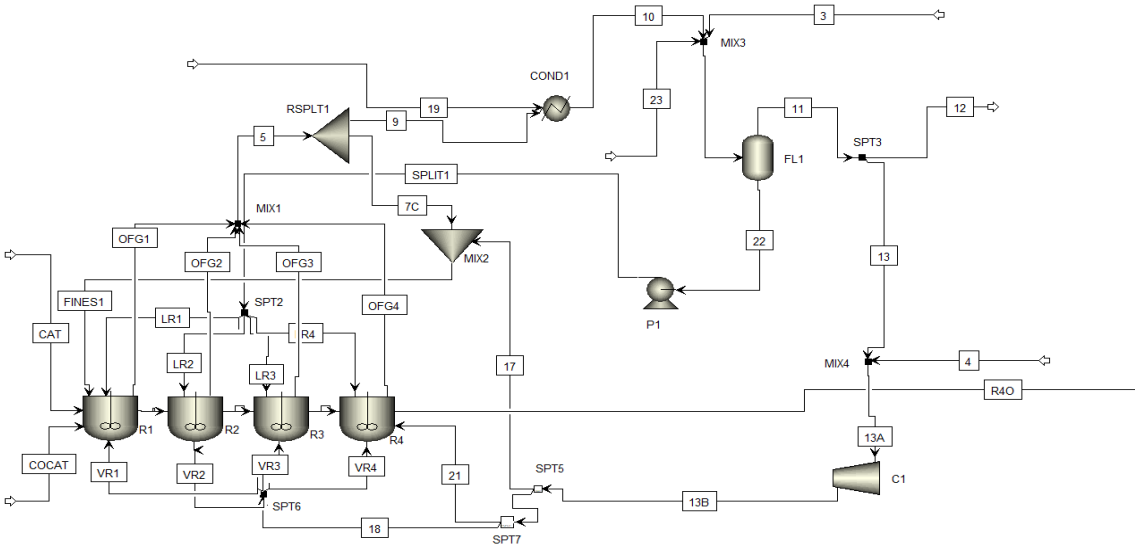

Figure 5.66a The front end of a two-reactor system for producing gas-phase PP polymer using stirred-bed reactors (closed-loop).

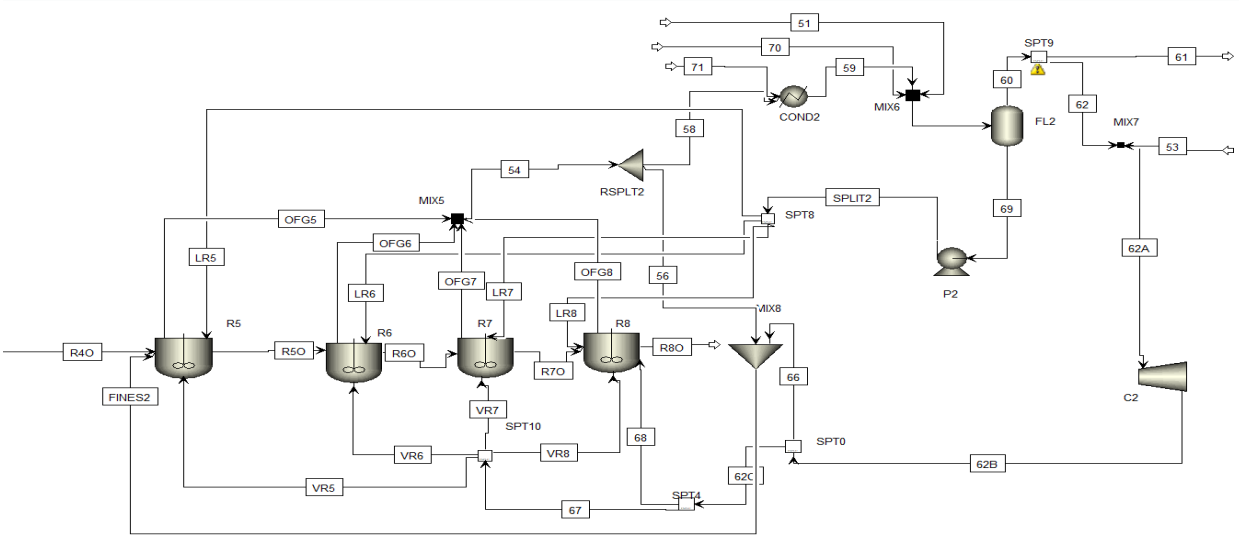

Figure 5.66b The rear end of a two-reactor system for producing gas-phase PP polymer using stirred-bed reactors (closed-loop).

Without changing other inputs and convergence parameters, we run the closed-loop simulation, and it converges. Table 5.20 compares the results of both open-loop and closed-loop simulations for the PP product stream R8O. We save the converged closed-loop simulation file as ***WS5.2 PP_Closed-Loop-Converged.bkp.***

Table 5.20 A comparison of open-loop and closed-loop simulation results

	Total monomer feed, kg/hr	**R8O (Open-Loop)**	**R8O (Closed-Loop)**
Temperature, °C		343.15	343.15
Pressure, MPa		21.7123	21.7123
Mass flow, kg/hr			
Propene	29286.83	5292.11	5487.4
Propane	1108.625	787.452	573.331
H2	14.3259	0.0095	0.0171
PP	0	28,996.8	29210.7
PP, ATFRAC		0.0384897	0.1359211
MWN		58861.4	69990.8
MWW		322,183	415,064
PDI		5.4736	5.93

5.7.9 Model Applications

We re-save the simulation file, ***WS5.2 PP_Closed-Loop-Converged.bkp***, as ***WS5.2a PP_Closed-Loop-PP Production vs TICL4 Mass Flow.bkp***, and use sensitivity analysis to quantify the effect of the mass flow rate of catalyst CAT (=$TiCl_4$) on the PP production, and the resulting MWN, MWW and PDI. Figures 5.67a and 5.67b show the manipulated variable ("Vary") and the dependent variables ("Define") for th analysis.

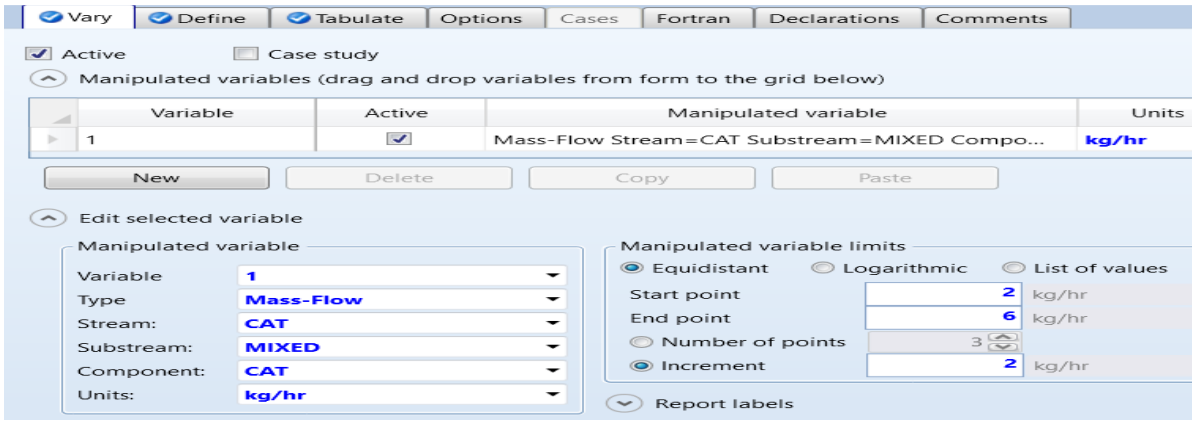

Figure 5.67a Define the manipulated variable of the sensitivity analysis

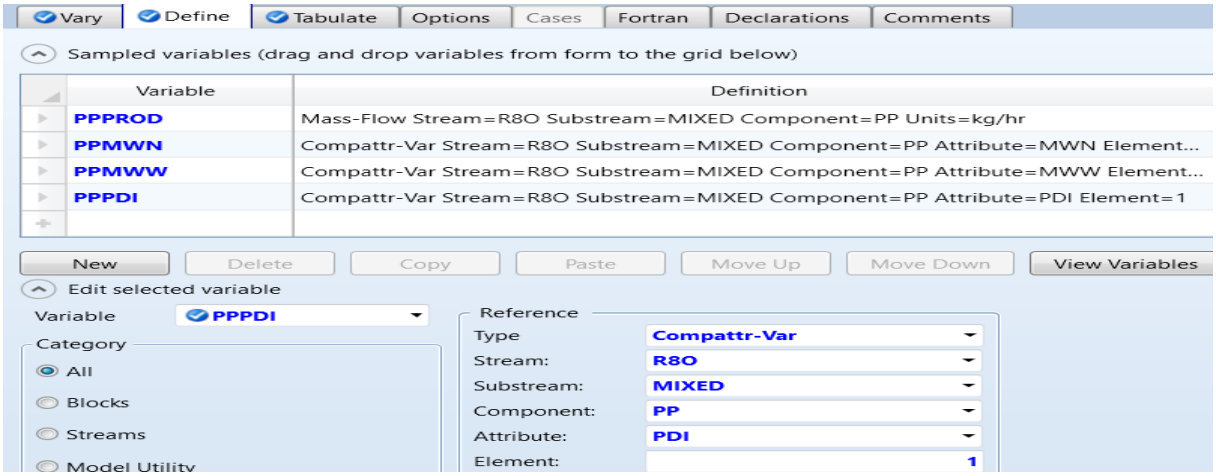

Figure 5.67b Define the dependent variable of the sensitivity analysis

Figures 5.68 and 5.69 illustrate the effects of the catalyst mass flow on the PP production (kg/hr), and on the resulting MWN and MWW.

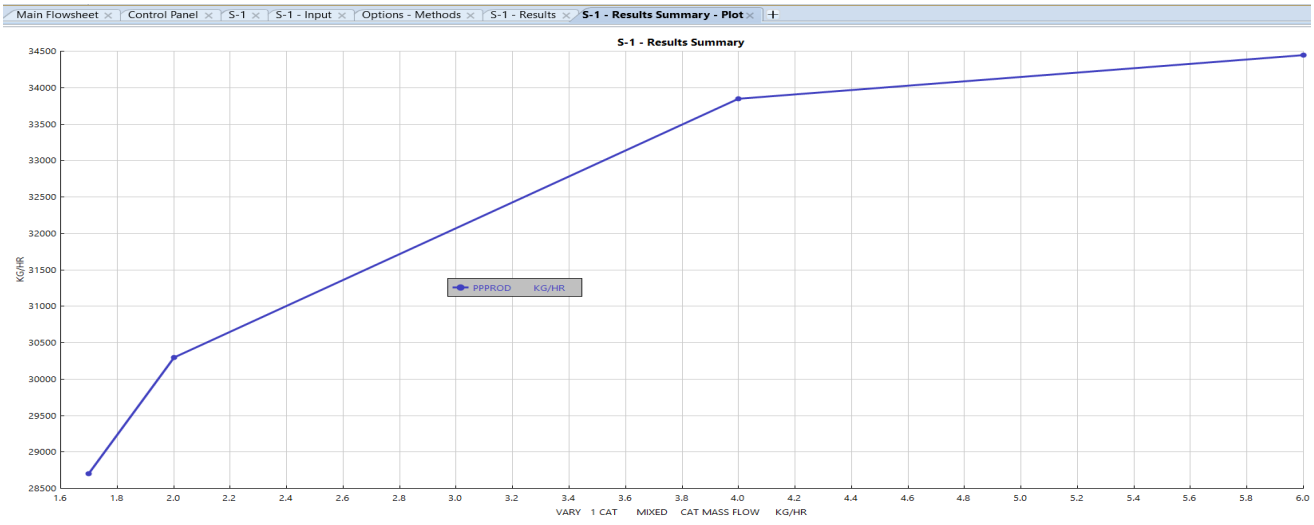

Figure 5.68 Effect of catalyst mass flow rate on the PP production.

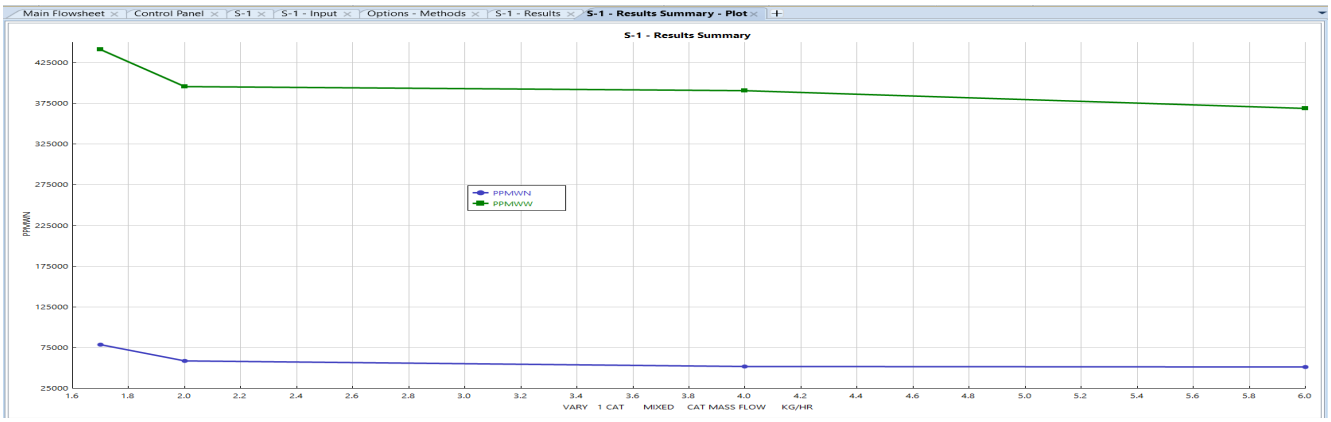

Figure 5.69 Effect of catalyst mass flow rate on the MWN and MWW of PP.

5.8 Workshop WS5.3: Simulation of a Gas-Phase Fluid-Bed LLDPE Process with Condensed Mode Cooling

5.8.1 Objective

The objective of this workshop is to present the details of a steady-state simulation model of a gas-phase fluidized-bed process for producing LLDPE with condensed mode cooling. Previously, we showed in Figure 5.8 a simplified flowsheet of the gas-phase fluidized-bed process for producing PP [27] and LLDPE [23,25], and present in ***Supplement 5.1f*** the kinetic model for a LLDPE process. In this workshop, we demonstrate how to develop such a steady-state simulation model for LLDPE based on the literature [54]. In Section 7.8, we will further demonstrate the dynamic and control aspects of this LLDPE process.

An objective of this workshop is to introduce the concept of condensed mode cooling [55 to 47] to ethylene polymerization in fluidized-bed reactors. We use plant data from a UNIPOL fluidized-bed process for producing LLDPE in the Asia-Pacific and validate the model with plant data from two product grades.

5.8.2 Condensed Mode Cooling in Ethylene Polymerization in a Fluidized-Bed Reactor

U. S. patents 454399A and 4588790 [55,56] present the concept of condensed mode cooling in ethylene polymerization in a fluidized-bed reactor (FBR). According to [55], condensed mode cooling in a FBR for an exothermic polymerization reaction cools the recycle stream to below its dew point and returns the resulting two-phase fluid stream to the reactor in order to maintain the fluidized bed at a desired temperature above the dew point of the recycle stream. This can increase the yield of polymer production, among other significant benefits. McKenna [57] presents a comprehensive 27-page review and detailed analysis of condensed model cooing in ethylene polymerization. He illustrates the concept of condensed mode cooling with a flowsheet shown in Figure 5.70. We summarize his basic analysis below.

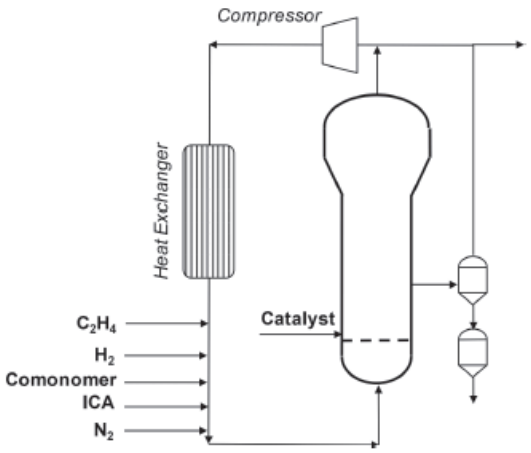

Figure 5.70 An illustration of a fluidized-bed reactor (FBR) system for ethylene polymerization under condensing mode operation [57]. In the figure, ICA represents an induced condensing agent.

First, we note that heat removal is the number one factor limiting the production rate of polyethylene on an industrial scale. For a fluidized-bed polymerization reactor system producing LLDPE and PP, such as the UNIPOL process of Figure 5.8 with modeling details in ***Supplement 5.1e***, McKenna [57] notes that the melting point of a typical LLDPE is on the order of 110°C, and a typical reactor operating temperature is 85°C to 95°C. Therefore, we have a very little margin for error in terms of heat removal. To understand the tools available for maximizing the heat removal, we present a simple enthalpy balance around a gas-phase FBR by McKenna [57] below.

$$F_{g,in}C_{pg,in}(T_{g,in} - T_{ref}) - F_{g,out}C_{pg,out}(T_{g,out} - T_{ref}) - F_{s,out}C_{ps,out}(T_{s,out} - T_{ref}) - UA(T_R - T_W) - Q_{vap} + R_p V_R(-\Delta H_p) = 0 \quad (5.14)$$

In the equation:

$F_{g,in}$ and $F_{g,out}$ = the inlet and outlet mass flow rates of process gas stream

$F_{s,out}$ = the outlet mass flow rate of the solid polymer stream

$C_{pg,in}$, $C_{pg,out}$ and $C_{ps,out}$
= the heat capacities of the inlet and outlet process gas stream, andof the solid polymer stream

$T_{g,in}, T_{g,out}, T_{s,out}$ and T_{ref} = the temperatures of the inlet and outlet proces gas stream, of the outlet solid polymer stream, and the reference temperature for the calculation of the enthalpy

U= the overall heat transfer coefficient

A = the surface area of contact between the reactor wall and the powder bed

T_R and T_W = the average teperatures of the reactor bed and the bed wall

Q_{vap} = the total enthalpy of change due to evaporation of any liquid in the reactor

R_p = the rate of reaction per unit volume of the reactor bed

V_R = the vuolume of the reactive bed

ΔH_p =the overall enthalpy of polymerization

McKenna [57] further assumes that $T_{ref} = T_R = T_{g,out}$, together with the following simplifications:

(1) The solid leaves the reactor at the same temperature as the gas

(2) The reactor is operating at a steady state with a uniform temperature T_R

(3) The enthalpy of the catalyst feed stream is negligible with respect to other streams;

(4) There are no significant heat losses.

With these assumptions and simplifications, we can rearrange Eq. (5.14) to give

$$R_p V_R = \frac{F_{g,in} C_{pg,in}(T_R - T_{g,in}) + UA(T_R - T_W) + Q_{vap}}{-\Delta H_p} \qquad (5.15)$$

What can we learn from this defining relationship for maximizing our polymer production rate, $R_p V_R$?

(1) The reactor temperature T_R $(85° \text{ to } 95°C)$ has a very narrow operating range for producing LLDPE, as the melting temperature of LLDPE is about 110°C and higher bed temperature tends to promote softening and sticking of the polymer particles.

(2) It is difficult to increase the overall heat transfer coefficient between the reactor wall and the powder bed. Increasing the gas velocity through the reactor may cause changes to the fluidizing medium.

(3) This basically leaves changes to the heat capacity $C_{pg,in}$ of the inlet process gas stream and to the total enthalpy due to evaporation of any liquid in the reactor Q_{vap} as our manipulative variables for maximizing the polymer production.

The conclusion is that we can use the composition and phase conditions of the feed stream (only the inert components obviously) to increase the amount of heat that can be removed, thus increasing the polymer production rate.

As illustrated in Figure 5.70, the feed to the bottom of the reactor below this distributor plate is composed of ethylene (monomer), nitrogen (inert), comonomer, hydrogen (chain transfer agent) and at least one *induced condensing agent (ICA)* that is a partially liquefied, chemically inert species. An ICA is typically an alkane. Isomers of butane, pentane and hexane appear to be most common, as referred to in the original patents [55,56]. McKenna [57] presents the data in Table 5.21 to suggest a guideline for the selecting an ICA.

Table 5.21 Capacities of gaseous ICA components commonly used in the polymerization of ethylene

ICA Component	Nitrogen	Propane	n-butane	Iso-butane	n-pentane	Iso-pentane	n-Hexane
Heat capacity[a]	7.0	17.4	23.3	23.1	28.6	28.4	34.5
Heat of Vaporization[b]		4.8	5.8	5.1	6.6	6.5	7.6

ICA solubility in LLDPE[c]		0.29	0.94	0.77	1.83	1.63	2.85
a: At 25°C, cal/K-mol. b: At 25°C, Kcal/mol. c: At 90° and 1.72 bar, g ICA per 100 g LLDPE (density = 0.918 g/cm3)							

If we consider replacing nitrogen as an inert alkane, such as iso-pentane, the heat capacity of the gas phase will increase. In addition, the solubility of a species in the amorphous polyethylene increases (longer, less branches), so does its heat of vaporization. Mckenna and his colleagues [59] present a detailed analysis of using n-hexane as an ICA in the production of LLDPE. In the commercial gas-phase fluidized-bed process for producing LLDPE that we simulate in this workshop, the ICA is iso-pentane.

5.8.3 Process Flowsheet

Figure 5.71 shows a simulation flowsheet for the gas-phase fluidized-bed reactor system of a UNIPOL process for producing LLDPE. In Section 5.3.1, we discuss that the high recycle ratios of the recycle gas lead to uniform temperature and low concentration gradient in the FBR, making it reasonable to represent the FBR as a CSTR. We note that the flowsheet includes two essentially identical sections with the suffix letters for stream and block names being different. We use suffix letters A and B in the stream and block names to indicate product grades A and B. Including both sections in the same simulation flowsheet enables us to identify a single set of kinetic parameters to match the production targets for both product grades with different feed component mass flow rate and compositions. We save the simulation file as ***WS5.3 LLDPE.bkp.***

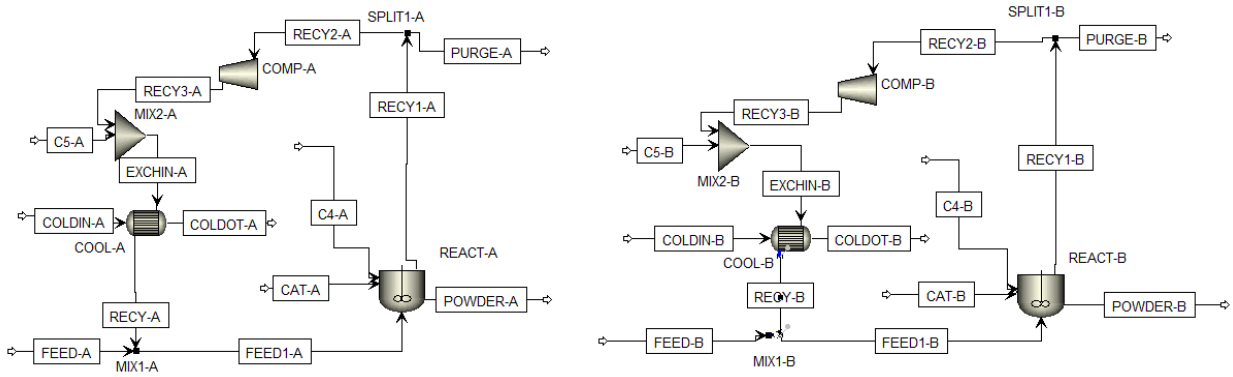

Figure 5.71 A simulation flowsheet of a gas-phase fluidized-bed reactor system for a UNIPOL process for producing LLDPE with condensed model cooling

5.8.4 Unit System, Components, Characterization of Oligomer, Polymer and Site-Based Species

We use METCATM unit system for this workshop by starting with new unit set named METCATM based on the MET unit set, and replacing the pressure unit from N/sqm to atm. Figures 5.72 shows the components involved.

Component ID	Type	Component name	Alias
E2	*Conventional*	ETHYLENE	C2H4
E-SEG	Segment	ETHYLENE-R	C2H4-R
BUTENE	*Conventional*	1-BUTENE	C4H8-1
B-SEG	Segment	1-BUTENE-R	C4H8-R-1
CAT	*Conventional*	TITANIUM-TETRACHLORIDE	TICL4
CCAT	*Conventional*	TRIETHYL-ALUMINUM	C6H15AL
LLDPE	Polymer	POLY(ETHYLENE)	PE
OLIGOMER	Oligomer		
IC5	*Conventional*	2-METHYL-BUTANE	C5H12-2
H2	*Conventional*	HYDROGEN	H2
CO	*Conventional*	CARBON-MONOXIDE	CO
N2	*Conventional*	NITROGEN	N2
H2O	*Conventional*	WATER	H2O

Figure 5.72 Component specifications for the LLDPE process

Ethylene (E2) and 1-butene (C4) are monomer and comonomer, respectively, with each having a repeated segment. Catalyst CAT is TICl4, and cocatalyst COCAT is triethyl aluminum. IC5 (iso-pentane or 2-methyl butane) is an induced condensing agent (ICA). Hydrogen is chain transfer agent, and CO is a poison. N2 is an inert, and water is a cooling medium. Following the path, Properties -> Components-> Polymers -> Characterization -> Oligomers, we define OLIGOMER according to Figure 5.73.

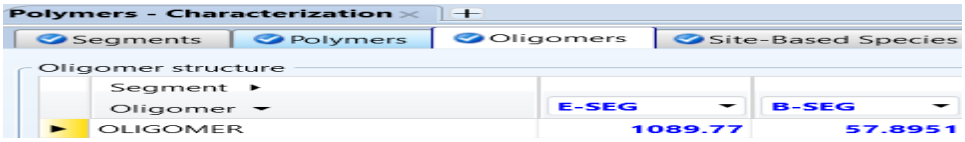

Figure 5.73 Specification of oligomer.

We follow Figures 5.22 and 5.23 to specify the repeat segments, E-SEG and B-SEG, and choose the same built-in Ziegler-Natta attributes for LLDPE. Figure 7.54 specifies the site-based species.

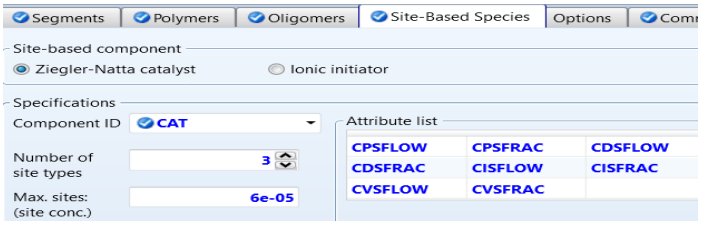

Figure 7.74 Specification o site-based species

In the following section, we give details of our deconvolution analysis of GPC data to determine the specification of three active catalyst sites.

5.8.5 Deconvolution Analysis of GPC Data to Determine the Number of Active Catalyst Sites

In Section 5.5.2.3, we explained how to follow the detailed instructions in Supplement 5.2, to apply a deconvolution Excel spreadsheet, ***Excel for deconvolution.xls***, to determine the number of active catalyst sites. Refer to the example file folders for Chapter 5, WS5.3, we see the GPC data for product grades A and B, ***Log(MW) versus d(wt)/d (log MW),*** where wt is the weight fraction of the slice, and MW is molecular weight of the slice. Following the step-by-step instructions of Supplement 5.2, we do deconvolution analysis of the GPC data assuming 3 and 4 active catalyst sites. See the resulting Excel files, ***WS5.3_Grade A_3 sites.xls, WS5.3_Grade A_4 sites, WS5.3_Grade B_3 sites.xls, WS5.3_Grade***

B_4 sites, in the example folder. Figures 7.75a and 7.75b compare the resulting plot of molecular weight distribution (MWD) and MWDs of individual catalyst sites for grade A, assuming three and four catalyst sites. Note the negative fractional area between the MWD and the x-axis for four catalyst sites. Therefore, we choose three catalyst sites.

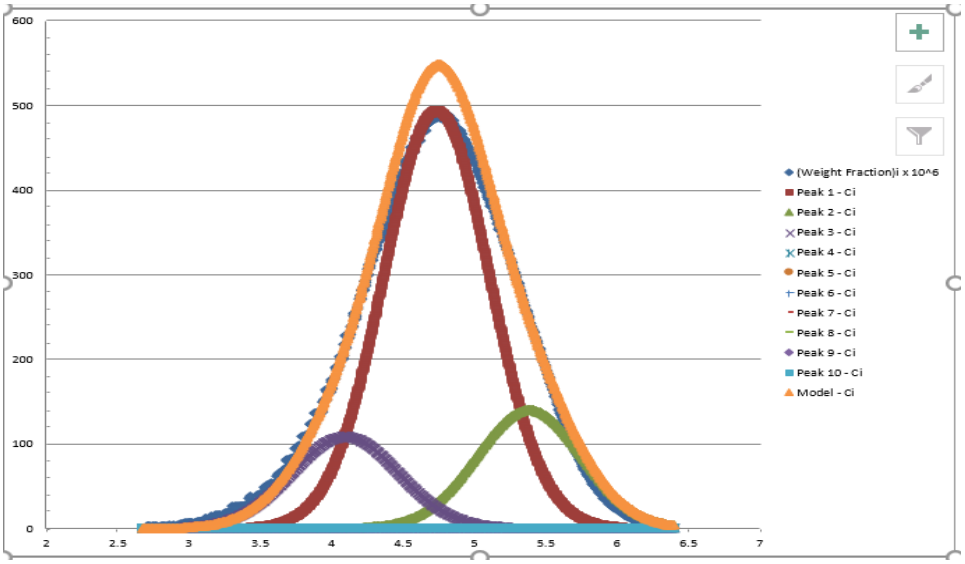

Figure 7.75a Weight fraction x10^6 versus log (molecular weight) resulting from GPC analysis of grade A data with three active catalyst sites

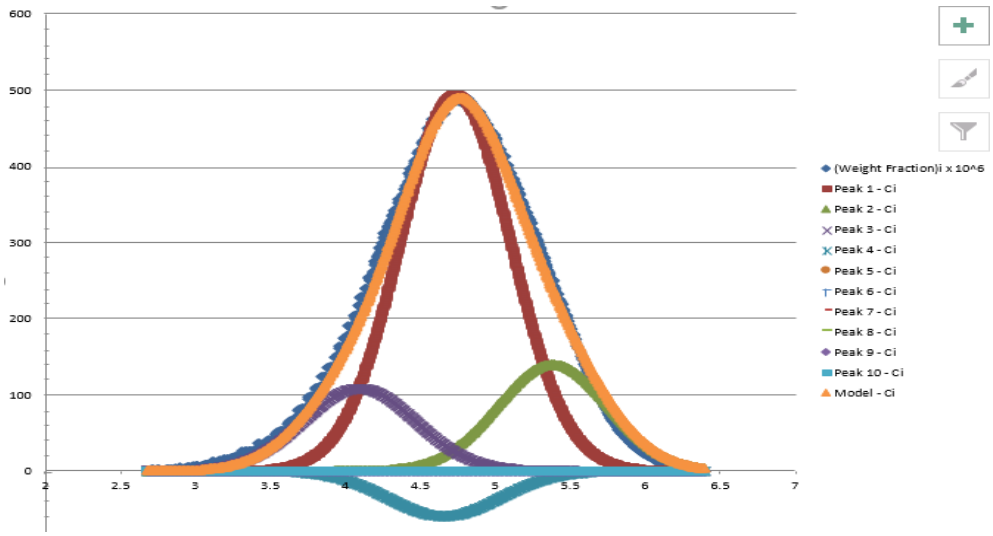

Figure 7.75b Weight fraction x10^6 versus log (molecular weight) resulting from GPC analysis of grade A data with four active catalyst sites

5.8.6 Thermodynamic Model and Parameters

Following the LDPE example in Section 4.6.4 and the PP example in Section 5.7.4, we choose polymer perturbed-chain statistical fluid theory (POLYPCSF) equation of state (Section 2.8) as our thermodynamic method. Based on the original references for POLYPCSF [51,52], the Aspen Polymers Spheripol high impact PP copolymer example [35], our previous article [5], and a search of Aspen Polymers online help on "Parameters (POLYPCSF)", we input the pure component parameters: Properties -> Methods-> Parameters-> Pure Components ->New -> Scalar -> Change name from Pure-1 to PCSAFT -> Enter values as in Figure 5.76.

Pure component scalar parameters

	Parameters	Units	Data set	Component CAT	Component CCAT	Component E2	Component BUTENE	Component H2	Component N2	Component IC5	Component H2O	Component CO	Component E-SEG	Component B-SEG
	PCSFTM		1	20	20	1.55873	2.27766	0.828469	1.2053	2.5617	2.92912	1.3097		
	PCSFTU	K	1	287.028	287.028	179.412	222.314	12.5276	90.96	230.75	316.794	92.15	287.028	230
	PCSFTV		1	4.57764	4.57764	3.43405	3.65228	2.97294	3.313	3.8296	2.04668	3.2507	4.57764	4.2
	PCSFTR		1										0.0183853	0.014

Figure 5.76 POLYPCSF pure component parameters.

Following Section 4.4.5 and Figure 4.22, we use the PCES (Physical Constant Estimation System) to estimate all missing property parameters. The reader may refer to the simulation file, ***WS5.3 LLDPE.bkp***, for the estimated property parameters. Following the path: Properties -> Methods _> Parameters -> Pure Components, we see parameter values from four sources: (1) Aspen enterprise databases- DB-PURE37 (i.e., APV110 PURE 37) and DB-POLYMER (i.e., APV110 Polymer); (2) Results of PCES - R-PCES; (3) User inputs. Figure 5.77 shows the user inputs for parameters of the temperature-dependent correlation ideal-gas heat capacity correlation CPIG-1. This figure follows the component parameter values for H2, E2 and E-SEG, and includes additional parameter values for 1-butene, B-SEG and IC5 that we regressed from NIST property values (e.g., https://www.chemeo.com/cid/13-178-0/1-Butene). By clicking on the "help" button displayed in Figure 7.77, we can see the explicit temperature-dependent correlation for each parameter.

Parameter CPIG Help Data set 1

Temperature-dependent correlation parameters

	Component	Source	Temperat units	Property units	1	2	3	4	5	6	7	8
	H2	USER	K	J/kmol-K	27140	9.274	-0.0138	7.65e-06	0	0	0	1000
	E2	USER	K	J/kmol-K	3806	156.6	-0.835	1.76e-05	0	0	0	1000
	BUTENE	USER	C	J/kmol-K	47859	152.06						
	E-SEG	USER	K	J/kmol-K	52417.3	458.823	-0.636152	0.00037622	0	0	0	1000
▶	IC5	USER	C	J/kmol-K	16321	431.71						
	B-SEG	USER	C	J/kmol-K	82932	115.29						

Figure 5.77 Parameters for CPIG correlation

Figure 5.78 shows the assumed properties values for catalyst CAT and cocatalyst CCAT under PURE-1. We create this folder by following the path: Properties -> Methods-> Parameters-> Pure Components ->New-> Type: Scalar-> Name: PURE-1 -> Enter parameter name, unit, component name and value according to Figure 5.78.

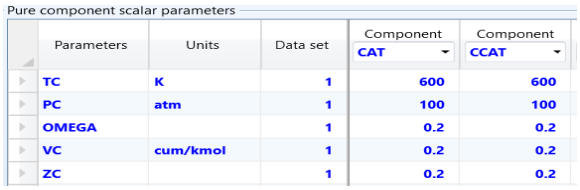

Figure 5.78 Assumed property values for catalyst and cocatalyst

Figure 5.79 shows the parameter for the enthalpy of formation used by the van Krevelen method, DHFVK. We assume the same value for LLDPE as that reported for LPDE by Bokis et al. [61]. This parameter is important to the calculation of heat of polymerization.

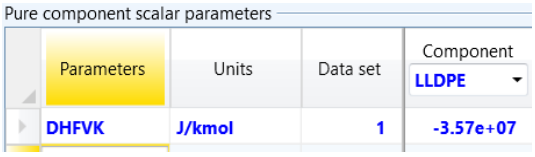

Figure 5.80 Assumed parameter for the enthalpy of formation for LLDPE

5.8.7 Inlet Stream Specifications for Grades A and B

Table 5.22 specifies the inlet streams and Table 5.23 gives the initial estimates of recycle steams. Referring to Figures 5.24 and 5.33, we specify the catalyst stream and its component attributes in Figure 5.81 for catalyst stream CAT-A. For component attributes displayed in the figure, we need to fill in the following: attribute ID – CPSFLOW, element CPSFLOW, value =0; attribute ID – CPSFRAC, element CPSFRAC, value =1; attribute ID – CDSFLOW, element CDSFLOW, value =0; attribute ID – CDSFRAC, element CDSFRAC, value =0; attribute ID – CVSFRAC, element S_1, value =0; element S_2, value = 0; element S_3, value =0. For catalyst stream CAT-B, we repeat the same specifications as for CAT-A in Figure 5.81, except to enter new catalyst mass flow rates of CAT = 0.165 kg/hr, and CCAT = 5.06 kg/hr.

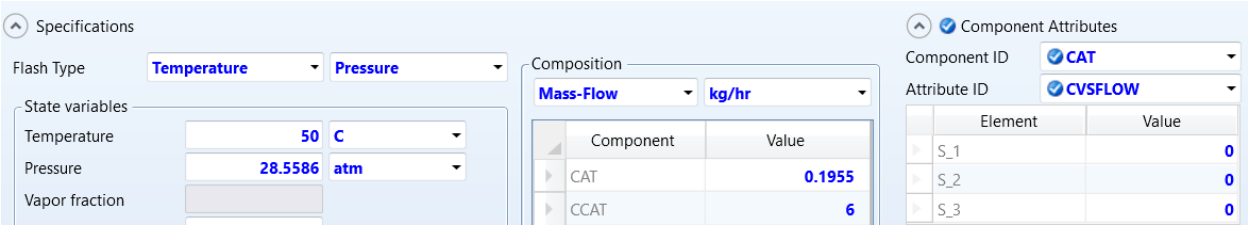

Figure 5.81 Specification of catalyst stream and component attributes

Table 5.22 Specifications of inlet streams for grades A and B

Streams	Feed-A (Feed-B)	C4-A (C4-B)	C5-A (C5-B)	CAT-A (CAT-B)	Coldin-A (Coldin-B)
Temperature, °C	5	39	45	50	26.59
Pressure, atm (kPag)	29.6077 (2898.67)	31.5946 (3100)	34.5554 (3400)	28.5586 (2792.38)	1 (0)
Mass flow, kg/hr	49054 (45900.5)	5300 (3800)	70 (70)	6.1955 (5.225)	1.86918E6
E2	49000 (45825)				
Butene		5300 (3800)			
H2	9 (30.5)				
N2	25				
CO	20				
CAT				0.1955 (0.165)	
CCAT				6 (5.06)	
IC5			70 (70)		
H2O					1.86918E6

Table 5.23 Recycle stream estimates for grades A and B

Streams	RECY1-A (RECY1-B)	RECY-A (RECY-B)
Temperature, °C	64	51.4
Pressure, atm	23	22.4
Mass flow, kg/hr	209026	918570
E2	41480	434690
Butene	47710	124140
H2	656	19870
N2	98350	253910
CO	20	
IC5	20830	85960

5.8.8 Specifications of Unit Operation and Chemical Reactor Blocks

Table 5.24 specifies the unit operations and chemical reactors.

Table 5.24 Block specifications

Block	Specifications
React-A (React-B)	86°C, 23.2035 atm (2250kPag); vapor-liquid; reactor volume and phase volume; Reactor volume =150 cum; condensed phase, volume= 30 cum; streams Recy1-A (Recy1-B)= vapor, Powder-A (Powder-B) = liquid; kinetic R-1
Split1-A (Split1-B)	Split fraction, Purge-A (Purge-B) = 0.1
Comp-A (Comp-B)	Isentropic, discharge pressure = 23.149 atm
Mix1-A (Mix1-B); Mix2-A (Mix2-B)	Pressure = 0 atm (no pressure drop)
Cool-A (Cool-B)	Design mode; hot stream outlet temperature = 49.7552°C; minimum approach temperature = 10°C; Pressure drop, hot side, outlet pressure = -0.68046 atm (pressure drop); U methods, constant, U = 0.85 kW/sqm-K

5.8.9 Ziegler-Natta Kinetics Specifications

Following Figure 5.35, we create a Z-N reaction set, named R-1. Figure 5.82 shows the species specifications of the ZN reactions.

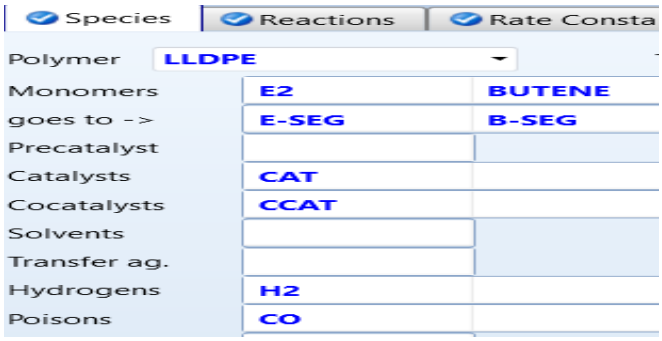

Figure 5.82 Species specifications for ZN reactions

Based on deconvolution of GPC data for this process, we specify previously in Section 5.8.5 that the number of active catalysts as 3. Supplement 5.4 gives the details of these 63 reactions, together with the relevant kinetic parameters. These reactions include:

(1) 3 spontaneous catalyst site activation reactions (ACT-SPON), with one reaction per active catalyst site;
(2) 3 catalyst activation reactions (ACT-COCAT) by cocatalyst with one reaction per active catalyst site;

(3) 6 catalyst activation reactions (ACT-MON) by monomer C2H4 and comonomer C4H8 with two reactions per active catalyst site;

(4) 6 chain initiation reactions (CHAIN-INI) by monomer C2H4 and by comonomer C4H8, with two reactions per active catalyst site;
(5) 12 chain propagation reactions (PROP) of reacting polymer chain Pn[C2H4] with C2H4 and C4H8, and reacting polymer chain Pn[C4H8] with C2H4 and C4H8, totaling 4 reactions per active catalyst site;
(6) 12 reactions of chain transfer to monomer (CHAT-MON) by reacting polymer chain Pn[C2H4] with C2H4 and C4H8, and by reacting polymer chain Pn[C4H8] with C2H4and C4H8, totaling 4 reactions per active catalyst site;
(7) 6 reactions of chain transfer to hydrogen (CHAT-H2) by reacting polymer chain Pn[C2H4] with H2, and by reacting polymer chain Pn[C4H8] with H2, with two reactions per active catalyst site;

(8) 6 reactions of spontaneous chain transfer (CHAT-SPON) by reacting polymer chain Pn[C2H4], and by reacting polymer chain Pn[C4H8], with two reactions per active catalyst site;

(9) 3 catalyst deactivation reactions by poison (DEACT-POISON), with one reaction per active catalyst site type;

(10) 3 spontaneous catalyst deactivation reactions (DEACT-SPON), with one reaction per active catalyst site type;
(11) 3 reactions of catalyst deactivation by hydrogen (DEACT-H2) with one reaction per active catalyst site.

To specify the reaction rate constants according to the Arrhenius form, Eq. (5.1), we follow the pre-exponential factors k_0 and the activation energy E for each reaction given in ***Supplement 5.4***.

5.8.10 Reactor and Flowsheet Simulation to Match Plant Production Targets

With inlet stream specifications in Table 5.22 and block specifications in Table 5.24, our modeling goal is to fine-tune the kinetic parameters to simulate the plant production targets for grades A and B. To speed up the simulation convergence of reactors REACT-A and REACT-B, we need to generate estimates of key component mass flow rates in exiting streams from these reactors, as seen in the "Estimates" folder in Figure 5.43. These estimates include the mass flow rates of monomer ethylene (E2) and comonomer 1-butene (Butene) in vapor streams RECY1-A and RECY1-B, and of polymer LLDPE in liquid streams Powder-A and Powder-A. We generate these estimates in two steps. First, we run the simulation file, ***WS5.3 LLDPE.bkp***, without these estimates, and save the resulting "unconverged" simulation file as ***WS5.3 LLDPE no estimates.bkp***. We obtain the simulated mass flow rates from this file, and then make estimates of the key component mass flow rates. Figure 5.83 illustrates the estimates for reactor REACT-A for producing grade A. Table 5.25 summarizes the estimates and simulation results. We save the converged simulation as ***WS5.3 LLDPE.bkp***.

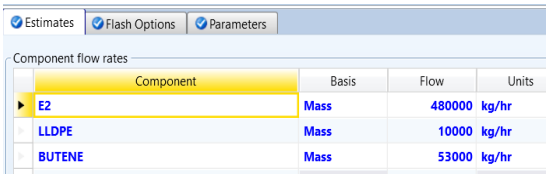

Figure 5.83 Estimates of key component mass flow rates for reactor REACT-A.

Table 5.25 Estimates and simulation results of key component mass flow rates

Key Component	Ethylene (E2) in RECY1-A	1-Butene (Butene) in RECY1-A	LLPDE in POWDER-A	Ethylene (E2) in RECY1-B	1-Butene (Butene) in RECY1-B	LLPDE in POWDER-B
Simulated mass flow, kg/hr; no estimates	489,996	52,999.7		458,250	38,000	
Assumed mass flow estimate, kg/hr	480,000	53,000	10,000	460,000	38,000	9,000
Simulated Mass flow, kg/hr with estimates (converged)	382,939	49169.2	**10,587.8**	361,288	35,368	**9474.79**

We follow Tables 5.4 and 5.9 to fine-tune the kinetic parameters to match the production targets. *Supplement 5.4* list the values of the resulting kinetic parameters. Table 5.26 compares the simulation results with plant production targets.

Table 5.26 Comparison between production targets and model results

Polymer grade	Grade A			Grade B		
	Production target	Model result	% Error	Production target	Model result	% Error
Production rate, kg/hr	10,500	10,587.8	0.84%	9,500	9474.79	0.27%
MWN	24,356	25131.1	3.18%	13,522	13,797	2.03%
MWW	105,496	104,081	1.34%	55,265	56,763	2.71%
PDI	4.33	4.15	4.15%	4.09	4.11	0.49%

5.8.11 Model Applications

We want to demonstrate a sensitivity analysis of the effects of hydrogen mole flow on the LLDPE melt index (MI) and density (DEN) [54,62]. Following Section 2.10.2, Eqs. (2.31) and (2.32), we assume the following correlations for the LLDPE MI and DEN:

$$MI=(125700/MWW)^{3.84} \qquad (5.16)$$

$$DEN = 0.936 - 0.02386*(SFRAC*100)^{0.514} \qquad (5.17)$$

where SFRAC is the mole fraction of comonomer, 1-butene, in the LLDPE product.

Frist, we define the MI and DEN correlations using a calculator block. Follow the path: Simulation -> Flowsheeting options -> Calculator -> New -> Name = C-1 -> Input -> (1) Define: See Figure 5.84 to define MWW, SFRAC, PROD, MI and DEN (note that comonomer, 1-butene, mole fraction in the LLDPE polymer is element 2 within the SFRAC array; element 1 is the mole fraction of monomer, ethylene) -> (2) Calculate: see Figure 5.85; and (3) Sequence: See Figure 5.86.

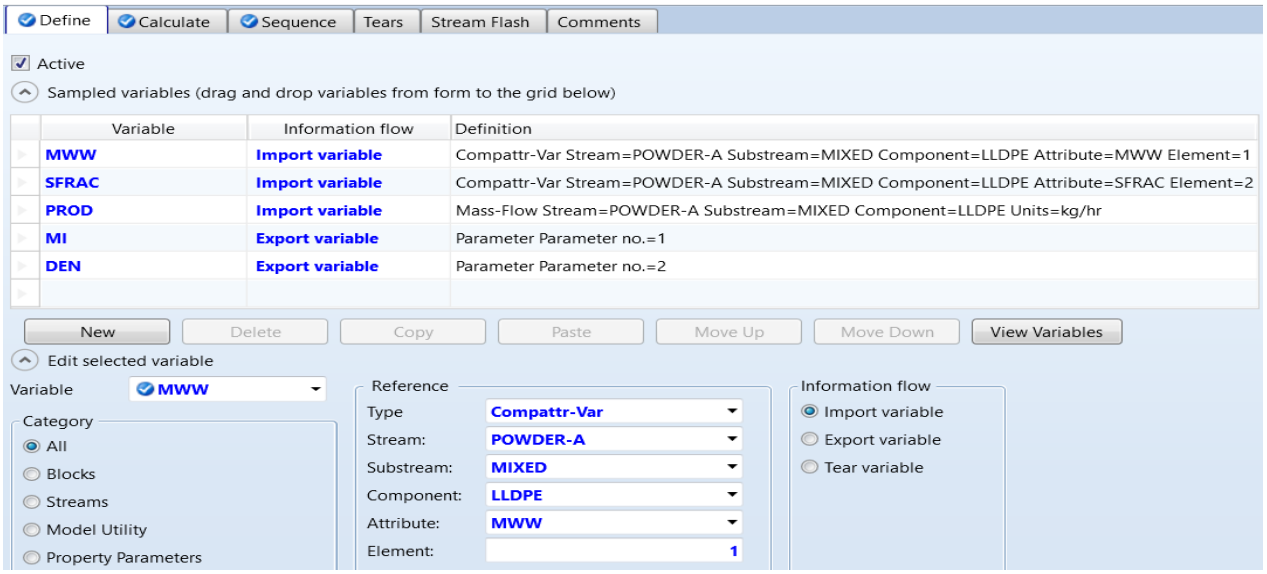

Figure 5.84 Define the variables and parameters

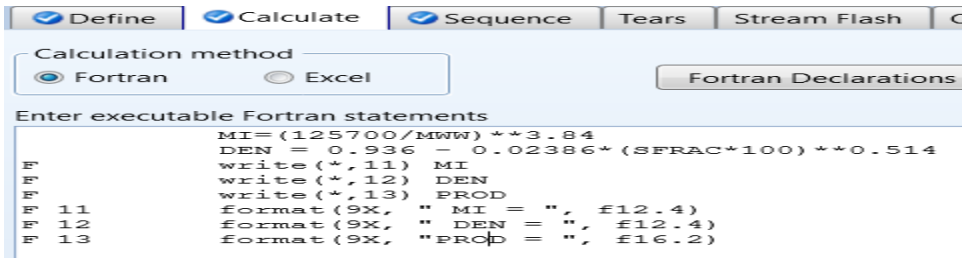

Figure 7.85 Specify Fortran equations for MI and DEN

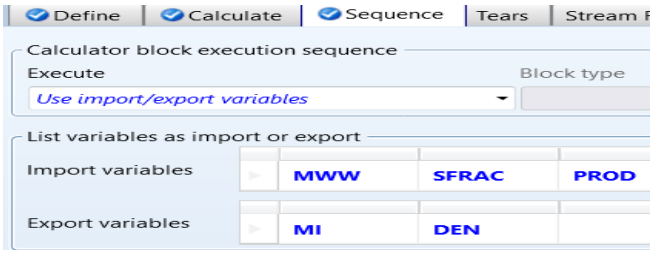

Figure 7.86 Define the calculation sequence

Next, we define the sensitivity analysis by following the path: Simulation ->Model analysis tools -> Sensitivity -> New -> Name = S-1 -> Input: (1) Vary: see Figure 7.87; (2) Define: see Figure 7.88; and (3) Tabulate: see Figure 7.89. Figure 7.90 plots the resulting MI and DEN values as a function of hydrogen mole flow in stream FEED-A. We save the resulting simulation file as ***WS5.3 LLDPE_MI and DEN vs H2 Mole Flow.bkp.***

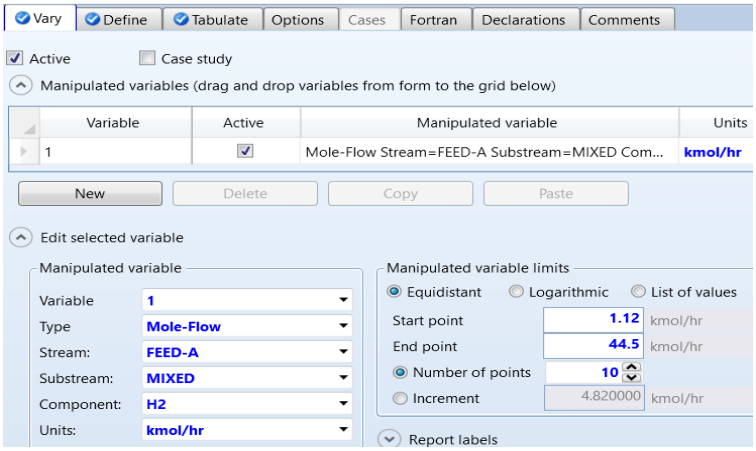

Figure 5.87 Define the manipulated variable, “Vary”

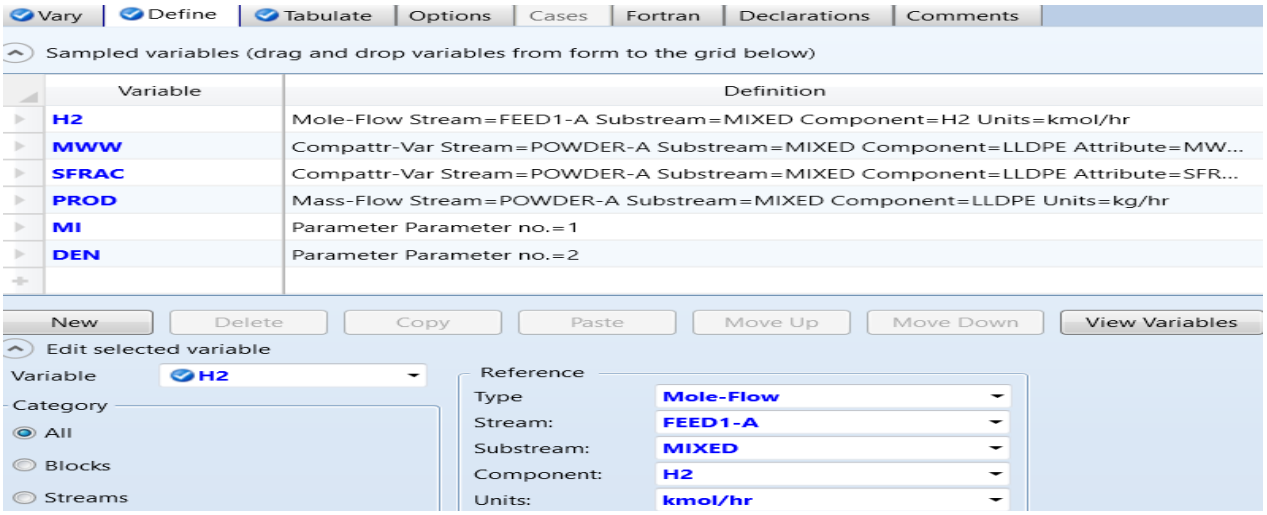

Figure 7.88 Define the dependent variables and parameters

Figure 7.89 Specify the tabulated variables

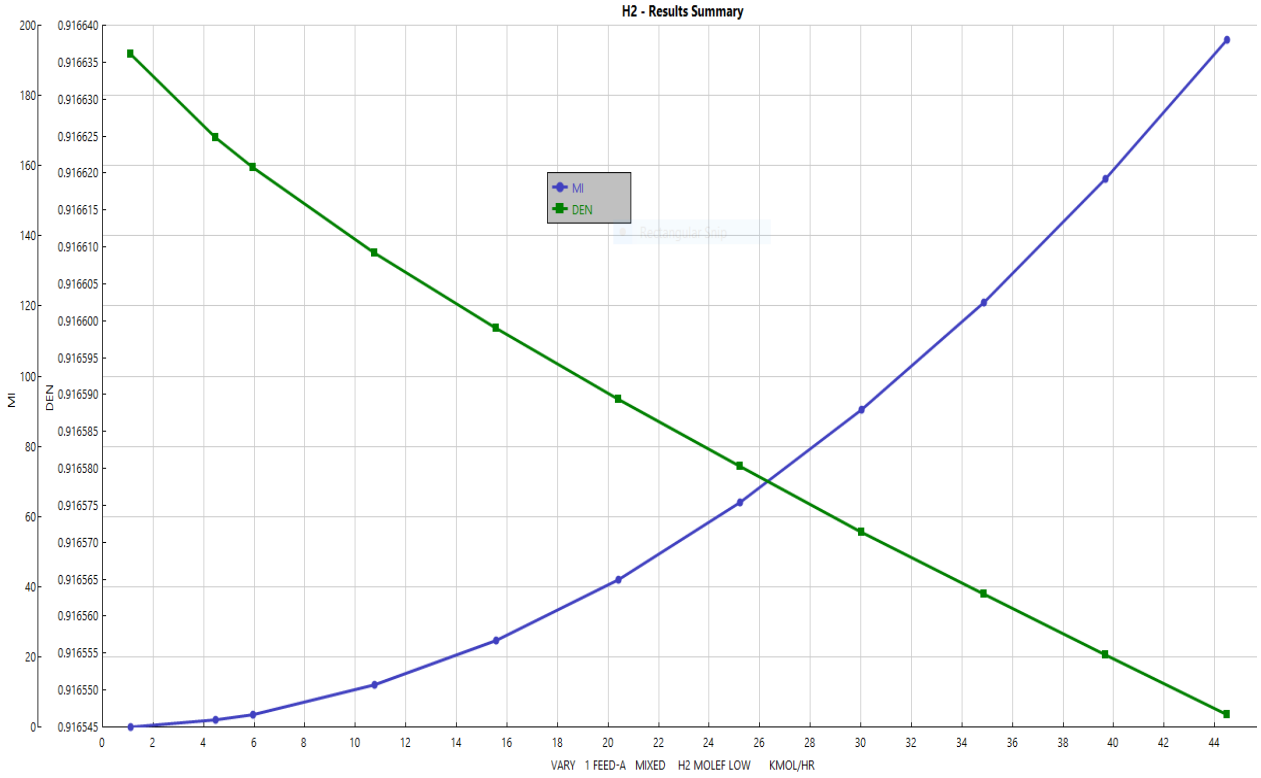

Figure 7.90 MI and DEN values as a function of hydrogen mole flow in stream FEED-A

5.9 Workshop WS5.4: Simulation of a Solution Polymerization Process for Producing Ethylene-Propylene Copolymer (EPM) or an Ethylene-Propylene-Diene Terpolymer (EPDM) with Metallocene Catalysts

5.9.1 Objective

The general objective of this workshop is to introduce the methodology to simulate a polyolefin manufacturing process using a metallocene catalyst system. A specific objective is to demonstrate how to simulate the production of an ethylene-propylene copolymer (EPM) or an ethylene-propylene-diene-terpolymer (EPDM) in a solution polymerization process. We explain the new features of the polymerization kinetics using a metallocene catalyst, and their implementation within Aspen Polymers. As the literature contains only very limited information about the process details and operating conditions, we focus on the methodology for simulating the process with assumed operating conditions. If plant data are available, the reader may modify the workshop details easily to obtain more accurate simulations.

5.9.2 Process Background

In a comprehensive review with over 500 literature references, Cesca [63] gives a detailed introduction to the chemistry of ethylene-propylene copolymer (EPM) and ethylene-propylene-diene terpolymer (EPDM) and presents the industrial solution and suspension polymerization process flowsheets. Van Duin, et. at [64] present a historical and technical summary of Keltan developments defining EPDM for the past and the next 50 years. Figure 7.91 gives a process block diagram of a typical solution polymerization for producing EPDM [65].

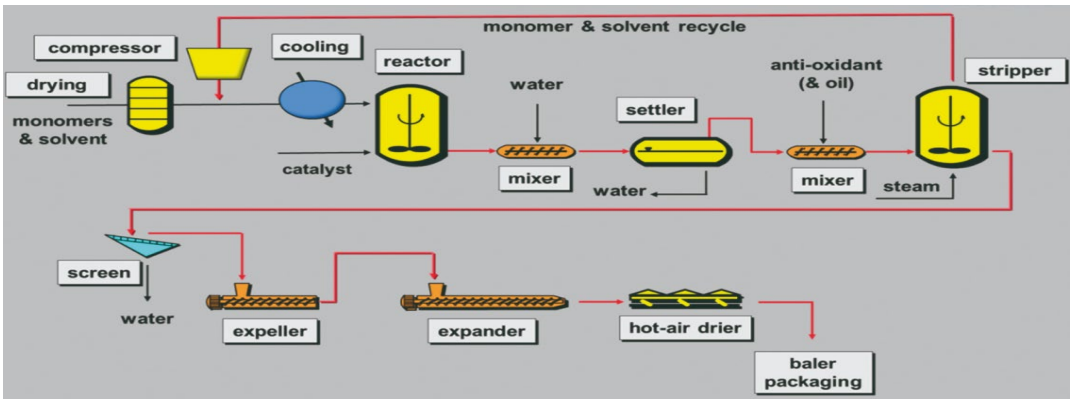

Figure 7.91 A process block diagram for solution polymerization for producing EPDM [65].

Eisinger et al. [65] demonstrate how to adopt the UNIPOL gas-fluidized process to produce EPM or EPDM. This workshop focuses on the adaption of the Ziegler-Natta polymerization kinetics model of Aspen Polymers to use a metallocene catalyst system.

For producing EPDM, the monomers include ethylene, propylene, and a diene. The typical diene monomer used includes: (1) ENB (ethylidene norbornene), CAS no. 16219-75-3, chemical formula C9H12, formula molecular weight 120.19, and molecular structure file ***16129-75.3.mol*** (see Figure 7.92) (https://www.chemicalbook.com/ProductChemicalPropertiesCB1309456_EN.htm). While we can import the molecular structure file to represent ENB and estimated its properties, Aspen Plus pure component database unfortunately does not contain any repeated segment related to ENB. (2) DPCD (dicyclopentadiene), CAS no. 77-73-6, chemical formula C10H12, formula molecular weight 132.2. It's available within Aspen Plus pure component database, as is its repeat segment, dicyclopentadiene-R (C10H12-R). To import its molecular structure into Aspen Plus for property estimation, the structure file ***77-73-6.mol***, is available (see Figure 7.92) (https://www.chemicalbook.com/Search_EN.aspx?keyword=dicyclopentadiene).

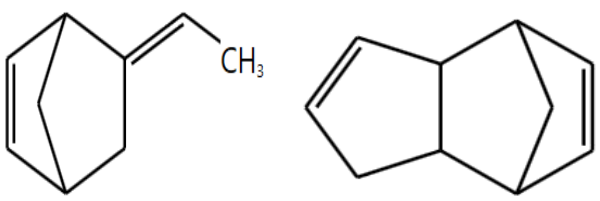

Figure 7.92 Molecular structures of the typical third monomer for EPDM terpolymer: (left) ENB (ethylidene norbornene; C9H12); and (right) DEPD (dicyclopentadiene;C10H12).

A typical Ziegler-Natta catalyst system used for producing EPM or EPDM is a vanadium catalyst-cocatalyst system, $VOCl_3$-$Al_2Et_3Cl_3$. Cozewith and his colleagues [66,67] were among the first to present the detailed Ziegler-Natta polymerization reactions and the associated experimental reaction rate constants for producing EPM or EPDM using vanadium-based catalysts in a continuous stirred-tank polymerization reactor, and in a semi-batch or a plug-flow polymerization reactor. Subsequently, a number of simulation and control studies based on the kinetic model of Cozewith have appeared [68 to 70]. Hagg et.al. [71] later present an experimental and modeling study in a semi-batch bubble column reactor to produce EPM and EPDM using vanadium-based catalysts, and compare the resulting Ziegler-Natta polymerization reaction rate constants with those from prior studies. Further modeling and experimental studies of EPM and EPDM using vanadium-based catalysts appear in [72 to 74].

Hamielec and Soares [75] present an excellent overview of the metallocene-catalyzed polymerization. They state that "metallocene catalysts are organometallic coordination compounds in which one or two cyclopentadienyl rings or substituted cyclopentadienyl rings are π-bonded to a transition metal atom (see Figure 7.93). The most remarkable feature of these catalysts is that their molecular strictures can be designed to create active center types *to produce polymers with entirely novel properties*".

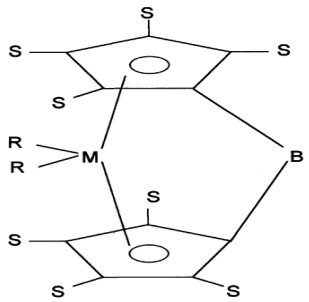

Figure 7.93 Generic structure of a metallocene catalyst

Continuing their previous study on the production of EPM copolymer and EPDM terpolymer using vanadium-based catalysts [71], Hagg et al. [76] present an experimental and modeling study using the same semi-batch bubble column reactor and a metallocene $Et(Ind)_2ZrCl_2$/MAO catalyst system. Here, "Et" stands for the ethyl group; "Ind" represents zirconium. $Et(Ind)_2ZrCl_2$ is not available with Aspen Plus pure component database. MAO represents $C12H16OS_2$, CAS no. 130184-19-9, and formula molecular weight 240.38. To import its structure file into Aspen Polymers for property estimation, the molecular structure file, ***130184-19-9.mol***, is available (see Figure 7.94) (https://www.chemicalbook.com/Search_EN.aspx?keyword=MAO).

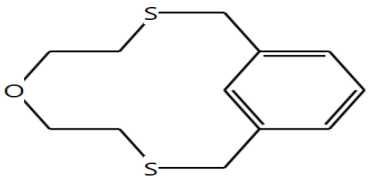

Figure 7.94 Molecular structure of MAO ($C12H16OS_2$), a component of a metallocene catalyst system

Figure 7.95 compares the polymer yields for producing the EPDM terpolymer using both the vanadium-based Ziegler-Natta catalyst system, $VOCl_3$-$Al_2Et_3Cl_3$, and the metallocene catalyst system, $Et(Ind)_2ZrCl_2$/MAO [76]. The three monomers are ethylene, propylene and ENB (ethylidene norbornene). The comparison shows the increased polymer yield when using a metallocene catalyst system.

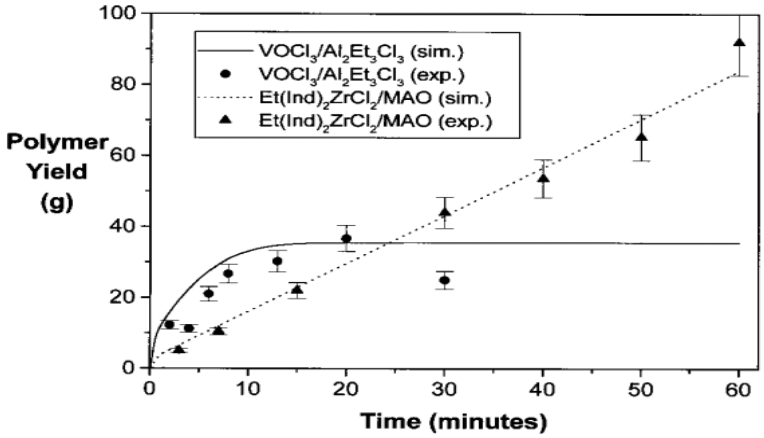

Figure 7.95 An illustration of increased EPDM terpolymer yields using a metallocene catalyst system when compared to a vanadium-based Ziegler-Natta catalyst system.

5.9.3 EPM Copolymerization Kinetics and EPDM Terpolymerization Using a Metallocene Catalyst System

Polymerization kinetics using a metallocene catalyst system include most of the reactions for Ziegler-Natta catalysts described in Section 2.2, except for two differences. First, a metallocene catalyst system mostly exhibits only a single active catalyst site, and results in a narrow molecular weight distribution with a polydispersity index of approximately 2. Second, a metallocene catalyst system includes additional reactions involving terminal double bond (TDB) end groups that are absent in the traditional Ziegler-Natta polymerization kinetics. We follow [77] to explain how to include the relevant TDB reactions in Aspen Polymers.

Polymerization with a metallocene catalyst system typically leads to the formation of long chain branching (LCB), but the LCB frequency is usually small. The long chain branches likely result from chain propagation reactions involving a growing polymer chain and a terminal double bond on a dead polymer chain. Polymer chains with terminal double bonds are formed by some of the chain-transfer reactions. To form long chain branches, the metal catalytic center must be open to provide a favorable reactivity ratio for the macromonomer.

Aspen Polymers tracks the concentration of TDB end groups on the dead polymer chains through a segment called *TDB Segment*, which typically has one less hydrogen atom than the related repeated segment. For example, we specify a *C3H5-TDB end segment* (C3H5-E) corresponding to *a C3H6-SEG repeated segment* (C3H6-R). TDB segments are generated through chain transfer reactions and are consumed through the TDB polymerization reaction.

We summarize the ethylene-propylene copolymerization kinetics using a metallocene $Et(Ind)_2ZrCl_2$/MAO catalyst system in Table 5.26 [76]. We also convert the reported reaction rate constant k (1/min) values in [76] to the corresponding pre-exponential factor k_0 (1/sec) values used in Aspen Polymers according

to the Arrhenius form, Eq. (5.1), assuming a reaction temperature *T* of 85°C or 358K in the equation. See Table 5.27. In the table, we follow [77] for the assumed values of the activation energies.

Table 5.26 Copolymerization kinetics for EPM (ethylene-propylene copolymer) using a metallocene $Et(Ind)_2ZrCl_2$/MAO catalyst system [76].

Reaction	Representation	Notes
1. Catalyst site activation by cocatalyst (CAT-COCAT)	CAT -> P_0	Assume a single active site. P_0 is a vacant site.
2. Chain initiation by monomer 1 (CHAIN-INI)	P_0 + M_1 (C2H4)-> P_1[C2H4-R]	M_1 is monomer 1, C2H4. P_1 is a propagation site with an attached polymer chin containing one segment.
2. Chain initiation by monomer 2 (CHAIN-INI)	P_0 + M_2 (C3H6)-> P_1[C3H6-R]	M_2 is monomer 2, C2H6.
3. Chain propagation (PROPAGATION)	Growing polymer chain +Monomer -> Propagating polymer chain P_n[C2H4-R] +C2H4 -> P_{n+1}[C2H4] P_n[C3H6-R] +C2H4 -> P_{n+1}[C2H4] P_n[C2H4-R] +C3H6 -> P_{n+1}[C3H6-R] P_n[C3H6-R] +C2H4 -> P_{n+1}[C3H6-R]	P_n and P_{n+1} are polymer chains of length n and n+1 segments.
4. Chain transfer to monomer (CHAT-MON)	Growing polymer chain + Monomer -> Dead chain + Growing monomer P_n[C2H4] +C3H6 -> D_n + P_1[C3H6-R] P_n[C3H6] +C3H6 -> D_n + P_1[C3H6-R]	D_n is a dead polymer chain of length n segments.
5. Chain transfer to agent (CHAT-AGENT or CHAT-H2)	Growing polymer chain + Transfer agent -> Dead chain + Vacant site P_n[C2H4] + Hydrogen ->D_n + P_0 P_n[C3H6] + Hydrogen ->D_n + P_0	
6. Spontaneous Catalyst Deactivation (DEACT-SPON)	P_0 -> DCAT P_n -> D_n + DACT	DACT is a deactivated catalyst site.
7. TDB polymerization reaction (TDB-POLY)	P_n[C2H4-R] +D_m[TDB-Seg] ->P_{n+m}[C2H4-R] P_n[C3H6-R] +D_m[TDB-Seg] ->P_{n+m}[C3H6-R]	TDB = terminal double bond

Table 5.27 Conversion of the reported reaction rate constant *k* (1/min) values in [76] to the corresponding pre-exponential factor k_0 (1/sec) values used in Aspen Polymers

Reaction	Comp 1	Comp 2	*k,1/min* [76]	*k,1/sec*	*Ea* cal/mol	Exp[Ea/RT]	k_0 1/sec
CAT-COCAT	CAT	COCAT	40	0.66667	8000	1.30705E-5	51005.47
CHAIN-INI		C2H4	5E4	833.3333	7000	5.33035E-5	15633755
CHAIN-INI		C3H6	5E3	83.33333	7000	5.33035E-5	1563375
PROPAGATION	C2H4	C2H4	1E6	16666.67	7000	5.33035E-5	3.13E8
PROPAGATION	C3H6	C2H4	6E5	10000	7000	5.33035E-5	1.88E8
PROPAGATION	C2H4	C3H6	2.1E6	35000	7000	5.33035E-5	6.57E8
PROPAGATION	C3H6	C2H4	5.3E5	8833.333	7000	5.33035E-5	1.66E8
CHAT-MON	C2H4	C3H6	6	0.1	8000	1.30705E-5	7650.821
CHAT-MON	C3H6	C3H6	6	0.1	8000	1.30705E-5	7650.821
CHAT-H2	C2H4	H2	3457	57.61667	8000	1.30705E-5	4408148
CHAT-H2	C3H6	H2	3457	57.61667	8000	1.30705E-5	4408148
DEACT-SPON	Active site P_0		80	1.33333	8000	1.30705E-5	102010.9
DEACT-SPON	Polymer chain P_n		80	1.33333	8000	1.30705E-5	102010.9
TDB-POLY	C2H4		2.1E6	35000	8000	1.39131E-5	2.68E9
TDB-POLY	C3H6		5.3E5	8333.333	8000	1.39131E-5	6.76E8

5.9.4 Unit System, Components and Characterization of Polymer

We choose to set up a unit system based on the MET unit set and replace the temperature from K to °C, and pressure from atm to psig. We make these changes, as we simulate the operating conditions of a UNIPOL gas-fluidized-bed process to produce EPM using a metallocene catalyst system in U.S. patent no. 6,011,128 [65].

Figure 5.96 shows our component specifications. As METCAT1, catalyst $Et(Ind)_2ZrCl_2$, is not available within Aspen Plus pure component database, we use TICl4 to represent this component (but will enter the correct molecular weight of 420.81 later in Figure 5.100). We define the cocatalyst (COCAT) MAO of Figure 5.95 by importing its molecular structure file, ***130184-19-9.mol*** (https://www.chemicalbook.com/Search_EN.aspx?keyword=MAO) (available in the workshop folder for this chapter). We follow the path: Properties -> Components -> Molecular structure -> COCAT -> Structure and functional group -> Draw/import/edit: import ***130184-19-9.mol*** -> Calculate bonds -> General -> Atom number and atom type automatically defined by Aspen Plus. We save the simulation file as ***WS5.4 EPM_metallocene kinetics.bkp.***

In Figure 5.96, ethylene and propylene are monomers, and their repeated segments are E-SEG and P-SEG. TDB-SEG is a terminal double bound end segment, with one less hydrogen atom than the repeated segment P-SEG. EPM is the ethylene-propylene copolymer. It's not available within the Aspen Plus polymer component database, so we specify it as a generic polymer component. N-hexane is a solvent, hydrogen is a chain transfer agent, and nitrogen is an inert gas.

Component ID	Type	Component name	Alias
METCAT1	Conventional	TITANIUM-TETRACHLORIDE	TICL4
COCAT	Conventional		
ETHYLENE	Conventional	ETHYLENE	C2H4
PROPYLEN	Conventional	PROPYLENE	C3H6-2
HEXANE	Conventional	N-HEXANE	C6H14-1
HYDROGEN	Conventional	HYDROGEN	H2
EPM	Polymer	POLY(ETHYLENE-PROPYLENE)	P(E&P)
E-SEG	Segment	ETHYLENE-R	C2H4-R
P-SEG	Segment	PROPYLENE-R	C3H6-R
TDB-SEG	Segment	VINYL-E	C2H3-E
NITROGEN	Conventional	NITROGEN	N2

Figure 5.96 Component specifications

Next, we follow the path: Properties -> Components -> Polymer and specify the polymer segments according to Figure 5.97.

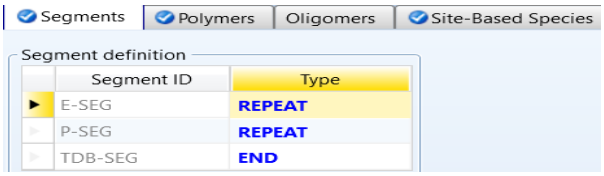

Figure 5.97 Segment definition for polymer

For the Polymers folder, we choose built-in attribute group, Ziegler-Natta selection for our polymer EPM. Figure 5.98 shows the specifications for the Site-Based Species.

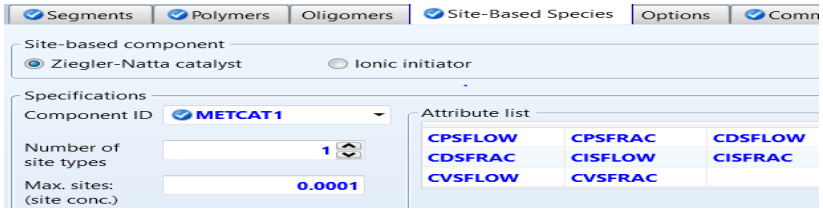

Figure 5.98 Specification of site-based species

5.9.5 Thermodynamic Method and Property Parameters for Components and Polymer

Our solution polymerization reactor for EPM operates at 300 psig [65], which is close to the operating pressure of our gas-phase stirred-tank reactor for PP in Section 5.7. Therefore, we choose POLYPCSF as our thermodynamic method. Following our examples for LDPE (Section 4.4.4), EVA (Section 4.6.4) and PP (Section 5.7.4), we enter the pure component parameters for POLYPCSF by following the path: Properties -> Methods -> Parameters -> Pure Components -> New -> Scalar -> Change name from Pure-1 to PCSF -> enter values as in Figure 5.99. We assume that TDB-SEG segment has the same parameter values as E-SEG.

Pure component scalar parameters

Parameters	Units	Data set	Component METCAT1	Component COCAT	Component ETHYLENE	Component PROPYLEN	Component HYDROGEI	Component E-SEG	Component P-SEG	Component TDB-SEG
PCSFTM		1	20	20	1.55873	1.9598	0.828469			
PCSFTU	K	1	287.028	287.028	179.412	207.19	12.5276	237.088	267.732	237.088
PCSFTV		1	4.57764	4.57764	3.4305	3.5356	2.97294	3.25929	3.49356	3.25929
PCSFTR		1						0.0481045	0.0402106	0.0481045

Figure 5.99 POLYPCSF pure component parameters

We follow the same procedure in creating the pure component parameter folder PCSF to generate a pure component parameter folder named CAT and enter the values as in Figure 5.100. Note the molecular weight (MW) for our catalyst METCAT1, $Et(Ind)_2ZrCl_2$.

Pure Components - CAT

Input | Comments

Pure component scalar parameters

Parameters	Units	Data set	Component METCAT1	Component COCAT
TC	K	1	600	600
PC	atm	1	100	100
OMEGA		1	0.2	0.2
VC	cum/kmol	1	0.2	0.2
ZC		1	0.2	0.2
MW		1	420.81	

Figure 5.100 Assumed pure component parameters for METCAT1 and COCAT

Figure 5.101 shows the parameters for the ideal gas heat capacity, CPIG-1. These parameter values came from references [4,5,35]. We estimate the parameter values for COCAT by applying the estimation tool, based on the structure of Figure 7.94 and the molecular structure file, ***130184-19-9.mol.*** Specifically, we follow the path: Properties -> Estimation ->Input -> Setup -> -> Estimation option -> Estimate all missing parameters. After obtaining the estimated parameter values as shown by R-PCES for COCAT in Figure 5.101, we change the estimation option to “Do not estimate any parameters”.

Parameter CPIG | Help | Data set 1

Temperature-dependent correlation parameters

Components	Source	Temperature units	Property units	1	2	3	4	5	6	7	8	9	10	11
E-SEG	USER	K	J/kmol-K	-24096.9	244.16	-0.11	-4.09859e-05	0	0	250	1000	36029.2	1.0708e-54	23.4104
P-SEG	USER	K	J/kmol-K	-33286.7	399.74	-0.165649	0	0	0	250	1000	36029.2	0.811659	1.93918
TDB-SEG	USER	K	J/kmol-K	-24096.9	244.16	-0.11	-4.09859e-05	0	0	250	1000	36029.2	1.0708e-54	23.4104
ETHYLENE	USER	C	J/kmol-K	3806	156.6	-0.0835	1.76e-05	0	0	273.15	1273.15			
PROPYLEN	USER	C	J/kmol-K	3710	234.5	-0.116	2.21e-05	0	0	273.15	1273.15			
COCAT	R-PCES	C	J/kmol-K	231244	872.015	-0.749763	0.000302549	0	0	6.85	826.85	36029.2	42.9328	1.5

Figure 5.101 Parameters for ideal gas heat capacity, CPIG-1

Figure 5.102 displays the parameter values for enthalpy of formation by the van Krevelen method, DHFVK. These values came from ***WS4.3*** of Section 4.6.

Pure component scalar parameters

Parameters	Units	Data set	Component E-SEG	Component P-SEG	Component TDB-SEG
DHFVK	J/kmol	1	-4.097e+07	-5.3299e+07	-5.5699e+07

Figure 5.102 Parameter values for enthalpy of formation by the van Krevelen method, DHFVK

The reader may see other parameter values for DHVLWT-1 (heat of vaporization), KLDIP-1 (liquid thermal conductivity), MULAND-1 (liquid viscosity), PLXANT-1(liquid vapor pressure) and SIGDIP (liquid surface tension) resulting from property estimation (R-PCES) from the simulation file ***WS5.4 EPM_metallocene_kinetics.bkp.***

5.9.6 Process Flowsheet and Inlet Stream and Block Specifications

Figure 5.103 depicts the fluidized-bed reactor system in our UNIPOL process for producing EPM copolymer.

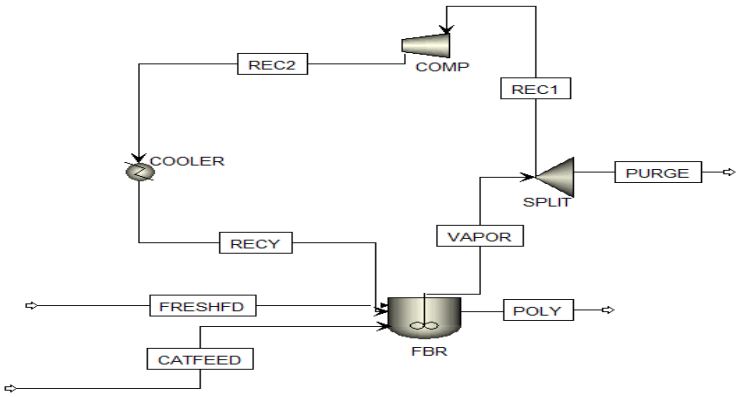

Figure 5.103 Fluidized-bed reactor system for producing EPM copolymer.

Figure 5.104 shows the specification of CATFEED stream.

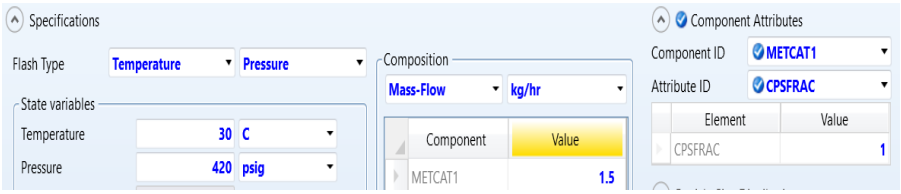

Figure 5.1045 Specifications of CATFEED stream

For component attributes displayed in Figure 5.104, we need to continue specifying the following attributes: CPSFLOW = CDSFLOW =CDSFRAC= CVSFLOW =CVSFRAC =0.

For feed steam, FRESHFD, we specify 5°C, 400 psig, and component mass flow rate (kg/hr): COCAT =30, Ethylene=25000, Propylene =5000, H2 =5, and N2 = 20. Table 5.28 gives the block specifications. We note that the reactor operating pressure of 300 psig (20.42 atm) follows the metallocene catalyst examples for polyolefins in [65, 77] and the PP and LLDPE examples in WS5.2 and 5.3. The reader may change this pressure with available plant data.

Table 5.28 Block specifications

Block	T,°C	Pressure psig	Specifications
SOLREACT	85	300	(1) Setup: Vapor-liquid phase; reactor volume and phase volume; reactor volume= 300 cum; condensed phase volume =88 cum; streams: Vapor-vapor phase, POLY- liquid phase; kinetics: R-1. (2) Convergence (see Section 3.6): estimates- component mass flow, EPM =10,000 kg/hr; flash options: maximum iterations =200; convergence parameters: mass balance convergence solver- Newton, maximum iterations -100, and "initialize using integration"
SPLIT			Split fraction: PURGE- 0.001
COMP			Isentropic; discharge pressure = 325 psig
COOLER	85	-10	Pressure = - 10 psia (pressure drop);flash options - maximum iteration = 200

5.9.7 Base-Case Simulation Results

In our base-case simulation, the actual reactions and their kinetic parameters are slightly different from those listed in Table 5.27 based on the literature, to obtain reasonable monomer and copolymer yields, MWN, MWW and PDI, as well as SFRACs (mole fractions of monomer and comonomer in the polymer product). See Tables 5.29 and 5.30 present the kinetic parameters, and stream results for feed and polymer product.

Table 5.29 Actual reactions and kinetic parameters for base-case simulation

	Type	Site No.	Comp 1	Comp 2	Pre-Exp 1/sec	Act-Energy cal/mol	Order	Tdb Frac	Ref. Temp. C
►	ACT-COCAT	1	METCAT1	COCAT	703000	8000	1		1e+35
	CHAIN-INI	1	ETHYLENE		3.3675e+07	7000	1		1e+35
	CHAIN-INI	1	PROPYLEN		875000	7000	1		1e+35
	PROPAGATION	1	ETHYLENE	ETHYLENE	3.3675e+07	7000	1		1e+35
	PROPAGATION	1	PROPYLEN	ETHYLENE	3.3675e+06	7000	1		1e+35
	PROPAGATION	1	ETHYLENE	PROPYLEN	8.75e+06	7000	1		1e+35
	PROPAGATION	1	PROPYLEN	PROPYLEN	8.75e+06	7000	1		1e+35
	CHAT-MON	1	ETHYLENE	ETHYLENE	1000	7200	1	1	1e+35
	CHAT-MON	1	PROPYLEN	ETHYLENE	1000	7200	1	1	1e+35
	CHAT-MON	1	ETHYLENE	PROPYLEN	1000	7200	1	1	1e+35
	CHAT-MON	1	PROPYLEN	PROPYLEN	1000	7200	1	1	1e+35
	CHAT-H2	1	ETHYLENE	HYDROGEN	3000	8000	0.5		1e+35
	CHAT-H2	1	PROPYLEN	HYDROGEN	3000	8000	0.5		1e+35
	DEACT-SPON	1			0.0006	10000	1		1e+35
	TDB-POLY	1	ETHYLENE	TDB-SEG	0.02	7000	1		1e+35

Table 5.30 Stream results for feed and polymer

Stream	CATFEED	FRESHFD	POLY
Temperature, °C	35	5	85
Pressure, psig	420	400	300
Mass flow, kg/hr			
METCAT1	1.5		1.5
COCAT		30	29.9641
ETHYLENE		25000	150.882
PROPYLEN		5000	54.692
HYDROGEN		5	0.0262353
EPM			10302.4
NITROGEN		20	0.0262353
Polymer attributes MWN			134463
MWW			268975
PDI			1.99888
SFRAC E-SEG			0.807252
P-SEG			0.192524
TDB-SEG			0.000224064

We see the total monomer conversion of 10302.4/(25000 +5000), or 34.34%. The mole fractions of ethylene, propylene and TDB segment in the EPM copolymer are 0.807252, 0.192524, and 0.000224, respectively. The MWN is 134463, and MWW is 268975, giving a PDI of 1.99888. Should the reader have plant data for these results, it's not difficult to fine-tune the kinetic parameters to match the plant production targets by following examples in previous workshops of this chapter. We save the simulation file as ***WS 5.4 EPM_Solution_Metallocene_Final.bkp.***

5.9.8 Extension to EPDM (Ethylene-Propylene-Diene Terpolymer)

As discussed in Section 5.9.2, Aspen Plus version 11 can represent the components involved in producing an EDPM terpolymer using DPCD (dicyclopentadiene) as the diene monomer. In the simulation files for WS5.4, we have included a completed component and property files, WS ***5.4 EPDM_metallocene_properties.bkp,*** for using DPCD as the diene monomer and a metallocene $Et(Ind)_2ZrCl_2$/MAO catalyst system [73]. Figure 5.106 shows the component specifications. Here, the details of the metallocene catalyst and cocatalyst are identical to that of the EPM copolymer example in WS5.4. The reader can refer to the simulation file to learn more about the components and properties involved.

Component ID	Type	Component name	Alias
METCAT1	Conventional	TITANIUM-TETRACHLORIDE	TICL4
COCAT	Conventional		
ETHYLENE	Conventional	ETHYLENE	C2H4
PROPYLEN	Conventional	PROPYLENE	C3H6-2
DPCD	Conventional	DICYCLOPENTADIENE	C10H12-D0
E-SEG	Segment	ETHYLENE-R	C2H4-R
P-SEG	Segment	PROPYLENE-R	C3H6-R
DPCD-R	Segment	DICYCLOPENTADIENE-R	C10H12-R
TDB-SEG	Segment	VINYL-E	C2H3-E
EPDM	Polymer	GENERIC-POLYMER-COMPON...	POLYMER
HEXANE	Conventional	N-HEXANE	C6H14-1
HYDROGEN	Conventional	HYDROGEN	H2
NITROGEN	Conventional	NITROGEN	N2

Figure 5.106 Component specifications for simulating the manufacturing of an ethylene-propylene-DPCD terpolymer

Hagg, et al. [76] have presented a generic reaction mechanism, reaction rate equations and experimental reaction rate constants for an EPDM terpolymerization using a metallocene

Et(Ind)2ZrCl2/MAO catalyst system. The third monomer, ENB (ethylidene norbornene), and its related repeat segment are not available within Aspen Plus pure component and segment databases, we do not simulate the EPDM work of Hagg et al. [76]. However, when adequate polymerization kinetic data become available for DCPD as the diene monomer, and ENB and its repeat segment become available in Aspen Plus databases, we can apply the same modeling methodology for the EPM (ethylene-propylene copolymer) to the ethylene-propylene-DCPD terpolymerization using a metallocene catalyst system.

5.10 Conclusions

In this chapter, we have demonstrated an effective methodology for estimating kinetic parameters for Ziegler-Natta polymerization for commercial processes producing polyolefins, such as HDPE, PP, LLDPE and EPDM. We consider the catalyst activation, initiation, propagation, chain transfer, deactivation, and other polymer-specific reactions. We have identified the reaction rate constants in Ziegler-Natta polymerization kinetics that have most significant impacts on common production targets, which greatly simplifies the kinetic parameter estimation for simulation and optimization models for polyolefin processes using plant data.

Our methodology begins with a kinetic model considering a single active catalyst site, followed by converting the single-site model into a model assuming multiple active catalyst sites. We apply deconvolution analysis to characterize the GPC MWD data to determine the most probable chain length distribution for each catalyst site assuming a Flory distribution. The deconvolution analysis identifies the expected number of active catalyst sites together with the weight fraction and number-average molecular weight for each active catalyst site.

We demonstrate an effective methodology in Figures 5.9a and 5.9b to use efficient software tools, such as data fit, sensitivity analysis and design specification in Aspen Polymers, to *simultaneously* estimate multiple reaction rate constants for Ziegler-Natta kinetics to match several datasets of production targets, such as production rates, MWN, SFRAC, etc. in a computer-aided step-by-step procedure. This differentiates our study from most of the previous studies which *sequentially* estimate these reaction rate constants. Our methodology in Figure 5.9 also greatly simplifies the kinetic parameter estimation for the multisite model, in that we only need to regress *selected* kinetic parameters for the multisite model to match the plant data for PDI and related production targets, such as the atactic fraction for PP production.

Our methodology in Figures 5.9a and 5.9b results in part from our insights and experiences from applying our methodology to several dozen commercial polyolefin processes at two of the world's largest petrochemical companies in the Asia-Pacific over the past two decades. Applying our

methodology using efficient software tools results in validated simulation and optimization models that we can use to quantify changes in process operations, process capacity scale-up, polymer quality control, product grade change, etc.

Our detailed supplements of modeling examples and Excel modeling spreadsheet will be useful to practicing engineers interested in applying process modeling and optimization to commercial polyolefin production.

This chapter is published with Wiley publication in the book *Integrated Process Modeling, Advanced Control and Data Analytics for Optimizing Polyolefin Manufacturing by Liu & Sharma.*[78-89]

This chapter also presents four detailed hands-on workshops for simulating HDPE, PP, LLDPE and EPM (ethylene-propylene copolymer) using Ziegler-Natta catalyst and metallocene catalysts-cocatalyst, and demonstrate how to apply the efficient simulation software tools such as data fit, sensitivity analysis and design specifications for kinetic parameter estimation, process improvement, and optimization.

5.10 Bibliography

1. Soares, J. B. P.; McKenna, T. F. L. (2012) *Polyolefin Reaction Engineering,* Wiley-VCH: Weinheim, Germany.

2. Dotson, N. A.; Galvan, R.; Laurence, R. L.; Tirrell, M. (1996) *Polymerization Process Modeling*; Wiley-VCH Publishers, Inc., New York: New York.

3. Sharma, N.; Liu, Y. A. (2019) 110th Anniversary: An Effective Methodology for Kinetic Parameter Estimation for Modeling Commercial Polyolefin Processes from Plant Data Using Efficient Software Tools, *Ind. Eng. Chem. Res.*, **58**, 14209.

4. Khare, N.P.; Seavey, K. C.; Liu, Y.A.; Ramanathan, S.; Lingard, S.; Chen, C. C. (2002) Steady-state and Dynamic Modeling of Commercial Slurry High-Density Polyethylene (HDPE) Processes. *Ind. Eng. Chem. Res*. **41**, 5601.

5. Khare, N. P.; Lucas, B.; Seavey, K. C.; Liu, Y. A.; Sirohi, A.; Ramanathan, S.; Lingard, S.; Song, Y.; Chen, C. C. (2004) Steady-State and Dynamic Modeling of Commercial Gas-Phase Polypropylene Processes Using Stirred-Bed Reactors. *Ind. Eng. Chem. Res*. **43**, 884.

6. Touloupidis, V. (2014) Catalytic Olefin Polymerization Process Modeling: Multi-Scale Approach and Modeling Guidelines for Micro-Scale/Kinetic Modeling. *Macromol. React. Eng*. **8**, 508.

7. Zacca, J. J.; Ray, W. H. (1993) Modeling of Liquid Phase Polymerization of Olefins in Loop Reactors. *Chem. Eng. Sci*. **48**, 3743.

8. Chen, K.; Tian, Z.; Luo, N.; Liu, B. (2014) Modeling and Simulation of Borstar Bimodal Polyethylene Process Based on a Rigorous PC-SAFT Equation of State Model. *Ind. Eng. Chem. Res*. **53**, 19905.

9. Zhang, C.; Shao, Z.; Chen, X.; Yao, Z.; Gu, X.; Biegler, L. T. (2014) Kinetic Parameter Estimation of HDPE Slurry Process from Molecular Weight Distribution: Estimability Analysis and Multistep Methodology. *AIChE J.* **60**, 3442.

5. Meng, W.; Li, J.; Chen, B.; Li, H. (2013) Modeling and Simulation of Ethylene Polymerization in Industrial Slurry Reactor Series. *Chin. J. Chem. Eng.* **21**, 850.

11. Zhao, X.; Guo, X.; Chen, P.; Niu, L.; Yang, J.; Xu, X. (2012) Simulation and Analysis of an Ethylene Slurry Polymerization System Using Supercritical Propane. *Ind. Eng. Chem. Res.* **51**, 682.

12. Zheng, Z. W.; Shi, D. P.; Su, P. L.; Luo, Z. H.; Li, X. J. (2011) SteadyState and Dynamic Modeling of the Basell Multireactor Olefin Polymerization Process. *Ind. Eng. Chem. Res.* **50**, 322.

13. Lu, C.; Zhang, M.; Jiang, S.; Song, D. (2006) Application of ASPEN PLUS in Large-Scale Polypropylene Plant. *Qilu Petrochemical Technology.* **34**, 404.

14. Touloupides, V.; Kanellopoulos, V.; Pladis, P.; Kiparissides, C.; Mignon, D.; Van-Grambezen, P. (2010) Modeling and Simulation of an Industrial Slurry-Phase Catalytic Olefin Polymerization Reactor Series. *Chem. Eng. Sci.* **65**, 3208.

15. Seavey, K. C.; Khare, N. P.; Liu, Y. A.; Bremner, T.; Chen, C. C. (2003) Quantifying Relationships among the Molecular Weight Distribution, Non-Newtonian Shear Viscosity and Melt Index for Linear Polymers. *Ind. Eng. Chem. Res*. **42**, 5354.

16. Mattos Neto, A. G.; Freitas, M. F.; Nele, M.; Pinto, J. C. (2005) Modeling Ethylene/1-Butene Copolymerizations in Industrial Slurry Reactors. *Ind. Eng. Chem. Res.* **44**, 2697.

17. Tian, Z.; Chen, K. R.; Liu, B. P.; Luo, N.; Du, W. L.; Qian, F. (2015) Short-chain Branching Distribution Oriented Model Development for Borstar Bimodal Polyethylene Process and Its Correlation with Product Performance of Slow Crack Growth. *Chem. Eng. Sci.* 130, 41.

18. Luo, Z. W.; Zheng, Y.; Cao, Z. K.; Wen, S. H. (2007) Mathematical Modeling of the Molecular Weight Distribution of Polypropylene Produced in a Loop Reactor. *Polym. Eng. Sci.* **47**, 1643.

19. You, C.; Li, S. (2007). Analysis and Application of Model Building Procedure in Polypropylene Plant. *Petrochemical Industry Technology*, **14**, No. 2, 56.

20. Luo, Z. H.; Su, P. L.; Shi, D. P.; Zheng, Z. W. (2009) Steady-State and Dynamic Modeling of Commercial Bulk Polypropylene Process of Hypol Technology. *Chem. Eng. J.* **149**, 370.

21. Kou, B.; McAuley, K. B.; Hsu, C. C.; Bacon, D. W.; Yao, K. Z. Mathematical Model and Parameter Estimation for Gas-Phase Ethylene Homopolymerization with Supported Metallocene Catalyst. *Ind. Eng. Chem. Res*. **44**, 2428.

22. Kou, B.; McAuley, K. B.; Hsu, C. C.; Bacon, D. W. (2005) Mathematical Model and Parameter Estimation for Gas-Phase Ethylene-Hexene Copolymerization with Metallocene Catalyst. *Macromol. Mater. Eng.*, **290**, 537.

23. Kashani, A. F.; Abedini, H.; Kalace, M. R. (2011) Simulation of an Industrial Linear Low Density Polyethylene Plant. *Chem. Prod. Process Model*. **6**, Art. 34, https://www.degruyter.com/document/doi/10.2202/1934-2659.1611/htML, accessed June 23, 2021.

24. Baughman, D. R.; Liu, Y. A. (1995) *Neural Networks in Bioprocessing and Chemical Engineering*; Elsevier: Atlanta, GA.

25. Knuuttila, H.; Lehtinen, A.; Nummila-Pakarinen, A. (2004) Advanced Polyethylene Technologies-Controlled Material Properties. *Adv. Polym. Sci*. **169**, 13.

26. Zheng, X. G. (2015) Operation Optimization of Dual-Loop Polypropylene Process by Polymers Plus Software. *Petrochemical Technology*, **44**, 612.

27. Shamiri, A.; Hussain, M. A.; Mjalli, F. S.; Mostoufi. (2010) Kinetic Modeling of Propylene Homopolymerization in a Gas-Phase Fluidized-Bed Reactor. *Chem. Eng. J.*, ***161,*** 240.

28. Gross, J.; Sadowski, G. (2001) Perturbed-Chain SAFT: An Equation of State Based on a Perturbation Theory for Chain Molecules. *Ind. Eng. Chem. Res*. **51**, 1244.

29. Sanchez, I. C.; Lacombe, R. H. (1976) An Elementary Molecular Theory of Classic Fluids. Pure Fluids. *J. Phys. Chem.*, **80**, 2352.

30. Lacombe, R. H.; Sanchez, I. C. (1976) Statistical Thermodynamics of Fluid Mixtures. *J. Phys. Chem.,* **80**, 2568.

31.Sanchez, I. C.; Lacombe, R. H. (1978) Statistical Thermodynamics of Polymer Solutions. *Macromolecules*, **11**,1145.

32. Tremblay, D. (2017) Modeling Polymerization Processes. Aspen Optimize Training, OPTIMIZE 2017, Houston, TX, April.

33. You, C. (2006) Modeling and Analysis of Polypropylene Process in Steady and Dynamic States. M.S. Thesis, College of Chemical Engineering, Tianjin University, June.

34. Soares, J. B. P.; Hamielec, A. E. (1995) Deconvolution of Chain-Length Distribution of Linear Polymers Made by Multiple-Site-Type Catalysts. *Polymer,* **36**, 2257.

35. Aspen Technology, Inc. (2021) Bessel Spheripol polypropylene process simulation example, see: https://esupport.aspentech.com/S_ Article id=000038267 (accessed March 11, 2021).

36. Bokis, C. P.; Orbey, H.; and Chen, C. C. (1999) Properly Model Polymer Processes. *Chem. Eng. Prog*. **95**, No. 4, 39.

37. Shepard, J. W.; Jezl, J. L.; Peters, E. F.; Hall, R. D. (1976). Divided Horizontal Reactor for the Vapor Phase Polymerization of Monomers at Different Hydrogen Levels. U.S. Patent 3,957,488.

38. Jezl, J. L.; Peters, E. F.; Hall, R. D.; Shepard, J. W. (1976). Process for the Vapor Phase Polymerization of Monomers in a Horizontal, Quench-Cooled, Stirred-Bed Reactor Using Essentially Total Off-Gas Recycle and Melt Finishing. U.S. Patent 3,965,083.

39. Peters, E. F.; Spangler, M. J.; Michaels, G. O.; Jezl, J. L. (1976). Vapor Phase Reactor Off-Gas Recycle System for Use in the Vapor State Polymerization of Monomers. U.S. Patent 3,971,768.

40. Jezl, J. L.; Peters, E. F. (1978). Horizontal Reactor for the Vapor Phase Polymerization of Monomers. U.S. Patent 4,129,701.

41. Buchelli, A.; Caracotsios, M. (1996). Polymerization of Alpha-Olefins. U. S. patent 5,504,166.

42. Choi, K. Y.; Ray, W. H. (1988). The Dynamic Behavior of Continuous Stirred-Bed Reactors for the Solid Catalyzed Gas Phase Polymerization of Propylene. *Chem. Eng. Sci*., **43**, 2587.

43. Kissel, W. J.; Han, J. H.; Meyer, J. A. (1999). Polypropylene: Structure, Properties, Manufacturing Processes, and Applications. In *Handbook of Polypropylene and Polypropylene Composites*; Karian, H. G., Ed.; Marcel Dekker: New York, p. 15.

44. Caracotsios, M. (1992). Theoretical Modelling of Amoco's Gas Phase Horizontal Stirred Bed Reactor for the Manufacturing of Polypropylene Resins. *Chem. Eng. Sci.*, **47**, 2591.

45. Zecca, J. J.; Dehling, J. A.; Ray, W. H. (1996). Reactor Residence Time Distribution Effects on the Multistage Polymerization of Olefins. I. Basic Principles and Illustrative Examples. Polypropylene. *Chem. Eng. Sci.* **51**, 4859.

46. Gorbach, A. B.; Naik, S. D.; Ray, W.H. (2000). Dynamics and Stability Analysis of Solid Catalyzed Gas-Phase Polymerization of Olefins in Continuous Stirred Bed Reactors. *Chem. Eng. Sci.* **55**, 4461.

47. Dittrich, C. J.; Mutsers, Stan M. P. (2007). On the Residence Time Distribution in Reactors with Non-Uniform Velocity Profiles: The Horizontal Stirred Bed Reactor for Polypropylene Production. *Chem. Eng. Sci.,* **62**, 5777.

48. Kouzai, I.; Fukuda, K. (2009). Modeling Study on Effects of Liquid Propylene in Horizontally Stirred Gas-Phase Reactors for Polypropylene. *Macromolecular Symposia,* **285**, 23.

49. Moore, E. P. (1996). Polypropylene (Commercial). In *Polymeric Materials Encyclopedia*; Salamone, J. C., Ed.; CRC Press: Boca Raton, FL, p. 6578.

50. Balow, M. J. (1999). Growth of Polypropylene Usage as a Cost-Effective Replacement of Engineering Polymers. In *Handbook of Polypropylene and Polypropylene Composites*; Karian, H. G., Ed.; Marcel Dekker: New York, p. 1.

51. Gross, J., Sadowski, G. (2001). Perturbed-Chain SAFT: An Equation of State Based on a Perturbation Theory for Chain Molecules. *Ind. Eng. Chem. Res.* **40**, 1244.

52. Gross, J., Sadowski, G. (2002). Application of Perturbed-Chain SAFT Equation of State to Associating Systems. *Ind. Eng. Chem. Res.* **41,** 5510.

53. Kissin, Y. V. (2003). Multicenter Nature of Titanium-Based Ziegler-Natta Catalysts: Comparison of Ethylene and Propylene Polymerization Reactions. *J. Polym. Sci. A: Polym. Chem*., **41**, 1745.

54. Wang, W. Q.(2008). Research on Modeling and Simulation for Industrial Polymerization Process. M.S. thesis, System Engineering, Zhejiang University, Hangzhou, China.

55. Jenkins, III, J. M.; Jones, R. L.; Jones, T. L. (1985). Fluidized Bed Reaction Systems. U. S. patent 4588790.

56. Jenkins, III, J. M.; Jones, R. L.; Jones, T. L.; Beret, S. (1986). Method for Fluidized Bed Polymerization. U. S. patent 4543399A.

57. McKenna, T. F. L. (2019). Condensed Mode Cooling of Ethylene Polymerization in Fluidized Bed Reactors. *Macromolecular Reaction Engineering*, **13**, 1800026.

58. Rainho, P.; Alizadeh, A.; Ribeiro, M. R.; McKenna, T. L. F. (2014). Pseudo-homogeneous CSTR Simulation of a Fluidized-Bed Reactor Operating in Condensed-Mode Including Sanchez-Lacombe n-Hexane Co-Solubility Effect. *J. Engineering for Rookies*, **1**, 56. http://citeseerx.ist.psu.edu/viewdoc/download?doi=10.1.1.1075.9872&rep=rep1&type=pdf, accessed June 23, 2021.

59. Utikar, R. P.; Harshe, Y. M.; Mehra, A.; Ranade, V. V. (2008). Modeling of a Fluidized-Bed Reactor Propylene Polymerization Reactor Operated in Condensed Mode. *J. Applied Polymer Science*, **108**, 2067.

60. Gross, J., and Sadowski, G. (2001) "Perturbed-Chain SAFT: An Equation of State Based on a Perturbation Theory for Chain Molecules." *Ind. Eng. Chem. Res.*, **40**, 1244.

61. Bokis, C. P., Ramanathan, S., Franjione, J., Buchelli, A., Call, M. L., Brown, A. L. (2002). Physical Properties, Reactor Modeling, and Polymerization Kinetics in the Low-Density Polyethylene Tubular Reactor Process. *Ind. Eng. Chem. Res.*, **41**, 1017.

62. Gao, T.; Zhao, Y. I. (2008). Application of Aspen Plus Process Simulation Software in LLDPE Plant. *Qilu Petrochemical Technology*, **36**, No. 1, 35.

63. Cesca, S. (1975). The Chemistry of Unsaturated Ethylene-Propylene-Based Terpolymers. (1975). *J. Polymer Sci. : Macromolecular Reviews*, **10**, 1.

64. Van Duin, M.; Van der Aar, I. N.; Van Dornemaele, G. (2017). Historical and Technical Summary of Keltan Developments Defining EPDM for the Past and the Next 50 Years. https://www.kgk-rubberpoint.de/en/21389/defining-epdm-for-the-past-and-the-next-50-years/, accessed June 29, 2021.

65. Eisinger, R. F.; Lee, K. H.; Hussein, F. D.; Zilker, Jr., D. P. (2000). Process for Conditioning a Gas-Phase Reactor to Produce an Ethylene-Propylene or Ethylene-Propylene-Diane-Rubber. U. S. Patent No. 6,011,128.

66. Cozewith, C. (1988). Transient Response of Continuous-Flow Stirred-Tank Polymerization Reactors. *AIChE J.*, **34**, 272.

67. Ver Strate, G.; Cozewith, C.; Ju, S. (1988). Near Monodisperse Ethylene-Propylene Copolymers by Direct Ziegler-Natta Polymerization. Preparation, Characterization, Properties., *Macromolecules*, 21, 3360.

68. Ogunnaike, B. A. (1994). On-Line Modelling and Predictive Control of an Industrial Terpolymerization Process. *Int. J. Control*, **59**, 711.

69. Meziou, A. M. (1993). Optimization and Advanced Control of an Industrial Polymerization Process. H.D. dissertation, Univ. Of Louisville, Louisville, KY.

70. Meziou, A. M., Deshpande, P. B., Cozewith, C.; Silverman, N. I.; Morrison, W. G. (1996). Dynamic Matrix Control of an Ethylene-Propylene-Diane Polymerization Process. *Ind. Eng. Chem. Research*, **35**, 164.

71. Hagg, M. C.; Henrique, J.; Dantos, J. H. Z. D.; Dupont, J.; Secchi, A. R. (1998). Dynamic Simulation and Experimental Evaluation of EPDM Terpolymerization with Vanadium-Based Catalyst., *J. Applied Polymer Sci.*, **70**, 1173.

72. Pourhossaini, M. R.; Vasheghani-Farahani, E.; Gholamian, Maryam; Gholamian, Mahmood (2006). Dynamic Simulation and Experimental Evaluation of Olefin Copolymerization with Vanadium-Based Catalysts., *J. Applied Polymer Sci.*, **100**, 3101.

73. Chen, H. J. (2016). Development of New Product Grades and Industrial Implementation of Ethylene-Propylene Rubber (EPDM). M. S. thesis, College of Life and Environmental Sciences, Shanghai Normal University, Shanghai, China.

74. Xu, C.-Z.; Wang, J.-J.; Gu, X.-P.; Fang, L.-F. (2018). Modeling of Molecular Weight and Copolymerization Composition Distributions for Ethylene-Propylene Solution Copolymerization. *AIChE J.*, **65**, e1663.

75. Hamielec A.E.; Soares J.B.P. (1999). Metallocene Catalyzed Polymerization: Industrial Technology. In: Polypropylene. Polymer Science and Technology Series, Vol 2. Karger-Kocsis J., Editor. Springer, Dordrecht. https://doi.org/10.1007/978-94-011-4421-6_62. Accessed June 29, 2021.

76. Hagg, M. C.; Henrique, J.; Dantos, J. H. Z. D.; Dupont, J.; Secchi, A. R. (2000). Dynamic Simulation and Experimental Evaluation of EPDM Terpolymerization with $Et(Ind)_2ZrCl_2$/MAO Catalyst System., *J. Applied Polymer Sci*., **76**, 425.

77. Aspen Technology, Inc. (2020). How to Model a Terminal Double Bond Polymerization in Aspen Polymers? Knowledge Article No. 000086916. AspenTech Online Support. https://esupport.aspentech.com/S_Article?id=000086916, accessed July 3, 2021.

78. Liu, Y. A., & Sharma, N. (2023). *Integrated Process Modeling, Advanced Control and Data Analytics for Optimizing Polyolefin Manufacturing*. Wiley-VCH GmbH (https://doi.org/10.1002/9783527843831)

79. Liu, Y. A., & Sharma, N. (2023). Introduction to Integrated Process Modeling, Advanced Control, and Data Analytics in Optimizing Polyolefin Manufacturing. In *Integrated Process Modeling, Advanced Control and Data Analytics for Optimizing Polyolefin Manufacturing* (Chapter 1, pp. 1-40). Wiley-VCH GmbH. https://doi.org/10.1002/9783527843831.ch1

80. Liu, Y. A., & Sharma, N. (2023). Selection of Property Methods and Estimation of Physical Properties for Polymer Process Modeling. In *Integrated Process Modeling, Advanced Control and Data Analytics for Optimizing Polyolefin Manufacturing* (Chapter 2, pp. 41-86). Wiley-VCH GmbH. https://doi.org/10.1002/9783527843831.ch2

81. Liu, Y. A., & Sharma, N. (2023). Reactor Modeling, Convergence Tips, and Data-Fit Tool. In *Integrated Process Modeling, Advanced Control and Data Analytics for Optimizing Polyolefin Manufacturing* (Chapter 3, pp. 87-114). Wiley-VCH GmbH. https://doi.org/10.1002/9783527843831.ch3

82. Liu, Y. A., & Sharma, N. (2023). Free Radical Polymerizations: LDPE and EVA. In *Integrated Process Modeling, Advanced Control and Data Analytics for Optimizing Polyolefin Manufacturing* (Chapter 4, pp. 115-162). Wiley-VCH GmbH. https://doi.org/10.1002/9783527843831.ch4

83. Liu, Y. A., & Sharma, N. (2023). Ziegler–Natta Polymerization: HDPE , PP , LLDPE, and EPDM. In *Integrated Process Modeling, Advanced Control and Data Analytics for Optimizing Polyolefin Manufacturing.* (Chapter 5, pp. 163-265). Wiley-VCH GmbH. https://doi.org/10.1002/9783527843831.ch5

84. Liu, Y. A., & Sharma, N. (2023). Free Radical and Ionic Polymerizations: PS and SBS Rubber. In *Integrated Process Modeling, Advanced Control and Data Analytics for Optimizing Polyolefin Manufacturing.* (Chapter 6, pp. 267-319). Wiley-VCH GmbH. https://doi.org/10.1002/9783527843831.ch6

85. Liu, Y. A., & Sharma, N. (2023). Improved Polymer Process Operability and Control Through Steady-State and Dynamic Simulation Models. In *Integrated Process Modeling, Advanced Control and Data*

Analytics for Optimizing Polyolefin Manufacturing. (Chapter 7, pp. 321-379). Wiley-VCH GmbH. https://doi.org/10.1002/9783527843831.ch7

86. Liu, Y. A., & Sharma, N. (2023). Model-Predictive Control of Polyolefin Processes. In *Integrated Process Modeling, Advanced Control and Data Analytics for Optimizing Polyolefin Manufacturing.* (Chapter 8, pp. 381-476). Wiley-VCH GmbH. https://doi.org/10.1002/9783527843831.ch8

87. Liu, Y. A., & Sharma, N. .2023. Application of Multivariate Statistics to Optimizing Polyolefin Manufacturing. In *Integrated Process Modeling, Advanced Control and Data Analytics for Optimizing Polyolefin Manufacturing* (Chapter 9, pp. 477-531). Wiley-VCH GmbH. https://doi.org/10.1002/9783527843831.ch9

88. Liu, Y. A., & Sharma, N. (2023). Applications of Machine Learning to Optimizing Polyolefin Manufacturing. In *Integrated Process Modeling, Advanced Control and Data Analytics for Optimizing Polyolefin Manufacturing.* (Chapter 10, pp. 553-650). Wiley-VCH GmbH. https://doi.org/10.1002/9783527843831.ch10.

89. Liu, Y. A., & Sharma, N. (2023). A Hybrid Science-Guided Machine Learning Approach for Modeling Chemical and Polymer Processes. In *Integrated Process Modeling, Advanced Control and Data Analytics for Optimizing Polyolefin Manufacturing.* (Chapter 11, pp. 651-698). Wiley-VCH GmbH. https://doi.org/10.1002/9783527843831.ch11